AD657564

CAL/USAAVLABS SYMPOSIUM PROCEEDINGS

AERODYNAMIC PROBLEMS ASSOCIATED WITH V/STOL AIRCRAFT

VOLUME III

AERODYNAMIC RESEARCH ON BOUNDARY LAYERS

Reproduced by the
CLEARINGHOUSE
for Federal Scientific & Technical
Information Springfield Va. 22151

22-24 June 1966

Statler-Hilton Hotel

Buffalo, New York

DISCLAIMER NOTICE

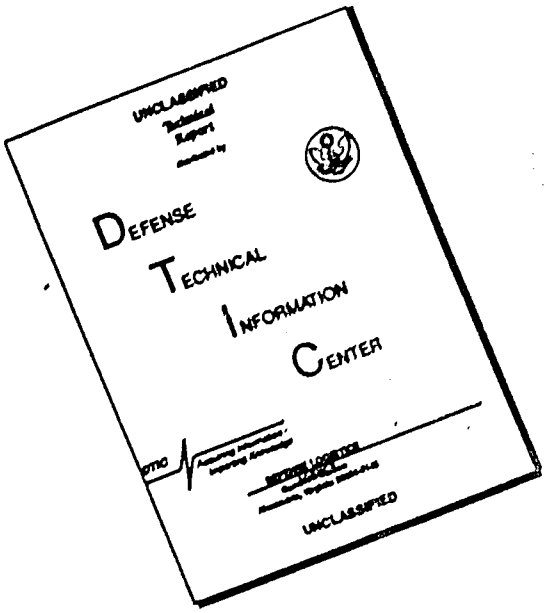

THIS DOCUMENT IS BEST QUALITY AVAILABLE. THE COPY FURNISHED TO DTIC CONTAINED A SIGNIFICANT NUMBER OF PAGES WHICH DO NOT REPRODUCE LEGIBLY.

CAL/USAAVLABS

SYMPOSIUM PROCEEDINGS

AERODYNAMIC PROBLEMS ASSOCIATED WITH V/STOL AIRCRAFT

Published in Four Volumes as Follows:

Volume I Propeller and Rotor Aerodynamics

Volume II Propulsion and Interference Aerodynamics

Volume III Aerodynamic Research on Boundary Layers

Volume IV Panels on Recommended V/STOL Aerodynamic Research, Panel Summaries, Featured Speakers, and Technical Paper Discussions

This is VOLUME III and contains those technical papers presented

Friday, 24 June 1966
Statler-Hilton Hotel
Buffalo, New York

has been approved for public release and sale; its distribution is unlimited.

SEP 7 1967

Statements and opinions contained herein are those of the authors and are not to be construed as reflecting the views of the Department of the Army nor the cosponsors of this Symposium – The U.S. Army Aviation Materiel Laboratories and Cornell Aeronautical Laboratory, Inc.

FOREWORD

The rapid advances made in helicopter and V/STOL aircraft development in the past few years have spotlighted areas in which significant aerodynamic problems have been encountered, and in some cases the problems still exist. Fortunately, a technological maturity has now been attained in the industry, making possible investigations through knowledgeable scientific approaches that have produced an enlightened understanding of the problems and, in many cases, have led to practical solutions. The next generation of flight vehicles, currently in the design and development stages, are offering challenges to the aerodynamicist and engineer, and it is evident that future vehicle developments will demand an ever-increasing rate of technological advance in the knowledge and understanding of aerodynamic phenomena.

Several years have passed since a technical specialists' meeting was held to direct attention specifically to the low-speed aerodynamic problem areas of helicopters and V/STOL vehicles. Therefore, in the interest of disseminating up-to-date information, the cosponsors of this symposium, the U.S. Army Aviation Materiel Laboratories (USAAVLABS) and Cornell Aeronautical Laboratory, Inc. (CAL), believe such a meeting among technical specialists in the field would be timely. It is hoped that this symposium will, through the presentation of selected technical papers, establish the state of the art of aerodynamic analysis in the basic problem areas and spotlight those critical areas where research is urgently needed. The ultimate objective is to identify those advances required in the state of the art that can assure the availability of the analytical tools needed to develop and analyze the next generation of helicopters and V/STOL aircraft.

In keeping with these objectives, five technical sessions, each dealing with specific basic areas of aerodynamic analysis associated with V/STOL aircraft, have been formed. In addition, a panel session has also been scheduled in which outstanding members of industry and government from three countries will present their recommendations for areas of research that need to be pursued if the state of the art is to advance at the required rate.

It is believed that the formal presentation of the selected papers and the panel presentations and recommendations will stimulate constructive discussions among the specialists in attendance. While a significant amount of time has been allotted during the sessions for this to be accommodated, it is hoped the sessions will, in addition, stimulate discussions and serious thought between the attendees and the technical members of the various organizations who were unable to attend. In order to foster this latter objective, the informal discussions (questions and answers, etc.) will be recorded, printed, and mailed to each attendee for inclusion in his copy of the proceedings.

The proceedings of the symposium have been bound in four volumes -- a separate volume for the technical sessions of each day, and one volume for the panel sessions. We are indebted to the authors for preparing their manuscripts in a form that could be directly reproduced. This material was published as provided by the authors and was neither checked nor edited by CAL or USAAVLABS.

The cosponsors of the symposium are grateful to the many people who contributed to its success. In particular, our thanks go to Colonel Harry L. Bush, Commanding Officer of the U.S. Army Aviation Materiel Laboratories, and Mr. Ira G. Ross, President of Cornell Aeronautical Laboratory, Inc., who opened the sessions; to Mr. Charles W. Harper, our keynote speaker; to Major General William Bunker, Deputy Commanding General, U.S. Army Materiel Command, for his address at the symposium banquet; to the five session chairmen --

Arthur Jackson, Hamilton Standard

Franklyn J. Davenport, Vertol Division of The Boeing Company

John W. White, U.S. Army Aviation Materiel Laboratories

Irven H. Culver, Lockheed-California Company

Sean C. Roberts, Mississippi State University

and to the two panel chairmen --

Larry M. Hewin, Technical Director, USAAVLABS

Harold A. Cheilek, Vice President - Technical Director, CAL

and, most especially, of course, to the authors and panel members without whom there could not have been this symposium on low-speed aerodynamic problems.

SYMPOSIUM TECHNICAL CHAIRMAN

Richard P. White, Jr., CAL
John E. Yeates, USAAVLABS

CONTENTS

VOLUME III

AERODYNAMIC RESEARCH ON BOUNDARY LAYERS

SPANWISE FLOW EFFECTS ON ROTOR PERFORMANCE
F. D. Harris
Vertol Division
The Boeing Company
Morton, Pennsylvania

A PRELIMINARY STUDY OF THE EFFECT OF A RADIAL PRESSURE GRADIENT ON THE BOUNDARY LAYER OF A ROTOR BLADE
H. R. Velkoff
Department of Mechanical Engineering
The Ohio State University
Columbus, Ohio

THE BOUNDARY LAYER OF THE HOVERING ROTOR
W. H. Tanner
Bell Helicopter Company
Fort Worth, Texas
and
P. Buettiker
Arlington State College
Arlington, Texas

AN INVESTIGATION OF THE FEASIBILITY OF A COMMON BOUNDARY LAYER CONTROL SYSTEM FOR HIGH-LIFT AND LOW-DRAG ON AN AIRFOIL SECTION
S. C. Roberts
Aerophysics Department
Mississippi State University
State College, Mississippi

TECHNICAL SESSION V

AERODYNAMIC RESEARCH ON BOUNDARY LAYERS

Friday Morning
24 June 1966

SESSION CHAIRMAN

S.C. Roberts
Aerophysics Department
Mississippi State University

SPANWISE FLOW EFFECTS ON ROTOR PERFORMANCE

by

FRANKLIN D. HARRIS

Chief, Rotor System Technology
Vertol Division, The Boeing Company
Morton, Pennsylvania

INTRODUCTION

Throughout the development of rotary-wing aircraft, consideration of radial (spanwise) flow effects on rotor performance has remained rather academic. Although brief analytical notice[1][2] has been given to this spanwise flow effect on rotor drag, no great emphasis has been directed at the actual boundary-layer characteristics of a rotating helicopter blade in forward flight. Helicopter operation at advance ratios less than 0.3 has presented useable agreement between test results and theory, but the accumulation of experimental flight test and model rotor data has revealed a stall delaying phenomenon while measured rotor drags are in excess of theory at higher advance ratios. Experimental results obtained by Sweet[3] and Jenkins[4] clearly re-emphasize our problems in dealing with "blade stall".

The ability of the rotor to experimentally disregard the classical presumptions of "blade stall" is shown in Figure 1[5]. Experimental results obtained with full scale rotors[6],[7], and other model rotor tests[8],[9],[10] indicate that the phenomena is not an isolated one. The question derived from the experimental observations is: Why does simple aerodynamic rotor theory, which assumes no loss in section lift coefficient at stall (constant lift curve slope), agree with experimental data for rotor thrust, while a large drag increment in section drag at stall is required to attain even a semblance of agreement between experimental data and theory?

As discussed in References 11 and 5, the effects of induced velocity distribution, blade elasticity, Mach and Reynolds numbers, time rate of change

of section angle of attack, and spanwise flow (radial flow due to pressure gradient, centrifugal and Coriolis forces, and blade sweep) in the boundary layer can all potentially contribute to the explanation of the rotor stall delaying phenomenon. Reference 11, however, suggested that time rate of change of section angle of attack and spanwise flow in the boundary layer quite probably are the greatest contributers to the phenomena.

The rotating blade will have a boundary layer affected not only by the potential flow velocity field, but also by the spanwise (and chordwise) pressure distribution and centrifugal and Coriolis force fields. The study of radial flow on rotor blades must therefore encompass the effects of :

1. Oblique or yawed flow to local sections of the blade due to the potential, free-stream velocity field
2. The chordwise pressure distribution
3. The spanwise pressure distribution associated with loading on a blade
4. Spanwise "pumping" due to the centrifugal force field
5. The chordwise accelerations of boundary-layer particles moving spanwise due to the Coriolis force field.

The gross effect of radial flow due to the first four items is the thinning of the boundary layer; while the fifth item acts like an additional chordwise pressure drop. Although the order of magnitude of each of these external fields remains open to discussion, preliminary review of analytical studies conducted on a hovering rotor indicated that item one (yawed flow to local sections) would most significantly alter the outboard stall pattern.

A discussion of Boeing Company Research into radial (spanwise) flow characteristics is presented in Reference 12 to be published in the July issue, Journal of the American Helicopter Society. Since submittal of that paper, additional theoretical and experimental studies have been completed.

After briefly reviewing the rotary-wing classical assumptions and background work of Reference 12, this paper will discuss this most recent work and finally, submit to you my interpretation of the blade stall phenomena.

FUNDAMENTAL ASSUMPTION OF ROTARY-WING THEORY

All popular airload and rotor-performance theoretical analyses accept the simple-sweep theory, also referred to as the independence principle. As applied to the rotating blade in forward flight, the statements of simple sweep theory or independence principle may be interpreted as follows: independent of the direction that the local relative wind velocity makes with the rotor blade span axis at a given rotor-blade radial element, only the component of velocity that falls in the plane perpendicular to the span axis defines the aerodynamic characteristics of the airfoil section such as angle of attack, Mach number, and Reynolds number which, together, define a lift and drag coefficient. The component of velocity parallel to the rotor-blade span axis may be neglected, therefore, in defining the elemental lift and drag. Figure 2 illustrates this underlying assumption.

With this assumption, airloads are derived from a blade-element or "strip" analysis which assumes two-dimensional airfoil-section properties of lift and drag coefficient. The industry has worked hard to establish reliable two-dimensional data showing variations in airfoil $C_{\ell_{max}}$ with Mach number, airfoil properties for reverse flow, and Reynolds number corrections. A distributed induced velocity has been introduced into these "strip" analyses to provide a more reasonable three-dimensional model that closely estimates the effect of the rotor-blade vortex patterns as well as the vortex interaction of the several blades that normally comprise a rotor system. Today, the industry is deeply concerned with unsteady aerodynamic characteristics feeling the need to augment our two-dimensional airfoil data with the effects of a time varying angle of attack. Underlying this broad theoretical and experimental approach, however, are the fundamentals of simple sweep theory - the independence principle.

The translation of two-dimensional airfoil data into the three-dimensional environment of the helicopter rotor is now open to question.

BRIEF REVIEW OF SWEPT AND YAWED WING EXPERIENCE

The wealth of experimental and theoretical swept and yawed wing

experience has provided an excellent source from which to draw conclusions about just how acceptable the independence principle will be for rotary wing studies. The preliminary study of radial flow effects on rotor blades reported in Reference 12 explored this data in depth and this background is reviewed in the following paragraphs.

Lift Trends with Angle of Attack and Yaw Angle

The very important experimentally determined phenomenon that a unit area of a yawed infinite wing can achieve higher section-lift coefficients than the same unit area unyawed was initially studied[11] by reducing three-dimensional data[13] of an aspect ratio - 6 rectangular wing of NACA 0012 airfoil. The data, when presented in the rotary wing, normal to the blade span axis, coordinate system is quite startling as shown in Figure 3. It is clear that at the lower angles of attack the independence principle is substantiated for yaw angles up to 45 degrees and could be considered as a satisfactory engineering approximation for yaw angles up to 75 degrees. In short the rotary wing practice of ignoring the spanwise flow in determining rotor thrust must be correct to the first order when the blade element angle of attack is below, say, the classically used 12 degrees.

The "stalling" of this yawed wing obviously does not follow from the two-dimensional data as suggested by the zero yaw angle results. We would expect, after assuming that the spanwise velocity component could be disregarded, that $C_{\ell_{max}}$ is also independent of yaw angle, but data such as Figure 3 negates this "best guess".

Further experimental study[14] obtained with a 45° yawed wing spanning a wind tunnel to approximate a yawed infinite wing demonstrated a similar maximum lift improvement as shown in Figure 4. It is therefore reasonable to conclude that if there is a high degree of separation on the yawed infinite wing (large angles of attack near or above stall), the independence principle should not be employed to determine the chordwise pressure distribution or, more importantly, the section lift coefficient.

Skin Friction Drag Trend with Yaw Angle

The use of the independence principle to determine minimum airfoil drag coefficient variation with yaw angle is experimentally and theoretically accepted in the swept wing field if the boundary layer is completely laminar. Presently, the technical position if the boundary layer is turbulent is no where near as firm. The majority of work however, including a most recent review[15], supports the conclusion that the independence principle is not applicable for turbulent boundary layer studies. The boundary layer growth in the plane containing the resultant velocity, as shown in Figure 5, is recommended. This leads to a requirement to define the minimum drag coefficient as effected by yaw angle. A first impression might suggest reducing the drag coefficient with yaw angle because the thickness ratio is decreasing; this trend with yaw angle has not been experimentally found for flat plates[16],[17]. Even at the angle of attack for minimum drag coefficient, the drag is composed of both skin friction and pressure drag, and the actual variation of airfoil drag coefficient with yaw angle will therefore be individual in character. The reviewed literature indicated that the correct variation of turbulent skin-friction drag coefficient with yaw angle has not been clearly defined; however, the principles of simple-sweep theory, as used in rotary-wing theory for instance, are far from correct. Figure 6 summarizes two likely variations of minimum section drag coefficient with yaw angle and illustrates a comparison to the independence principle as used in present-day rotary-wing theory.

Pressure Drag Below Stall

The experimental results of Reference 14 permit a comparison of theory to drag data for a 45-degree swept wing spanning a rectangular wind tunnel and to drag data for an unswept-wing. The data were corrected for image (tunnel-wall) effects and indicated that the central half of the wing closely simulated the two-dimensional or infinite-wing conditions. The total drag (skin-friction and pressure components) was measured by a wake-rake method and was presented in the wind-axis (parallel to free stream) reference

system. To evaluate these data, the angle of attack of the yawed wing presented in the wind-axis system (α_Λ) was transferred into an angle of attack measured perpendicular to the span axis (α), by:

$$\alpha = \frac{\alpha_\Lambda}{\cos\Lambda}$$

The total drag coefficient measured parallel to the free stream versus angle of attack measured perpendicular to the span axis is shown in Figure 7. The airfoil tested was an NACA 63_1-012 (symmetrical) section and, as noted by Figure 7, was of the laminar-flow type embodied with a "drag bucket" around the design lift coefficient of 0.0.

Since the total drag contains the skin-friction component, a component which is expected to vary with yaw angle quite differently from the pressure drag, a comparison of theory to experiment in the normal drag polar form of Figure 7 would be quite misleading. By assuming that the skin friction does not vary with angle of attack, however, the total drag may be plotted against α^2, and the slope of this data should vary as $\cos^3\Lambda$ as developed in Reference 12. In fact, as shown in Figure 8, the agreement between theory and experiment is excellent. It is concluded that present classical blade-element analysis utilizing the simple sweep theory should provide a close approximation to airfoil pressure drag.

Pressure Drag Above Stall

As noted in Reference 11, stalled infinite yawed wing test data are unavailable. An attempt to synthesize two-dimensional data from the yawed finite wing tests of Reference 13 is presented in Reference 11. The results of this synthesis are shown in Figure 9, where drag coefficient (based on the normal velocity and force normal to the span axis) is plotted against angle of attack (measured in a plane normal to the span axis). This figure is presented to examine the use of the independence principle in determining pressure drag above stall. To the first approximation (yaw angles up to 45 degrees), the yawed infinite wing appears to stall in a manner similar to the unyawed two-dimensional wing. In view of the conclusions regarding the effect of yaw on maximum lift coefficient (Figures 3 and 4), a situation of pseudo-

boundary-layer control on lift exists, but with a massive drag penalty. In other words, the independence principle is invalid for calculations of maximum lift coefficient but is a good approximation for pressure drag due to stall.

In all of the work that has followed from Reference 11, no clear explanation of this apparent inconsistency has been forthcoming.

RECENT STUDIES

Since submitting Reference 12 for publication, a theoretical evaluation of the effect on rotor performance of lift coefficient - angle of attack trends with yaw angle suggested by Figure 3 (or 4) has been made with comparisons to experimental results [9]. In addition, the experimental measurements of minimum rotor drag as a function of advance ratio[10] has illuminated the effects of yaw on skin friction drag. The following paragraphs report this progress.

Blade Stall Delay from Spanwise Flow

In the experimental evaluation [9] of a model rotor capable of providing large propulsive force at an advance ratio of .6, the rotor model was tested in a conventional configuration for comparative purposes. In this configuration it had a radius of 4 feet, constant chord of 6 inches, three blades, a solidity of .119, root cutout of 19 percent, and a twist of zero degrees. The tests were conducted at a tip speed of 252 ft/sec and tunnel speed of 151 ft/sec. With fixed collective pitch, the shaft angle was raised from a nose down position at which the thrust was nearly zero, up to a point at which the large flapping caused droop stop contact. The longitudinal cyclic varied from 6 degree to 14 degree forward, but the lateral cyclic was held zero.

A summary of the experimental data to which the theoretical results are to be compared is shown in Figure 10. The variation of rotor thrust, profile plus induced power, and total power coefficients with control axis angle (shaft angle plus longitudinal cyclic) at constant collective pitch

presented in Figure 10 clearly illustrates the inconsistency in the descriptive words "Blade Stall". It is worth a minute to recall from the fixed wing aerodynamicist the thought that stall is in fact a response to boundary layer separation and that visibility of this boundary layer separation is most widely publicized with curves of airfoil lift and drag coefficients versus angle of attack. These barometers of the state of the boundary layer always show a maximum lift coefficient and increase in airfoil drag as "stall" occurs. The rotary wing aerodynamicist, although familiar with this classical stall background, must determine what the "response to boundary layer separation" is for a rotor. In short, "blade stall" has today the connotation of blade lift loss and drag rise; Figure 10 indicates that a "lift stall" did not occur. The profile plus induced power coefficient indicates a drag stall did occur.

The profile plus induced power coefficient was obtained by subtracting the experimental parasite power (hub tares removed) from the experimental total power coefficient by the energy equation below:

$$\frac{C_{P_i}}{\sigma} + \frac{C_{P_o}}{\sigma} = \frac{C_P}{\sigma} - \frac{V}{\Omega R}\,\frac{C_X}{\sigma} \qquad \text{Eq. (1)}$$

The parameter $\frac{C_{P_i}}{\sigma} + \frac{C_{P_o}}{\sigma}$ provides a barometer of rotor stall with respect to airfoil drag rise and indicates that rotor thrust in excess of C_T/σ equal to .06 or .07 was obtained rather inefficiently.

The parallel of this rotor characteristic - lift but with a severe power penalty - to the previously discussed yawed wing data is very strong. To provide theoretical comparisons to the experimental data accounting for a yawed flow effect, the two-dimensional airfoil data (normally a function of only angle of attack and Mach number) was given the yaw angle variable to increase lift coefficient by the percentage changes over zero yaw angle data as provided by Figure 3. The airfoil drag properties were not changed. The rotor performance analysis[18] used has the usual non-uniform downwash, no small angle assumptions, etc. refinements over classical theory. The analysis was conducted by matching theoretically, the experimental thrust value at the measured shaft angle and longitudinal cyclic. The agreement between experimental and calculated power coefficients was then reviewed. Since the

lowest collective pitch data was most indicative of the stall problem (low total power because only a small amount of propulsive force is being produced), the collective pitch equals 16 degrees experimental results is to be examined in detail.

Figure 11 illustrates the total power theoretical comparison with no yaw effect on airfoil lift characteristics, then with the lift coefficient improvement suggested by Figure 3, and finally, with a complete unstalled characteristic. The same comparison to the induced plus profile power is presented in Figure 12. Although the airfoil drag characteristics as a function of angle of attack and Mach number remained the same for the three lift characteristics examined. the differences in lift characteristics alter the blade motion and hence the angle of attack distribution within the rotor disc. This alteration to local angle of attack redistributes and lowers principally the profile power, since the thrust and, therefore the induced power, is approximately the same at any given control axis angle. Although the effect of yaw significantly contributes to a delay in stall power rise, the theoretical trend is not satisfactory. A key, provided by Figure 12, is the more reasonable agreement obtained with the assumption of a complete unstalled lift characteristic.

A disagreement in correlation occurs, however, on review of the total power comparison shown in Figure 11 when the assumption is a complete unstalled lift characteristic. Herein lies the importance of accurate knowledge of the translation of two-dimensional airfoil lift properties into the three-dimensional rotor performance problem. Because the total power is less than the induced plus profile power, a component of accelerating torque (in the autogyro sense) is provided from the local blade element lift. After the lift coefficient contributes to a reasonable flapping motion, its orientation relative to the shaft plane by the inflow angle is extremely important to the total power solution.

The importance of section lift coefficient and inflow angle is illustrated in Figure 13 with details of the blade element environment at the .782 radius station, 270 degree blade azimuth position for the $C_T/\sigma = .143$.

α_{CA} = -8.5 degree point. The elemental lift shown in Figure 13 provides a component of force that at its radius station will reduce the rotor torque required; in effect offsetting the elemental drag. Any increment, therefore, in lift coefficient above standard two-dimensional C - α trends in the region of the disc where the inflow angle is positive will reduce the total power coefficient. Before summarizing a plausible interruption of the blade stall phenomena, the effect of spanwise flow on minimum rotor drag will be discussed.

Minimum Rotor Drag with Advance Ratio

Experimental model rotor minimum drag data[10] has provided an improved guide to the effects of spanwise flow on this important rotor performance parameter. As suggested in Reference 12, spanwise flow could easily be mistaken for aircraft equivalent parasite drag area or minimum airfoil drag coefficient if the classical theoretical approach to calculating this rotor performance were used. The trend of drag with rotor solidity would provide incorrect visibility and Reference 12 therefore suggested that the "bookkeeping" be revised to account for radial flow. A suggestion of refinement now appears possible.

Following definition of the coordinate system in which the spanwise flow problem should be approximated (shown in comparison to the classical coordinate system in Figure 14), the requirement to define the variation of minimum drag coefficient with yaw angle was satisfied in Reference 12 by

$$C_{d_\Lambda} = C_{d_o} \cos^{-\frac{1}{5}} \Lambda \qquad \text{Eq (2)}$$

The approximate effect of spanwise flow on rotor H force, torque, and profile power coefficients was then presented. In view of the recent experimental results, not varying minimum airfoil drag coefficient with yaw angle would appear more correct, i.e.

$$C_{d_\Lambda} = C_{d_o} \qquad \text{Eq (3)}$$

The variation of experimental minimum rotor drag coefficient, $D_E/qd^2\sigma$, is shown versus advance ratio in Figure 15. Comparisons of classical theory and radial flow to this test data is also shown. The model blades (three) had a

twist of -3 degrees, solidity of .085, a root cutout of 16 percent, and a radius of approximately 4 feet. The test was conducted at an advancing tip Mach number of .7 except for $\mu = 1.0$ which, because of the 180 knot tunnel speed limitation, was .542. By varying shaft angle at constant 4 degrees collective pitch, data of rotor drag versus lift was obtained from which the minimum rotor drag data has been extracted. Despite the fact that the drag to be measured is small and hub tares must be removed to obtain the desired "blades alone" drag, the data scatter is not too great.

The theoretical development leading to a calculated minimum rotor drag coefficient outlined in Reference 12 was followed with the following revised assumptions:

1. Section drag coefficient in reverse flow is twice that in normal flow
2. Blade begins at 16 percent radius station
3. $C_{d_\Lambda} = C_{d_o}$
4. Incompressible

The comparisons of classical theory and radial flow theory to experiment is presented in Figure 15. The value of C_{d_o} used, .0085, was obtained from zero lift, hover power measurements. The agreement of the radial flow theory appears satisfactory, except for $\mu > .7$. The point worth noting is that agreement from the classical theory would be achieved by increasing C_{do} to approximately .011 which really is not justified in view of the hover power measurements.

The agreement of either theory for advance ratios greater than .7 is less than satisfactory and appears to be tied to the assumption of the C_{d_o} in reverse flow being twice that in normal flow. Jenny[19] addressed himself to the calculation of minimum rotor drag and indicated the sensitivity of rotor drag to this assumption for advance ratios greater than one.

AN INTERPRETATION OF BLADE STALL

With the completion of this follow-on work to the publishing of

Reference 12, the contributions made by many others to the studies of non-uniform downwash and unsteady aerodynamics as well as contributions to the study of radial flow, an interpretation of blade stall based upon the integration of what is known might provide insight to future analytical and experimental programs. What appears most conclusive from the studies to date is that no one refinement to our theory (such as blade elasticity on non-uniform downwash) provides the correlation necessary to unwavering confidence in our analytical capability. Although no power computations are presented for the effect of unsteady aerodynamics, a lift hysteresis effect on the two-dimensional airfoil data has been submitted [20] which will delay stall - provided the angle of attack is increasing with time. This unsteady aerodynamic behavior is illustrated in Figure 16, and indicates a capability of the airfoil to achieve a 50 percent improvement in maximum lift coefficient during the positive rate portion of the angle of attack cycle. During the negative rate portion of the cycle - which the rotor blade experiences - extremely low maximum section lift would be expected, but this is not experimentally born out as shown by either Figure 1 or 10. In view of the angle of attack and yaw angle distributions in the rotor disc, a blade stall interpretation gathering in both spanwise flow and unsteady aerodynamics appears quite plausible.

The non-uniform downwash computed, angle of attack contours in the rotor disc are shown in Figure 17, for the most severe, experimentally achieved, rotor thrust of $C_T/\sigma = .142$, $\alpha_{CA} = -8.5$ degrees. The computation was made assuming unstalled airfoil lift characteristics. The additional interpretative data of lines of constant local yaw angle and the region of negative rate of change of local angle of attack are shown in Figure 18. With respect to the local yaw angle data shown in the upper half of Figure 18, the spanwise flow mechanism leading to the increased lift coefficients illustrated by Figure 3 may be expected to substantially reduce the region of the disc involved in "lift stall". This reduction in the "lift stall" region still leaves the area around the 270 degree azimuth position operating above some $C_{\ell_{max}}$ but perhaps this area will be seen to be reduced through favorable effects of pressure and force fields acting on the boundary layer.

Based on the analytical study of the laminar boundary layer flow on rotor blades in forward flight reported in Reference 21, the qualitative impression appears to be that radial flow including velocity, pressure, and force fields will delay separation. The third quadrant of the disc, 180 degrees to 270 degrees azimuth, however, is suspected of being less favorably effected by radial flow than the fourth quadrant. The fact that the third quadrant may not have as much lift augumentation as the fourth quadrant should not be an over-riding consideration, however, because this region is characterized by a positive time rate of change in angle of attack.

It seems to me, therefore, that when the blade is in the up wind azimuth region, say from 180 to 270 degrees, any indecision about the benefits of radial flow providing lift augmentation should be replaced by a positive decision due to favorable unsteady aerodynamic lift characteristics. In the downwind azimuth region from 270 degrees to 360 degrees, spanwise flow created from the velocity, pressure, and force fields are all acting favorably on the boundary layer to provide lift augmentation regardless of the unsteady aerodynamic characteristics. Complimenting each other in this way, the rotor cannot stall in the way suggested by two-dimensional C_ℓ - α airfoil data if in fact it stalls at all. Translating a two-dimensional airfoil $C_{\ell_{max}}$ into a three-dimensional rotor lift characteristic seems just plain wrong.

In view of the characteristic trends of yawed wing pressure drag with angle of attack, a translation of two-dimensional airfoil drag data versus angle of attack into the three-dimensional rotor environment in the manner practiced by the industry seems correct. In addition, the connotation of a characteristic two-dimensional stall angle of attack generally used in a discussion of blade stall could be associated with a drag rise of blade elements.

To quantitatively illustrate this interpretation of blade stall, a two-dimensional airfoil C_ℓ versus α characteristic crudely approximating the favorable effects of both spanwise flow and unsteady aerodynamics was given to the performance analysis for evaluation. The airfoil lift characteristic used is shown in Figure 19. The comparison to the experimental data pro-

vided by Figure 10 is shown in Figure 20 and 21. The agreement is very encouraging and indicates an improvement over conventional use of two-dimensional airfoil section lift properties in rotor performance studies.

CONCLUSIONS

In view of the progress to date, several significant conclusions are submitted.

1. Rotor lift stall does not occur. Complementing benefits from spanwise flow and unsteady aerodynamics occur during the translation of two-dimensional airfoil lift characteristics into the three-dimensional rotor environment.

2. The lift variation of the elements in the blade with angle of attack is perhaps, more closely approximated by $C_\ell = \frac{dC_\ell/d\alpha}{2} \sin 2\alpha$. The classical representation of $C_\ell = \frac{dC_\ell}{d\alpha}\,\alpha$ appears unduly optimistic while the refined "stall" characteristic derived from application of two-dimensional airfoil properties is very pessimistic.

3. The direct application of two-dimensional airfoil pressure drag characteristic arising with angle of attack to the classical blade element rotor analysis is substantially correct. Drags associated with stall and compressibility are included as pressure drag.

4. The classical blade element analysis utilizing the simple-sweep theory underestimates rotor power and drag components due to airfoil skin-friction drag. The resultant velocity at the blade element accounting for the local yaw angle should be used in this computation. No variation in section minimum drag coefficient with yaw angle should be assumed, i.e. $C_{d_\Lambda} = C_{d_o}$.

5. Study of the effect of spanwise flow in the reverse flow region remains a challenging technical task.

REFERENCES

1. Sikorsky, I.A., "Correlation of Helicopter Performance Equations", IAS Preprint No. 694, January 1957.

2. Bennett, J.A.J., "Horizontal Flight"....Part III of article "Rotary-Wing Aircraft" - Aircraft Engineering, Volume XII No. 133, March 1940.

3. Sweet, George E., Jenkins, Julian L. and Winston, Mathew M., "Wind Tunnel Measurements on a Lifting Rotor at High Thrust Coefficients and High Tip-Speed Ratios" NASA TND-2462, September 1964.

4. Jenkins, Julian L., "Wind Tunnel Investigation of a Lifting Rotor Operating at Tip-Speed Ratios from 0.65 to 1.45".

5. Sweet, George E., and Jenkins, Julian L., "Results of Wind-Tunnel Measurements on a Helicopter Operating at Extreme Thrust Coefficients and High Tip-Speed Ratios". Journal of the American Helicopter Society, Volume 8, No. 3, July 1963, pp 4-9.

6. McCloud III, John L., and McCullough, George B., "Wind-Tunnel Tests of a Full-Scale Helicopter Rotor with Symmetrical and with Cambered Blade Sections at Advance Ratios from 0.3 to 0.4". NACA TN 4367, September 1958.

7. McCloud III, John L., and McCullough, George B., "Comparison of Calculated and Measured Stall Boundaries of a Helicopter Rotor at Advance Ratios from 0.3 to 0.4". NASA TND-73 September 1959.

8. Rabbott, John P.,"Comparison of Theoretical and Experimental Model Helicopter Rotor Performance in Forward Flight", Sikorsky Aircraft Division United Aircraft Corp, ASTIA, AD273332, July 1961.

9. Ekquist, D.G., "Design and Wind Tunnel Test of a Model Helicopter Rotor Having an Independently Movable Inboard Blade Panel", USAAVLABS Technical Report 65-63 August 1965.

10. Cenko, A., "Study of Rotor Performance and Behavior at High Advance Ratios", Boeing Report D8-0368, May 1966.

11. Harris, F.D., "Some Thoughts About Blade Stall", Boeing-Vertol Memorandum 8-7003-3-328, October 22, 1962.

12. Harris, F.D., "Preliminary Study of Radial Flow Effects on Rotor Blades" to be published in the July 1966 issue of the Journal of the American Helicopter Society.

13. Purser, Paul E., and Spearman, M. Leroy,"Wind-Tunnel Tests at Low Speed of Swept and Yawed Wings Having Various Plan Forms", NACA Technical Note 2445, December 1951.

14. Dannenberg, Robert E., "Measurements of Section Characteristics of a 45° Swept Wing Spanning a Rectangular Low-Speed Wind Tunnel as Affected by the Tunnel Walls", NACA Technical Note 2160, August 1950.

15. Cooke, J.C., "The Drag of Infinite Swept Wings", Royal Aircraft Establishment Technical Note No. Aero 2966, June 1964.

16. Ashkenas, Harry and Riddell, Frederick R., "Investigation of the Turbulent Boundary Layer on a Yawed Flat Plate", NACA Technical Note 3383, April 1955.

17. Ashkenas, Harry, "Turbulent Shearing Stress in the Boundary Layer of Yawed Flat Plates", NACA Technical Note 4140, April 1958.

18. Nice, G., "Standard Helicopter Performance Calculation Method", Boeing Report D8-0346, March 1966.

19. Jenny, David S., Arcidacono, Peter J., and Smith, Arthur F., "A Linearized Theory for the Estimation of Helicopter Rotor Characteristics at Advance Ratio Above 1.0", Presented at the Nineteenth Annual National Forum of the American Helicopter Society, May 1963.

20. Clarke, A.E., "Recent Work at the Royal Aircraft Establishment on Helicopter Dynamic Loads, with Particular Reference to High Incidence Problems", Presented at the VTOL Dynamic Loads Symposium Buffalo New York, June 1963.

21. Ho, T.L., "A Theoretical Study of Laminar Boundary Layer Flow on Rotor Blades", Boeing-Vertol Division Aero Investigation III-275, September 1965.

22. Abbott, Ira H., von Doenhoff, Albert E., and Stivers, Louis S., Jr., "Summary of Airfoil Data", NACA Technical Report 824, 5 March 1945.

23. Harris, F.D., "Adaptation of Radial Flow Effects Subrouting to Present Non-Uniform Downwash Computer Programs", Vertol Interoffice Memorandum 8-74003-1-094 June 1965.

The help in the preparation of this paper of both the Rotor Systems and Aerodynamic Research Staffs and particularly A. Cenko is gratefully acknowledged.

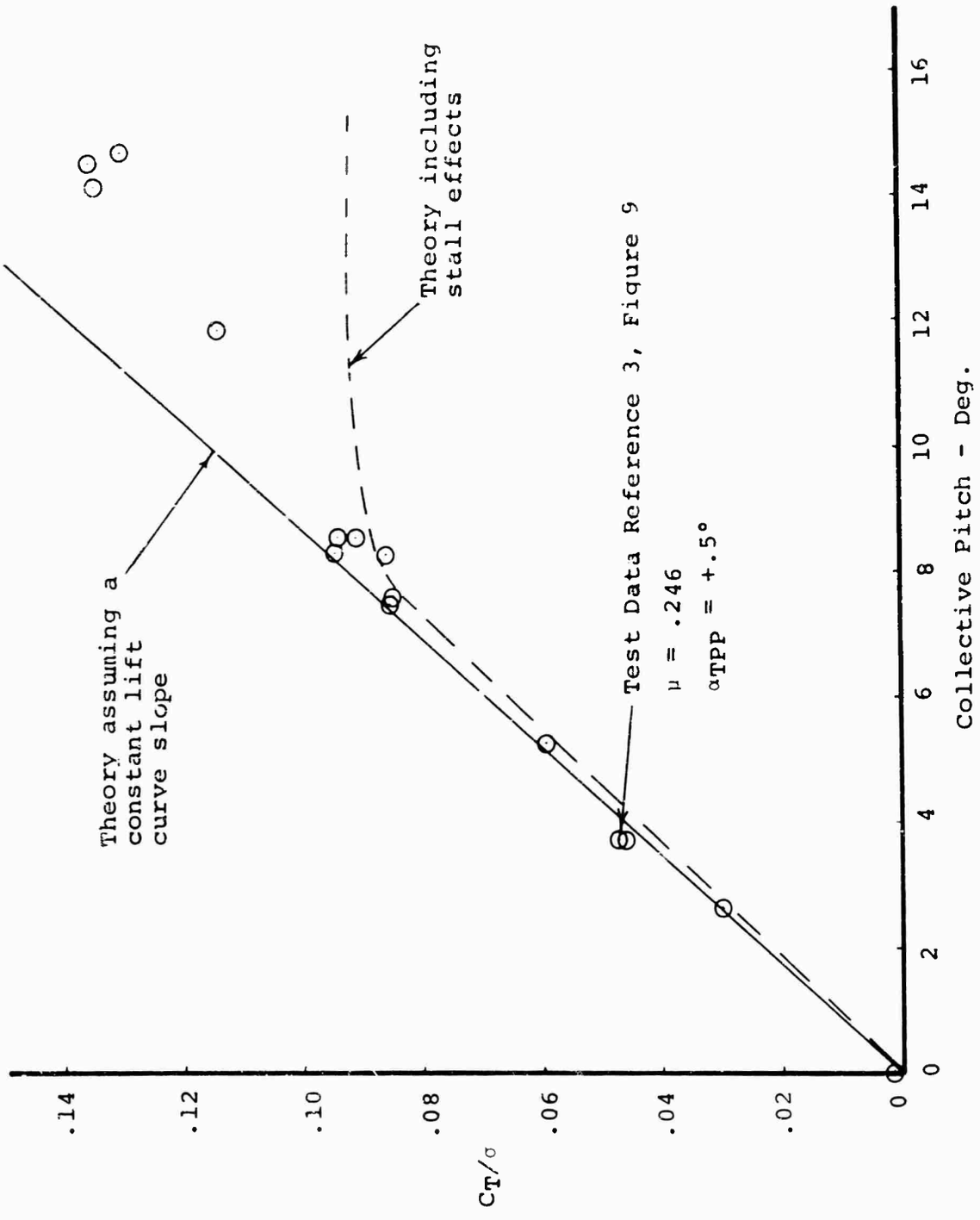

FIGURE 1 ROTOR LIFT CHARACTERISTICS THROUGH STALL.

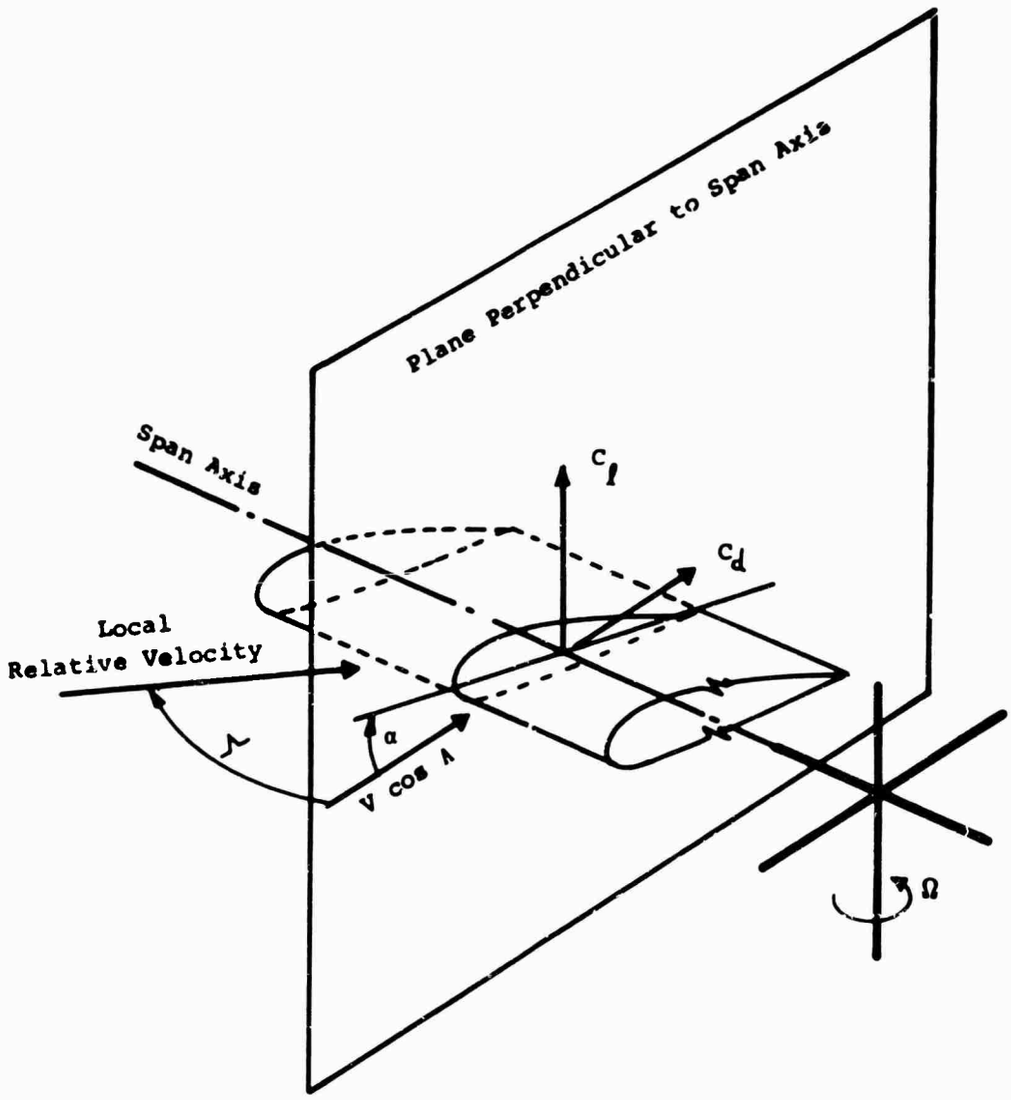

FIGURE 2 CLASSICAL BLADE-ELEMENT THEORY; EMBODIES INDEPENDENCE PRINCIPLE

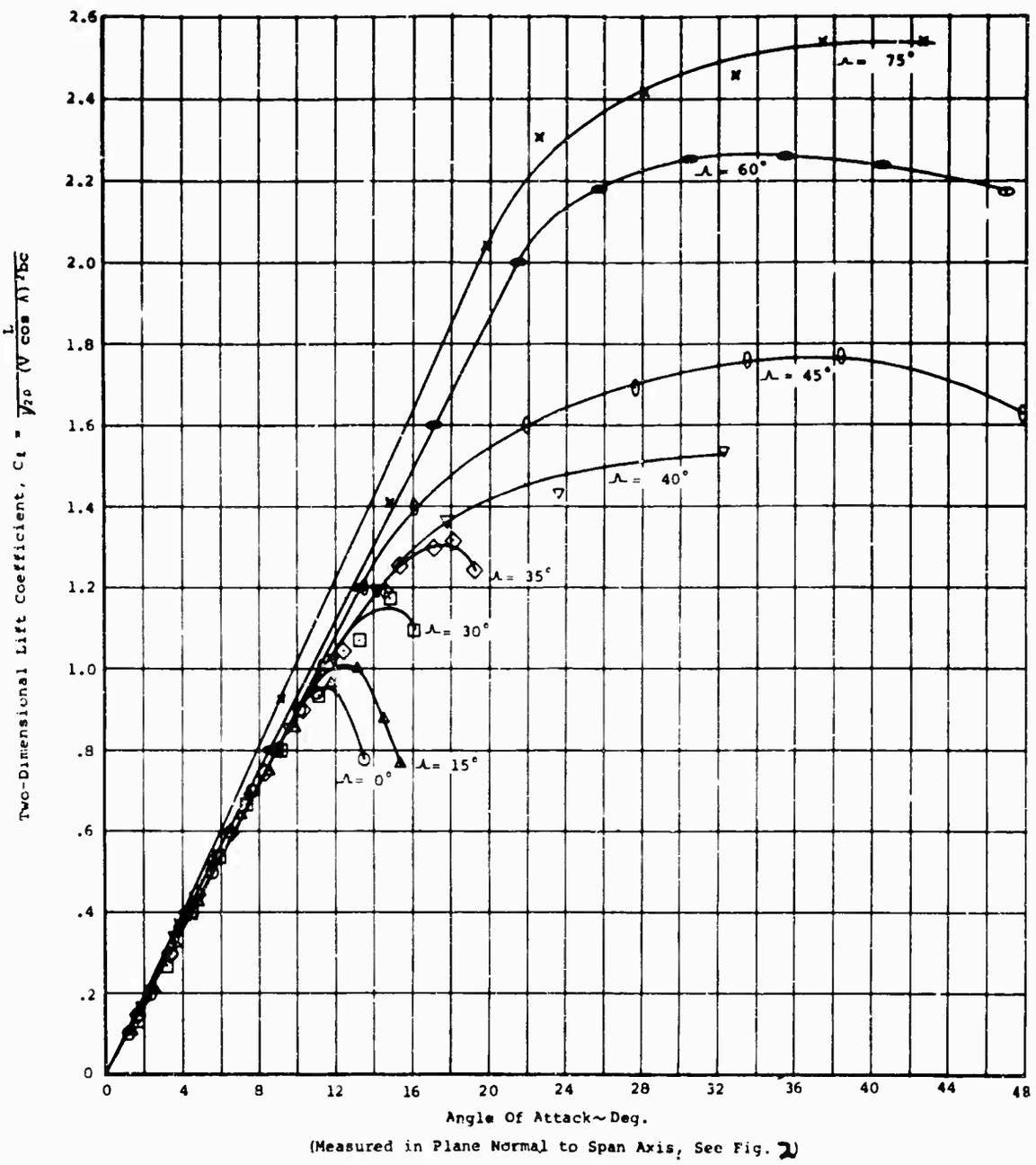

FIGURE 3 EFFECT OF YAW ANGLE ON SECTION LIFT COEFFICIENT (REFERENCE 13 DATA)

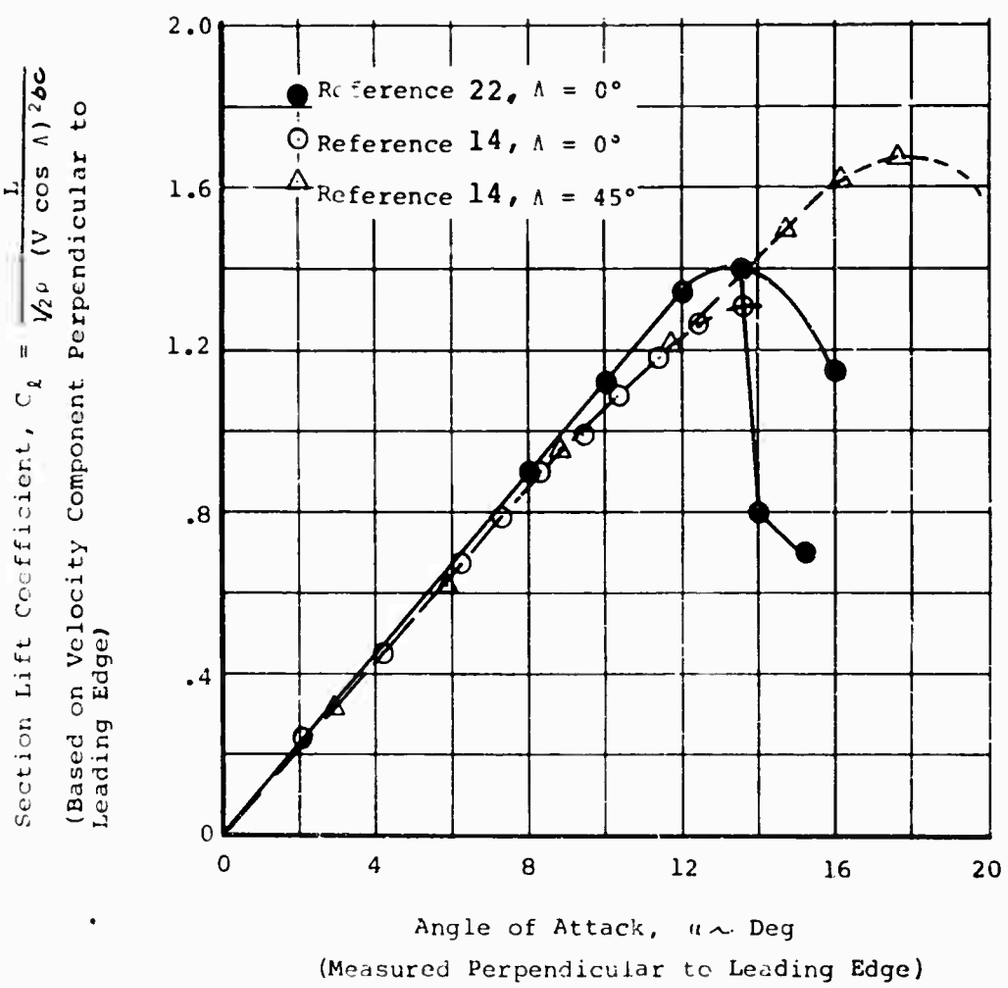

FIGURE 4 EFFECT OF YAW ANGLE ON SECTION LIFT COEFFICIENT (REFERENCE 14 DATA)

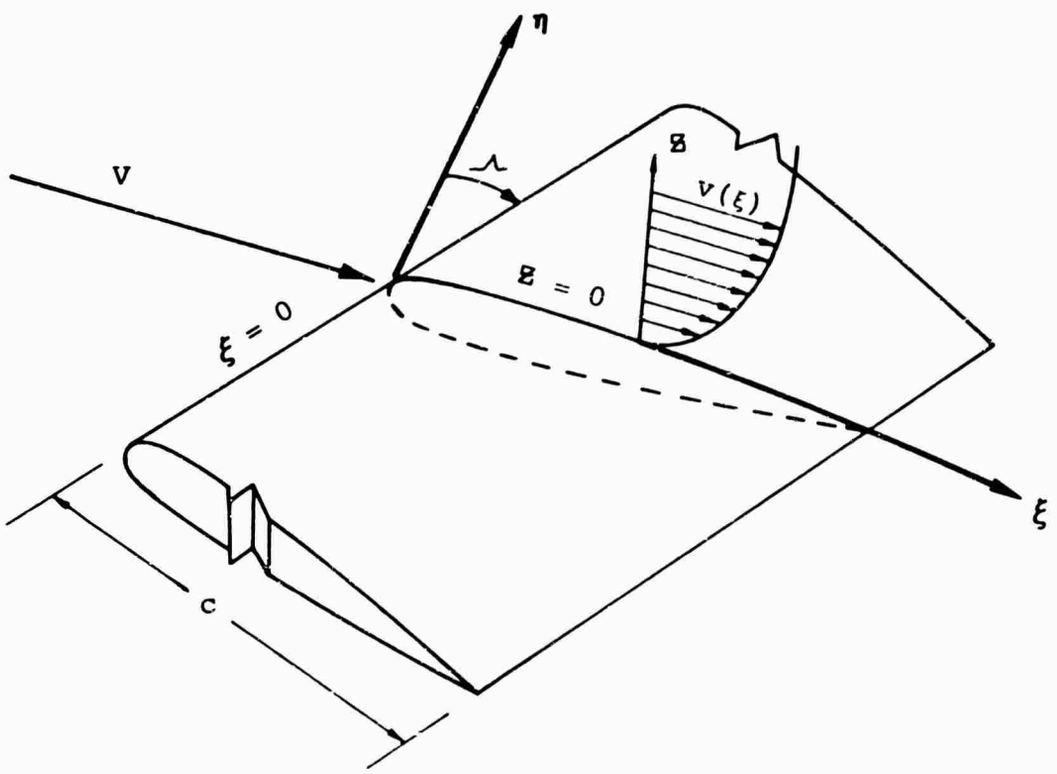

FIGURE 5 TURBULENT-BOUNDARY-LAYER COORDINATE SYSTEM FOR YAWED INFINITE WING

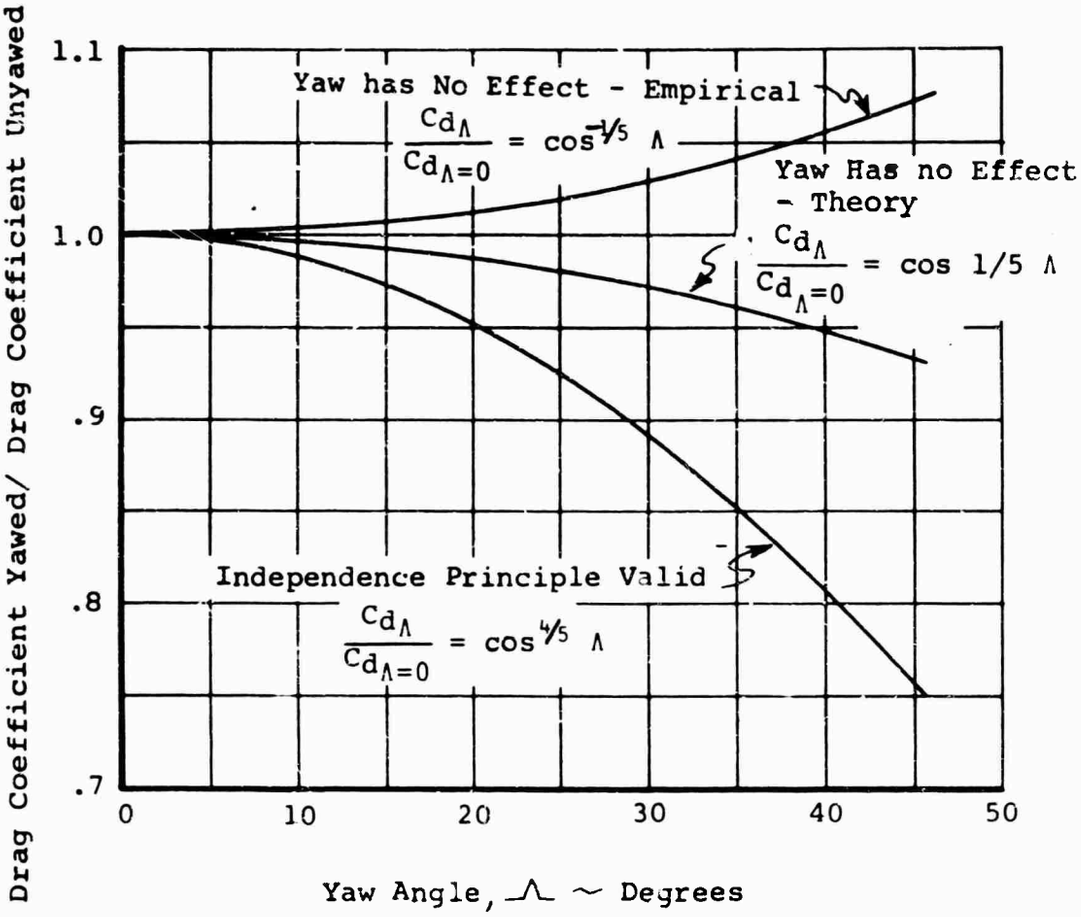

FIGURE 6 RATIO OF YAWED FLAT-PLATE DRAG TO UNYAWED DRAG; FULLY TURBULENT BOUNDARY LAYER

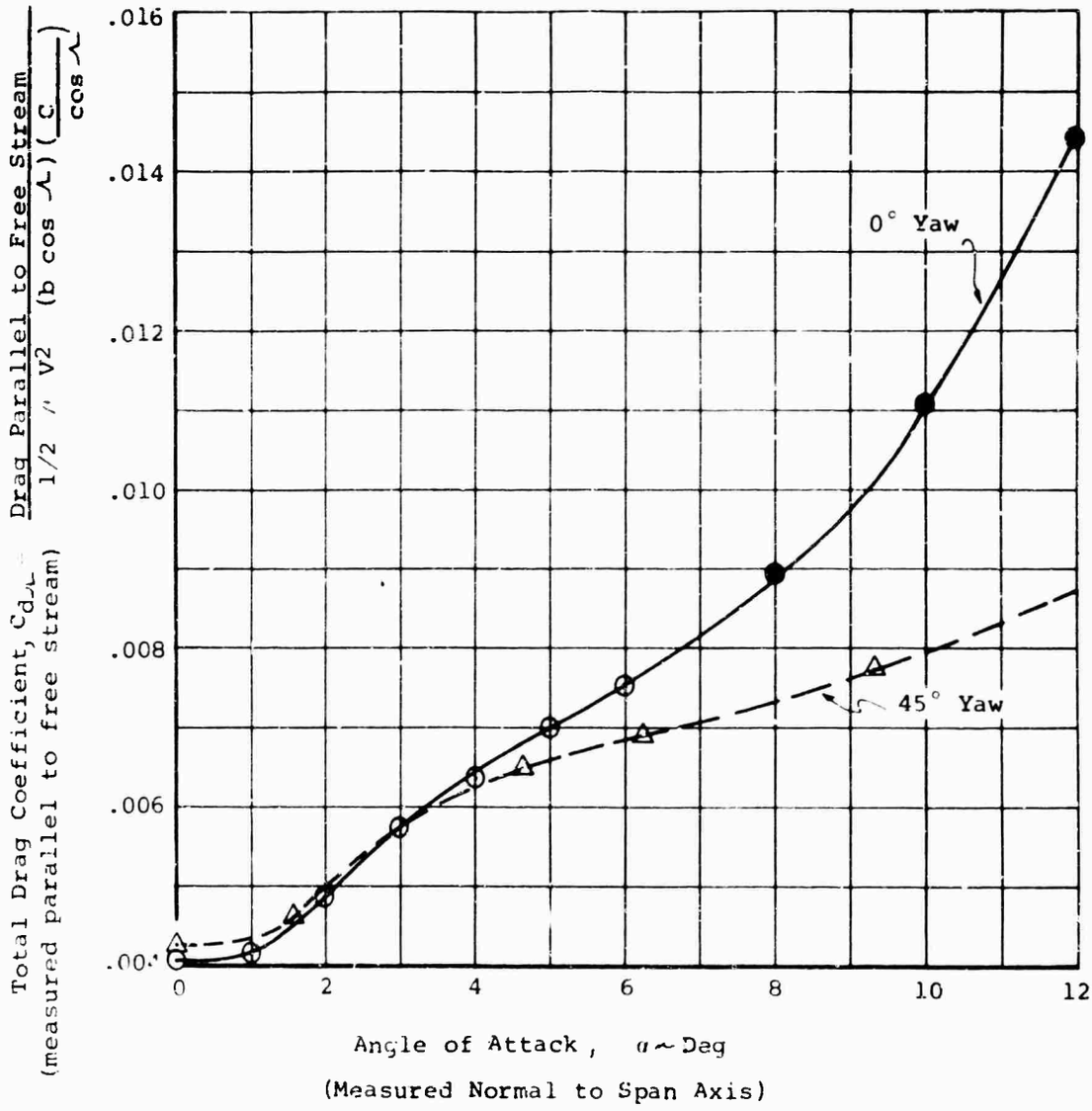

FIGURE 7 TOTAL SECTION DRAG COEFFICIENT VERSUS ANGLE OF ATTACK FOR 0-DEGREE AND 45-DEGREE YAW ANGLE

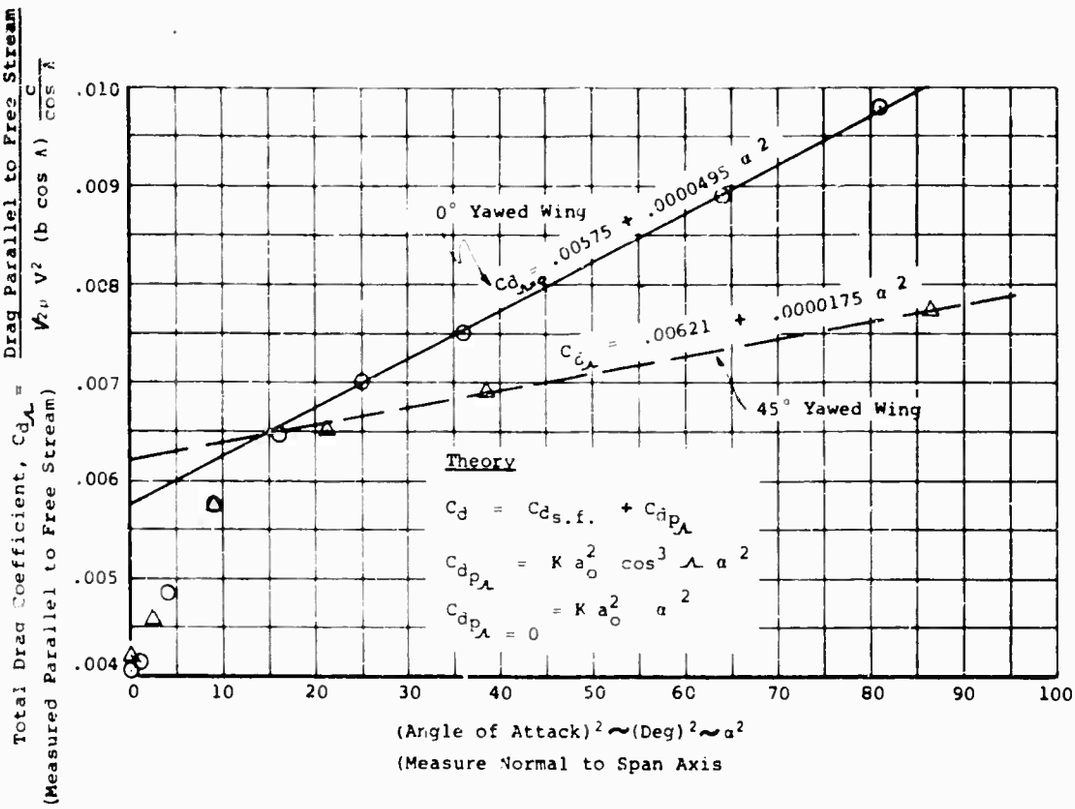

FIGURE 8 COMPARISON OF THEORY TO EXPERIMENT FOR THE SECTION PRESSURE DRAG

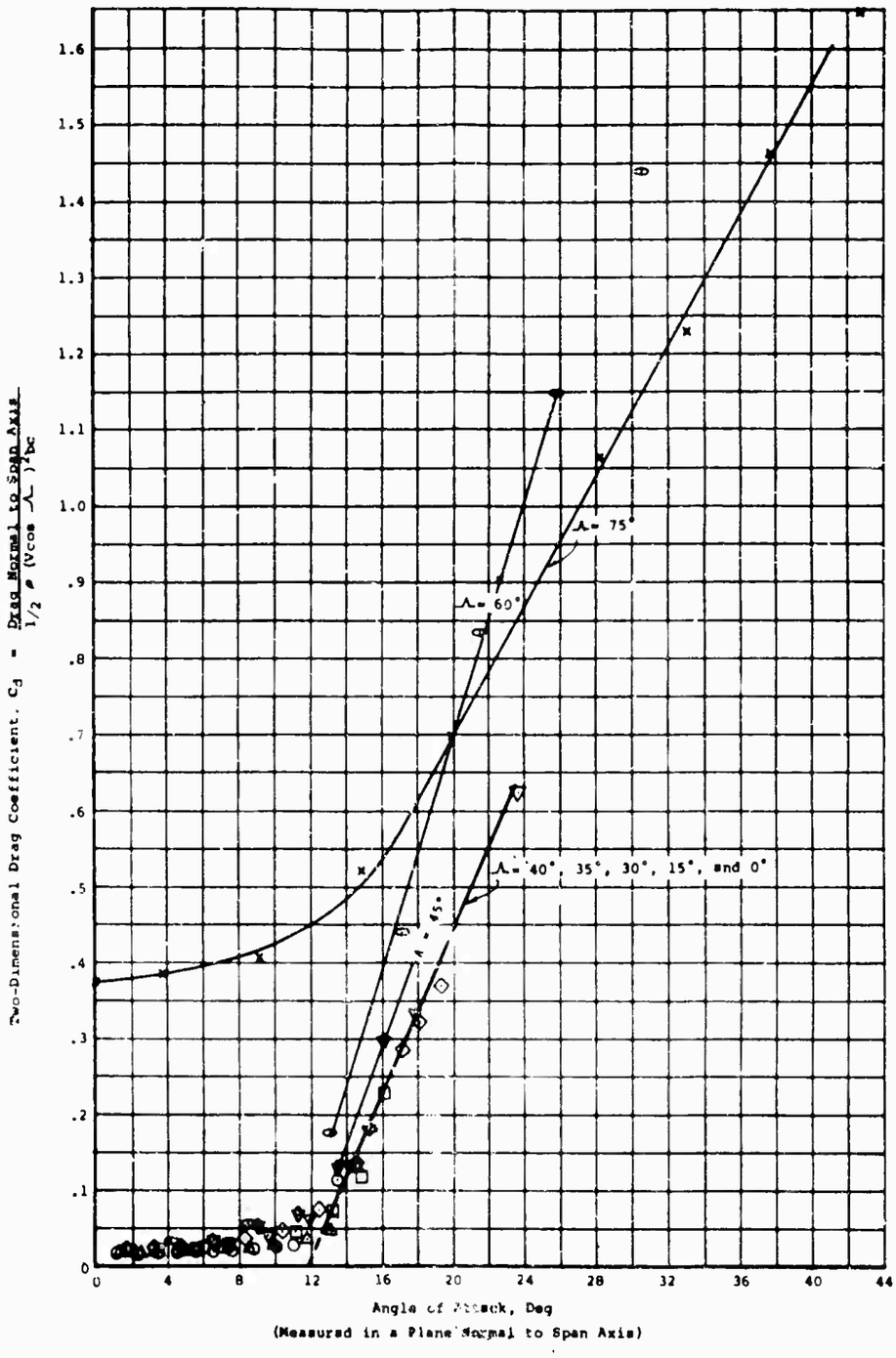

FIGURE 9 EFFECT OF STALL ON SECTION DRAG COEFFICIENT FOR SEVERAL YAW ANGLES

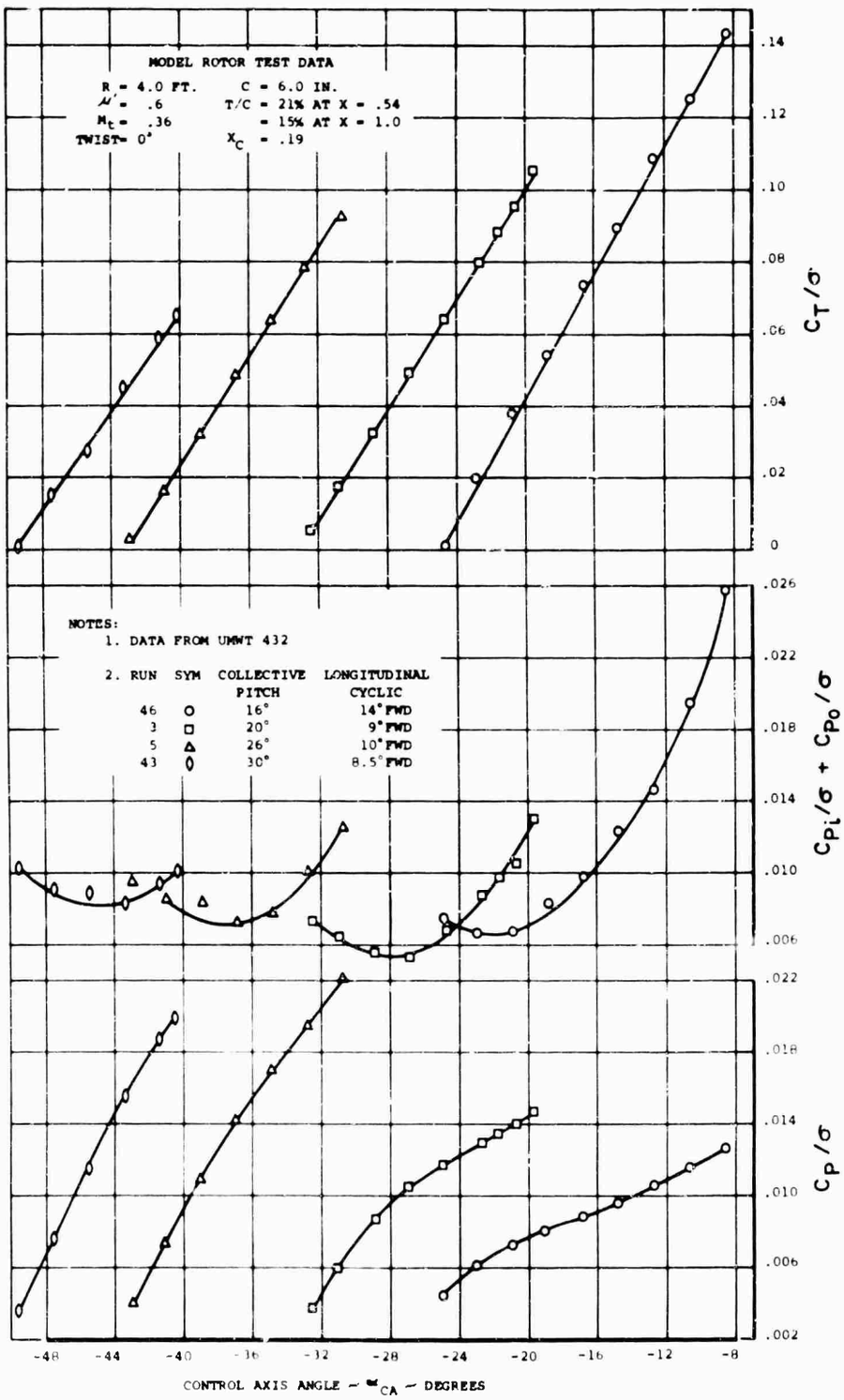

FIGURE 10 MODEL EXPERIMENTAL RESULTS

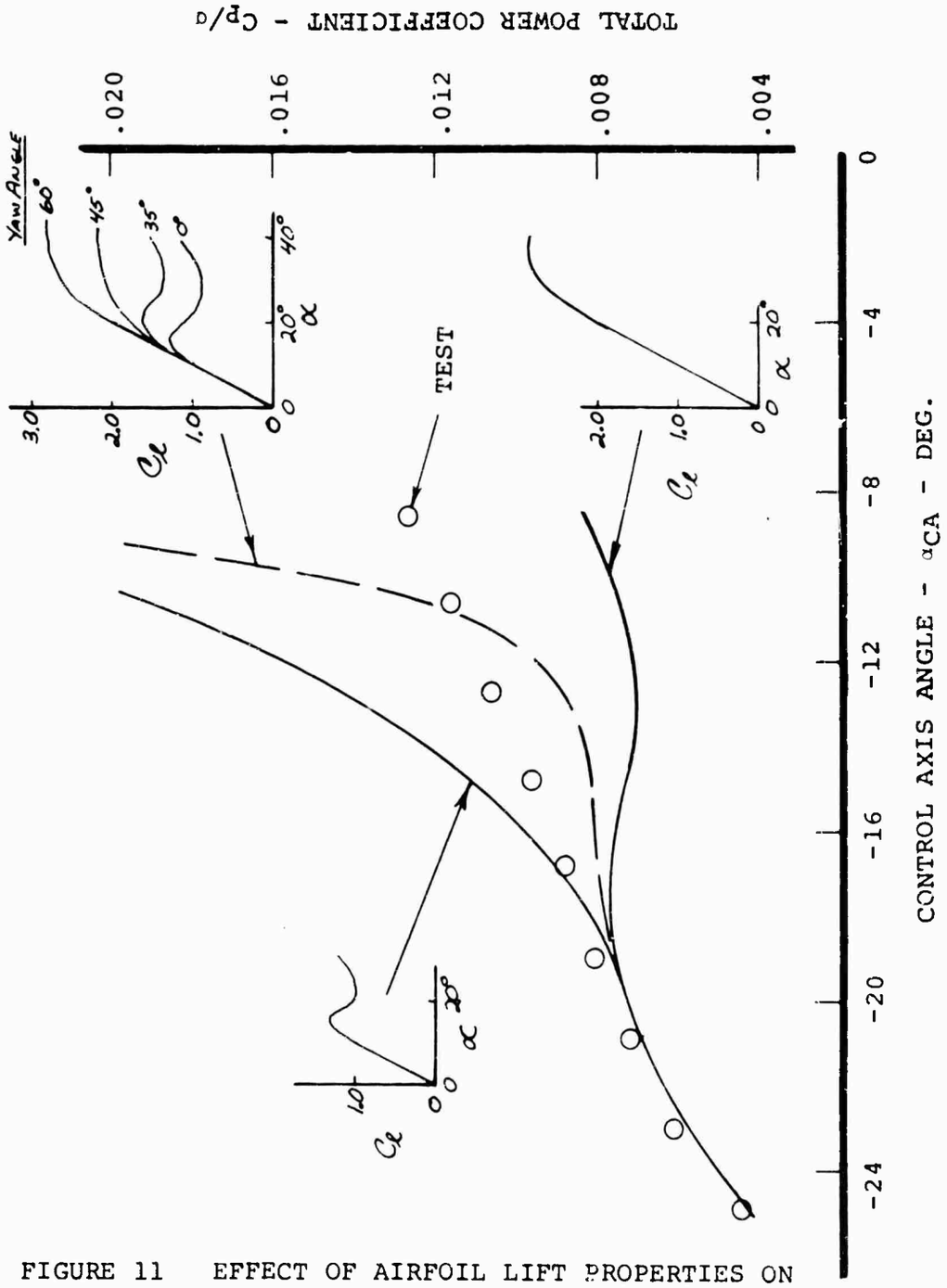

FIGURE 11 EFFECT OF AIRFOIL LIFT PROPERTIES ON TOTAL ROTOR POWER.

FIGURE 12 EFFECT OF AIRFOIL LIFT PROPERTIES ON INDUCED PLUS PROFILE POWERS.

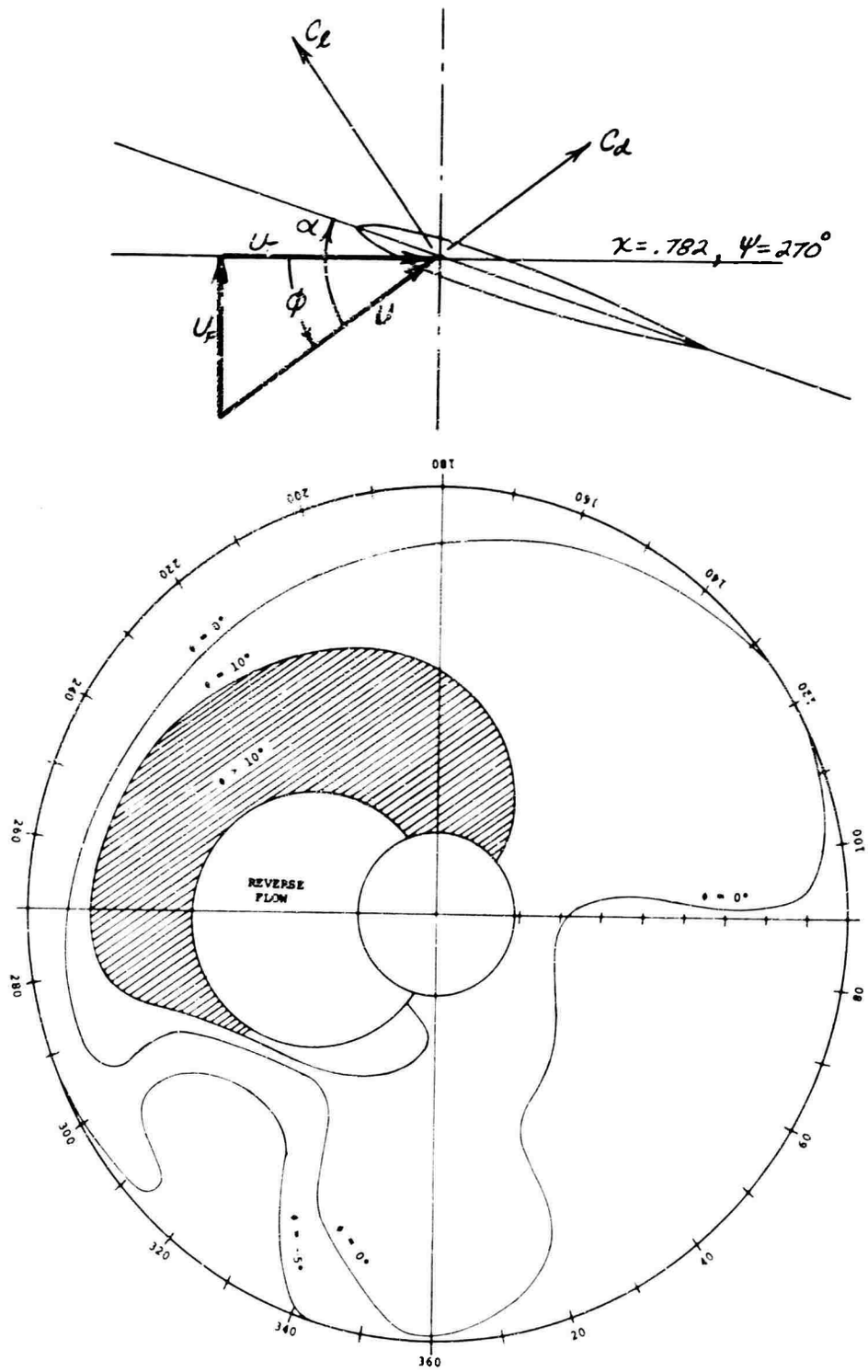

FIGURE 13 INFLOW ANGLE CONTOUR

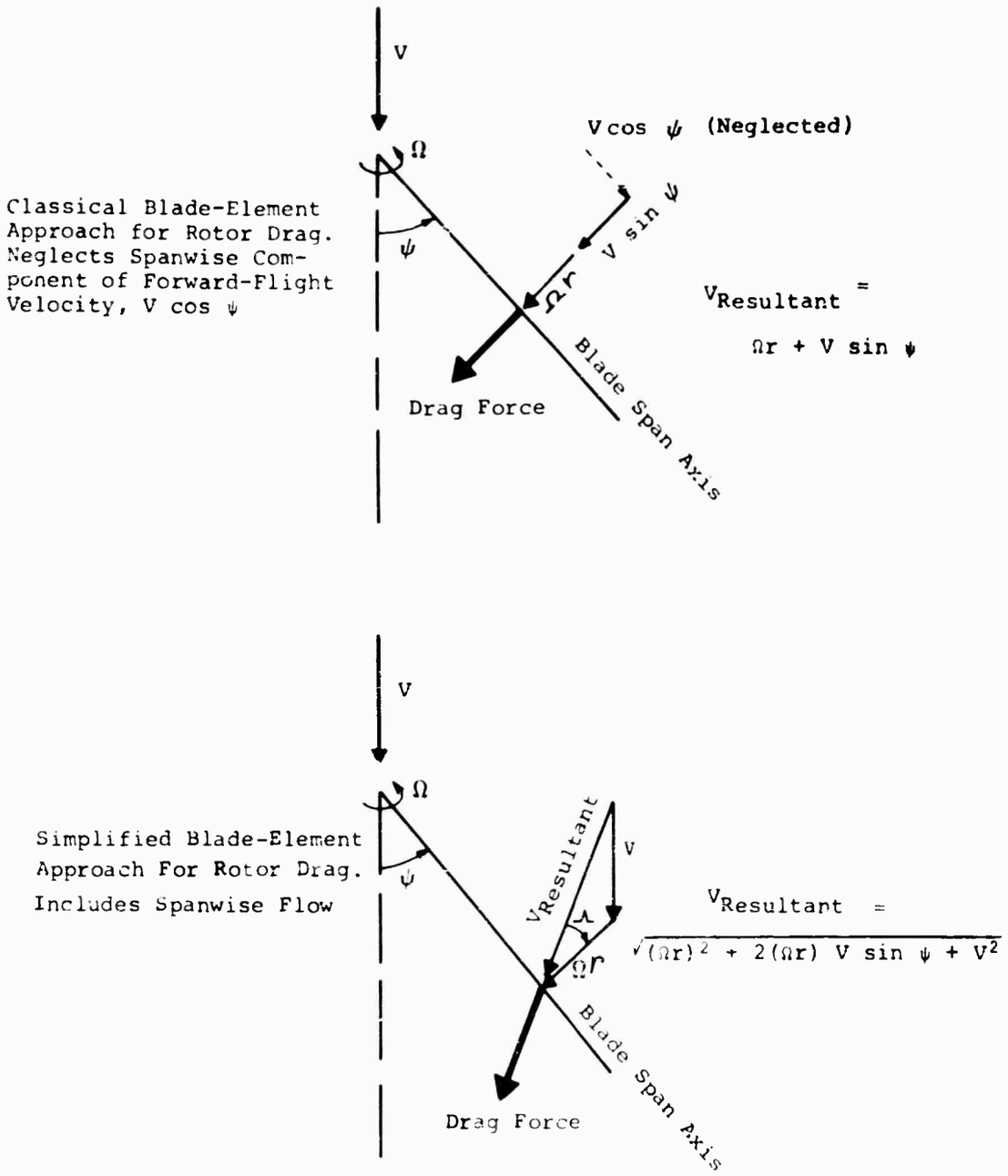

FIGURE 14 COMPARISON OF BLADE-ELEMENT THEORIES WITH AND WITHOUT SPANWISE (RADIAL) FLOW; SKIN-FRICTION DRAG

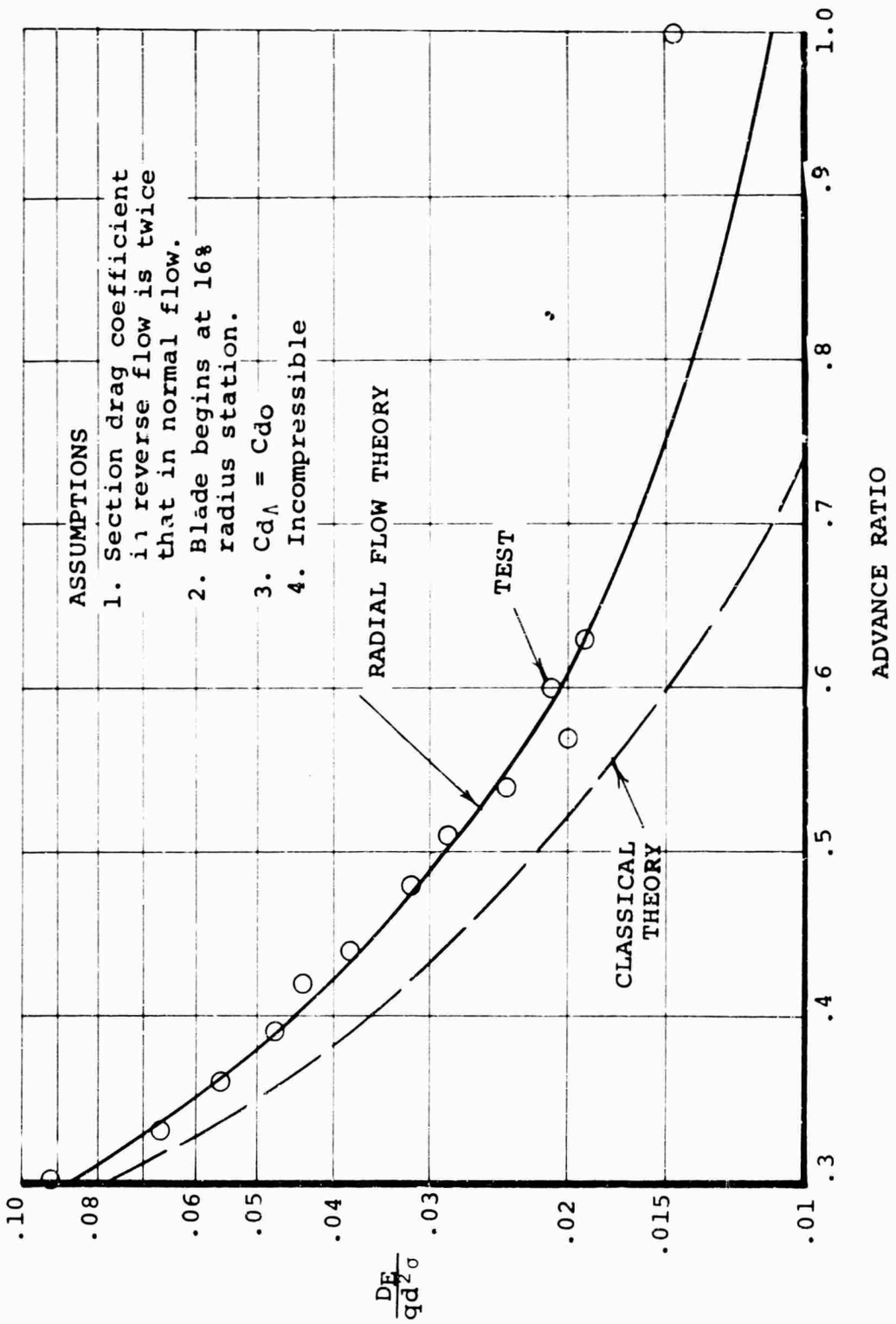

FIGURE 15 - MINIMUM ROTOR DRAG VS ADVANCE RATIO

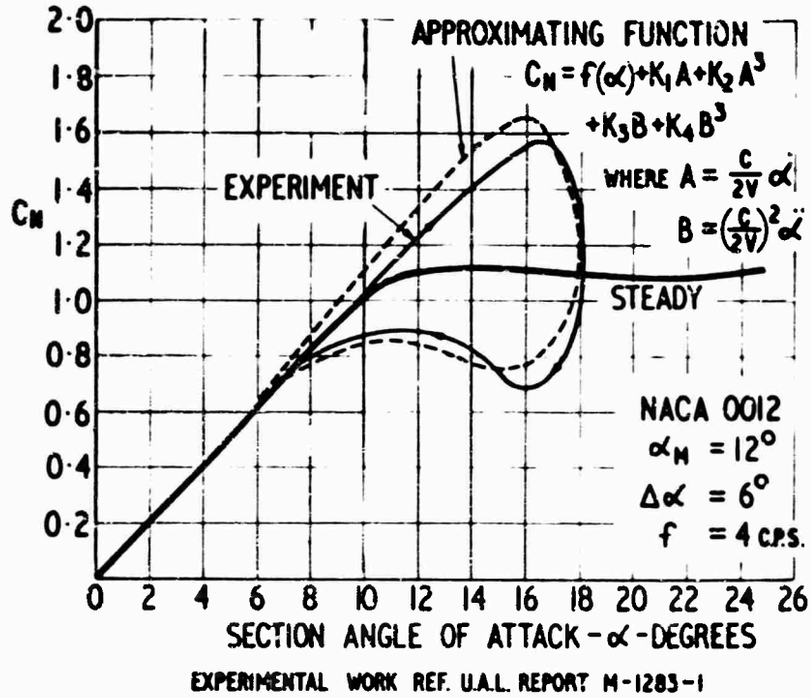

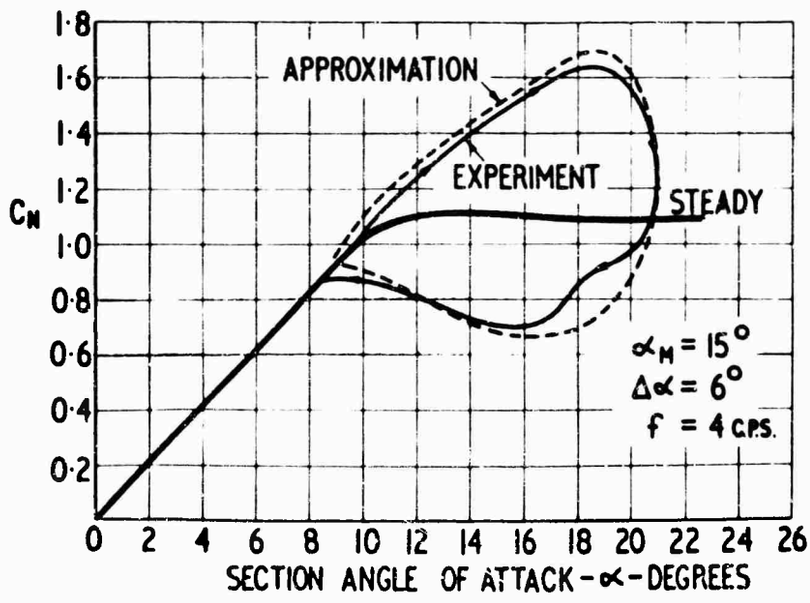

LIFT HYSTERESIS FROM PITCH OSCILLATIONS

FIGURE 16

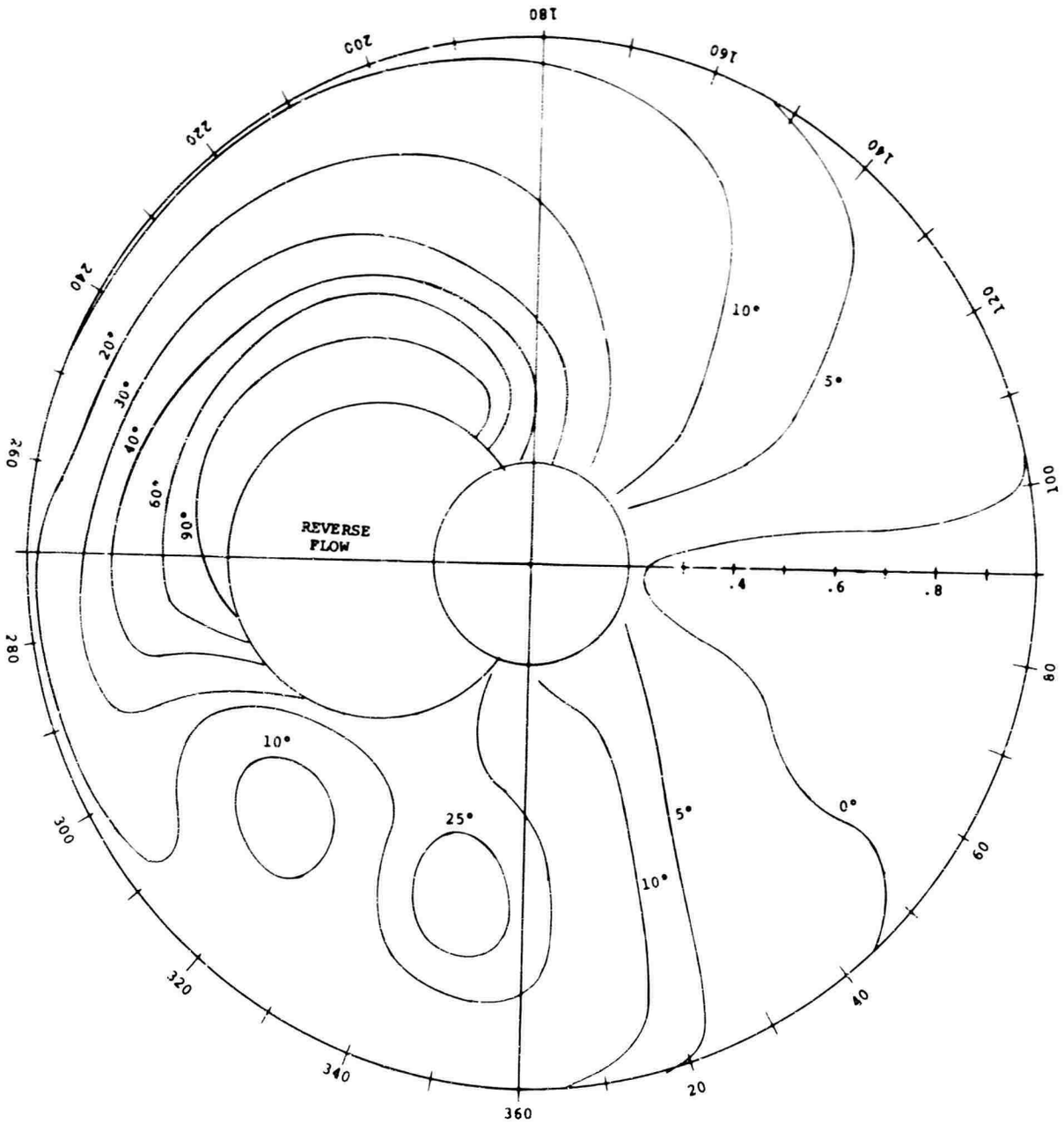

$C_T/\sigma = .142$

$\alpha_{CA} = -8.5°$

FIGURE 17 ANGLE OF ATTACK CONTOUR

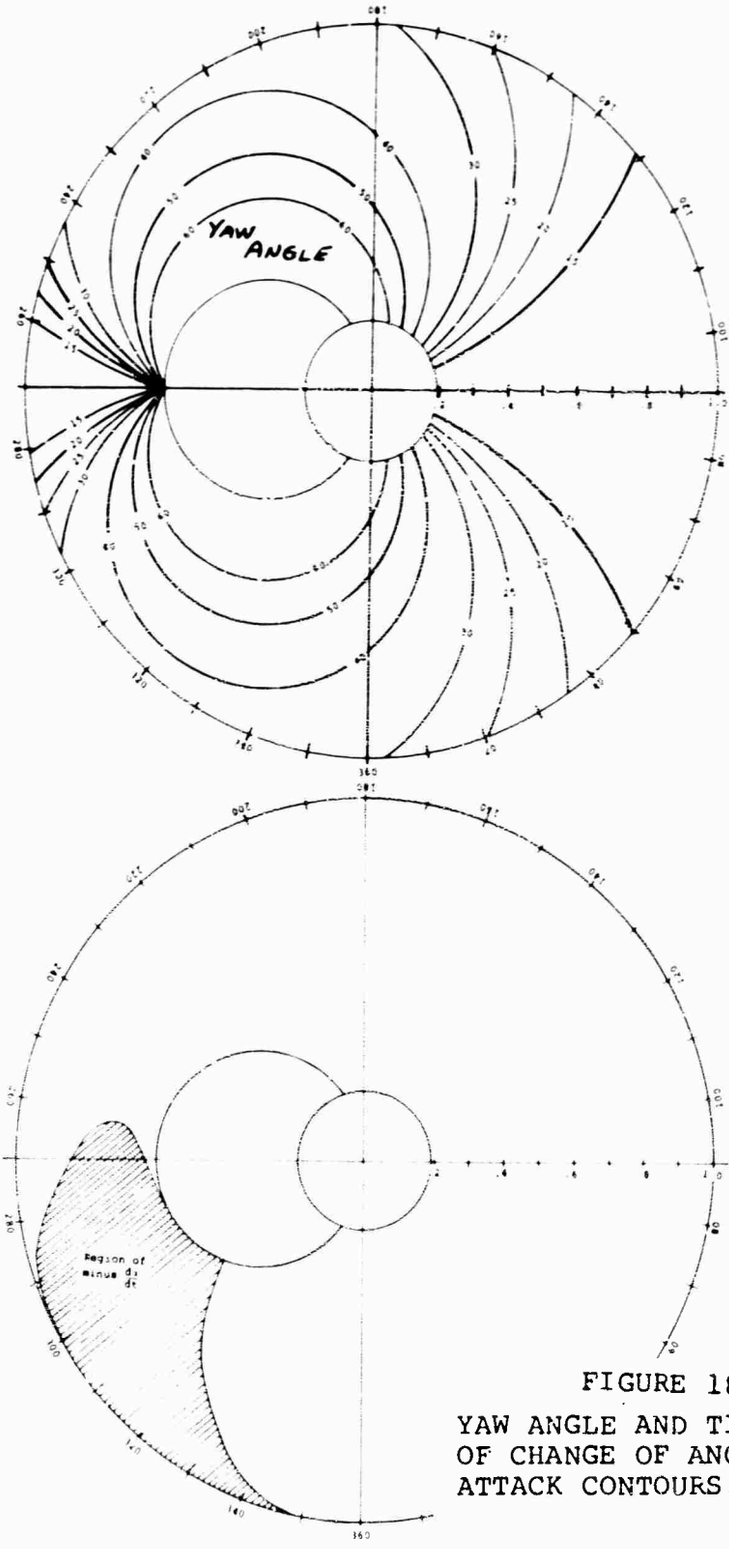

FIGURE 18
YAW ANGLE AND TIME RATE OF CHANGE OF ANGLE OF ATTACK CONTOURS.

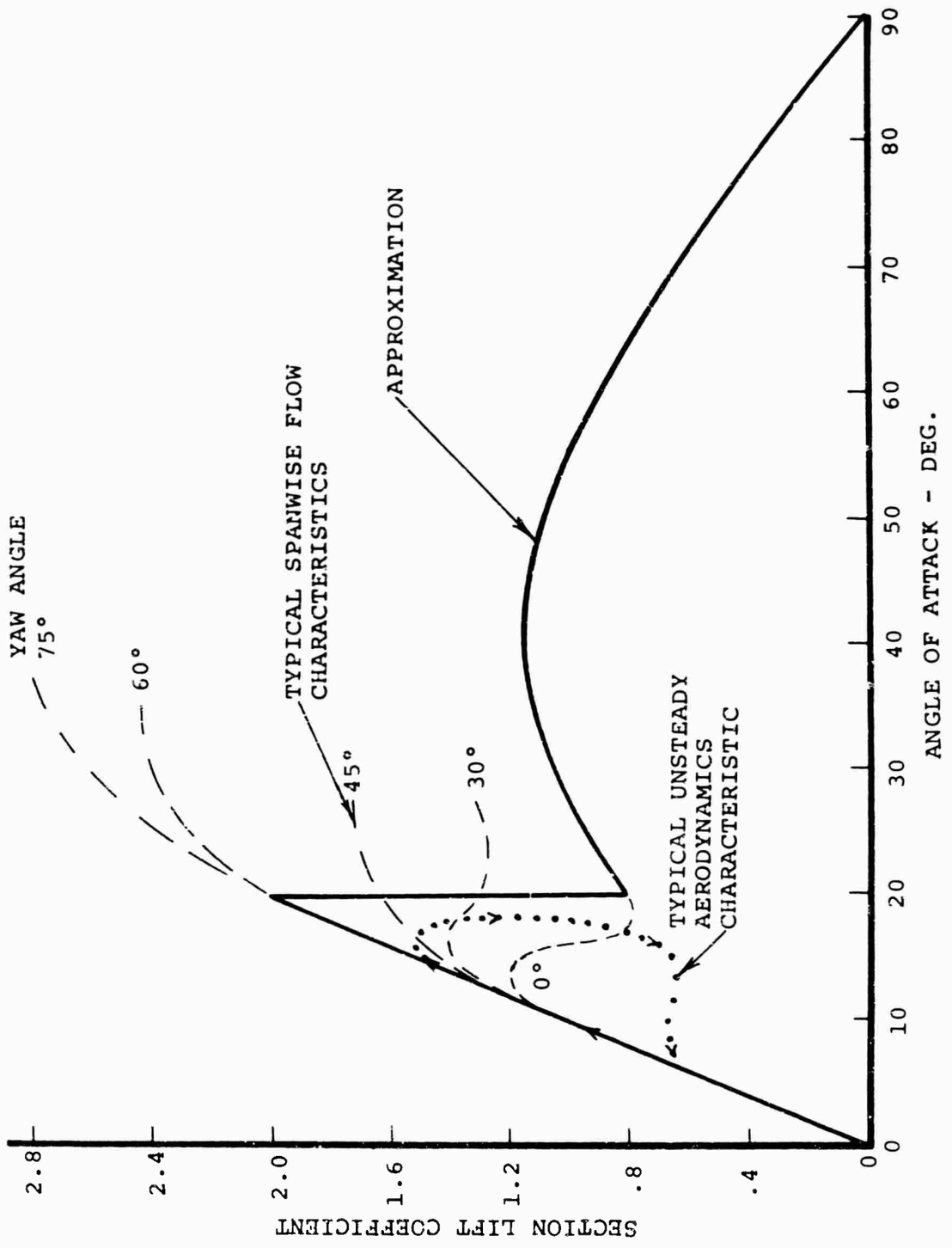

FIGURE 19 AIRFOIL C_ℓ-α APPROXIMATION

Figure 20 - Total Power Correlation with Figure 19 C_ℓ-α Approximation.

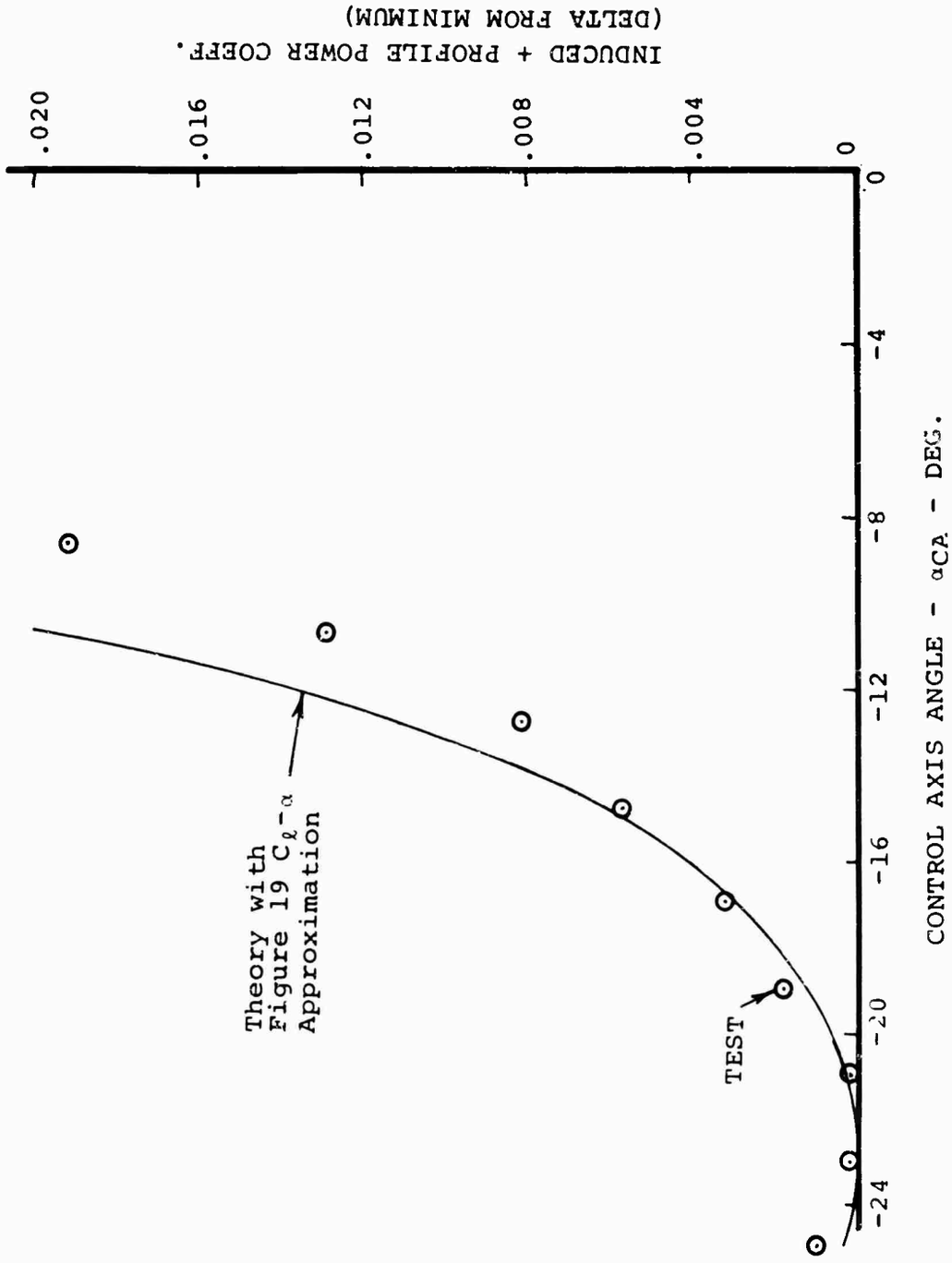

Figure 21 - Induced plus Profile Power Correlation with Figure 19 C_ℓ-α Approximation.

A Preliminary Study of the Effect of a Radial Pressure Gradient on the Boundary Layer of a Rotor Blade

by

Henry R. Velkoff

Department of Mechanical Engineering
The Ohio State University
Columbus, Ohio
U.S.A.

ABSTRACT:

Recent model rotor tests, tuft studies, and non-uniform inflow analyses have indicated that the phenomenon of "retreating blade stall" may be considerably different in nature than ordinary two-dimensional stall. An initial analysis was conducted using the Von Karman momentum integral equations to determine the possible effects on the boundary layer of the spanwise pressure gradients which can exist on rotors in forward flight. Using specified pressure and velocity distributions, an analytical solution was obtained which predicts a thinning of the boundary layer. The work presented represents an initial investigation and is presented in the interest of stimulating further research in the field of rotor blade boundary layers.

A Preliminary Study of the Effect of a Radial Pressure Gradient on the Boundary Layer of a Rotor Blade

by

Henry R. Velkoff

Department of Mechanical Engineering
The Ohio State University
Columbus, Ohio
U.S.A.

INTRODUCTION

Nineteen years ago at the 3rd Annual National Forum of the American Helicopter Society Dr. J. A. J. Bennett, the noted pioneer helicopter theoretician predicted flatly that the speed of the pure helicopter would be limited to 150 mph. Ten years later as a result of an intensive study sponsored by the Air Force, Hirsch of the Hughes Tool Co. reported that a maximum speed of up to 175 mph could be achieved by specialized rotor and aircraft design. Yet within the last three years we have witnessed flight speeds in excess of 200 mph by rotors not necessarily designed for high speed flight, and in the case of Sikorsky, the fuselage was definitely not designed for high speed flight. Extensive research sponsored by AvLabs has been instrumental in increasing the speed potential of pure rotary wing types greatly as evidenced by the work of Sikorsky, Bell, Lockheed and others.

One of the most unusual aspects of these speed increases is that they have been achieved without any real increased understanding of the physical mechanisms which underlie the basic limitations of rotary wing aircraft.

As a matter of interest, the approach used in considering the viscous flow actions on rotors today is practically the same as it was at the time of Dr. Bennett's overly pessimistic prediction.

Consider the basic limitations on the operations of a helicopter at high forward speed. It is well recognized that roughness, vibration, loss of control, sharply increased power, and high stresses are all the external indicators of the all too real limitation. Behind these manifest signs are rotor stall, compressibility effects, aeroelastic phenomena, and the detailed structure of the airflow through the rotor. The latter area, airflow, has been extensively investigated recently in AvLabs sponsored programs. The airflow and airloads work, however, does not consider the viscous flow effects , nor does it treat the transonic influences. It does not appear, however, that the nature of the airflow at the rotor where decoupled from stall and compressibility effects is a fundamental limitation to higher flight speeds.

Perhaps the most descriptive means of indicating the limitations on helicopter speed is through the use of the stall-compressibility boundary first discussed by Stuart. Figure 1 illustrates a typical Stuart plot used in a presentation by Legrand (1). The shaded area on the left indicates the retreating blade stall limitation, and the shaded area on the right the compressibility limitation. These particular limits are usually chosen based upon the experience of the particular helicopter design group. Typically the stall limitation is imposed as a certain value of angle of attack above two dimensional stall. This was and still is a common method, and one extensively covered in NASA work (2). A more realistic boundary

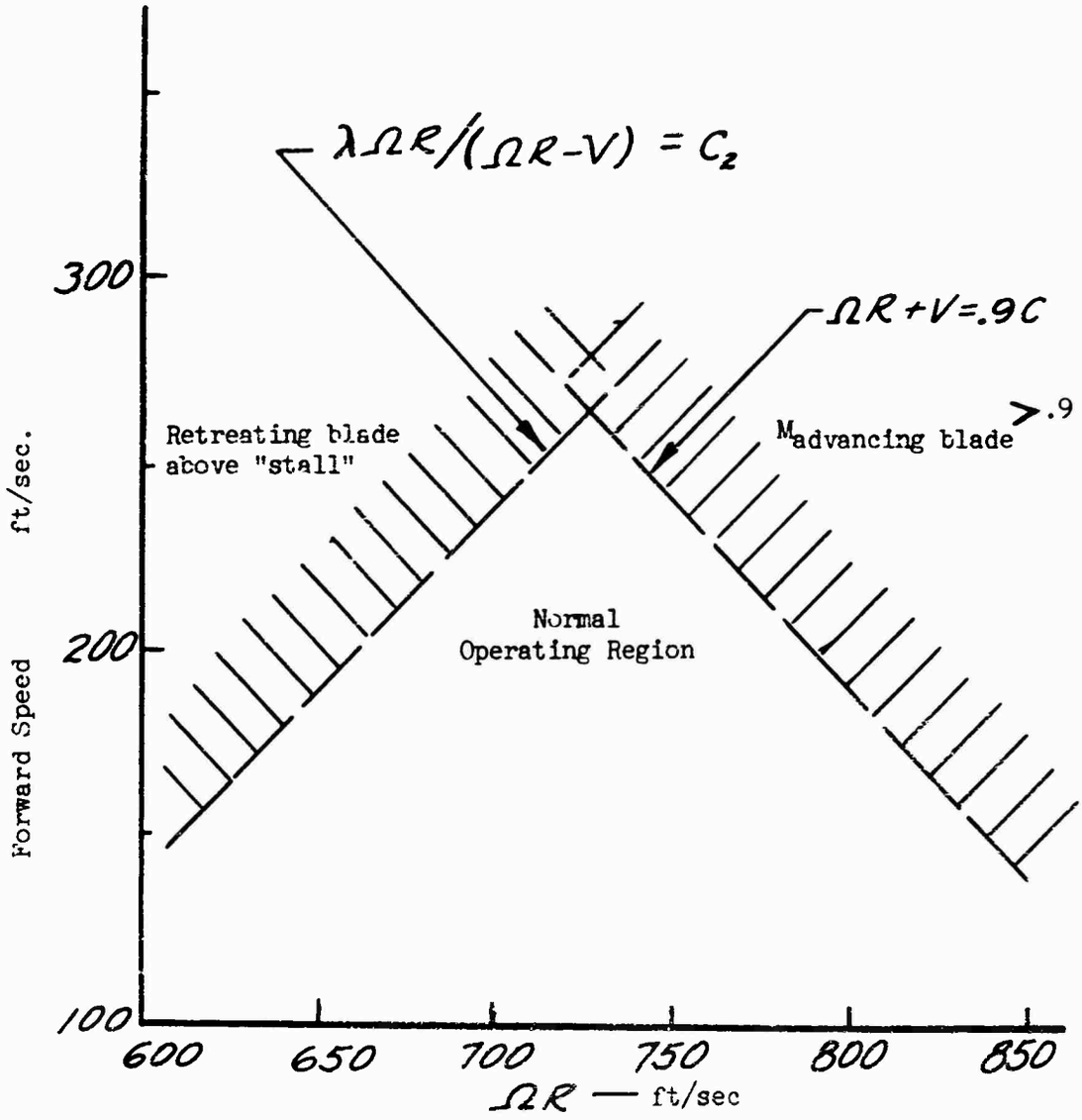

Figure #1 —— Stuart Plot

has evolved within the design groups based upon control loads. It was found that the high speed limitation was associated with a sharp increase in control loads. Sikorsky in their early XHR2S and H-37A experience were made painfully aware of this limitation, and more recently Vertol with the Chinook. The drift away from defining the limit as based on "stall" to one based upon control loads implied a realistic recognition that two dimensional stall may not be fully applicable to the rotor.

It is apparent from Figure 1 that if the critical "stall" shaded area could be moved upwardly then the speed of the pure helicopter could be increased correspondingly. The basic purpose of the work reported is to attempt to secure an understanding of the mechanism of "stall" on rotors as well as the true section drag of the individual blade elements. With such an understanding it may be possible to design airfoils to account for the particular viscous effects which take place and to develop boundary layer control devices which provide net improvements. The increases in speed obtained to date have achieved with almost no change in understanding of viscous effects on rotors since Dr. Bennett's statement. If an increased understanding of rotor boundary layers and "stall" can be obtained, then it is believed that even further significant gains in rotor performance can be achieved.

ROTOR BOUNDARY LAYER WORK

Even since the original comprehensive analysis of rotors based upon the work of Glauert, Lock, Wheatley and Bailey in the 30's, the assumption has been made in rotary wing theory that it was the component of flow normal to the blade span axis which was important. That is, in the analysis

of lift or drag of a section, one utilized two dimensional non-rotating section lift and drag coefficient data and applied them to the flow which occured over the airfoil normal to the blade span axis. The flow tangent to the blade span axis is ordinarily known as the spanwise flow. Under the usual assumption, this component of flow radially along the blade was considered to have little if any significant effect. In the case of lift forces this is considered to be a fairly good assumption over most of the blade. Since viscous effects ordinarily have little influence on the gross potential flow and lift, this assumption should be valid, so long as the angles of attack are low. In the case of drag, however. the picture is markedly different. Profile drag is completely dependent on the nature of the viscous flow actions at the surface of the rotating blade.

As partial justification for the ordinary approach used with drag, let us consider the boundary layer theory which evolved in the 1930's. In the analysis of swept wings it was found that the boundary layer equations applicable for spanwise and chordwise components of flow were decoupled for the case of thin airfoil sections. Because of this the theory predicted that the viscous boundary layer would grow independently in the chordwise and spanwise direction, if large over-riding pressure gradients did not exist. Since the two boundary layers were not coupled for the swept wing case it became possible to treat the wing in terms of a chordwise and spanwise component, and to use the two dimensional data with the chordwise component. (In the case of high speed flow, the use of sweep to effectively reduce the apparent thickness, or reduce the effective velocity component is well recognized). Based upon this fixed wing experience it became

logical to apply this approach to the helicopter rotor.

This standard technique of using only the chordwise component has led to good results for most practical helicopter work. There have been indications for some time that such a simple approach might not be fully adequate, and certainly with the higher flight speeds the deficiencies are more apparent. Specifically rotor power in hovering has almost always exceeded the very low values predicted by two dimensional theory and test for low drag airfoils. The low drags which should be obtainable from the "low drag bucket" have never been realized even on large rotors operating at high Reynolds numbers. Likewise "stall" phenomena on rotors have seldom been accurately predictable and gross indications of pitching moment are used, which of course include the drastic effects of the pitching moment break at high Mach number (M = .8-.9) as well as the C.P. shift at stall.

Most past efforts within the helicopter industry aimed at alleviating stall limitations have centered upon the use of relatively elementary or even crude boundary layer control techniques applied to rotors. Starting with the extensive work by Stalker of Michigan, through Rheem, Cessna, United Aircraft Research, and Sissingh net practical gains through the use of boundary layer blowing and suction on rotors has not provided useable gains worth the added complexity of the system used. To the best knowledge available, no comprehensive work was concentrated on what the boundary layer actually was like on a rotor in forward flight, yet considerable effort was directed at controlling something which was only imperfectly understood at best. In addition most of the work was based upon two dimensional tests,

which of course implied that the simple chordwise component approach was valid even in extremes of rotor operation. It is believed that the lack of success with these programs is largely due to a lack of knowledge of the actual boundary layer which exists on a rotor. Present work with the Dorand jet flap system may, however, evolve to provide useful gains.

STATEMENT OF THE TECHNICAL PROBLEM

A logical question arises at this point. Why is the boundary layer on a rotor blade potentially so different from that found on ordinary two dimensional type airfoil sections? Two fundamental forces are at work on an ordinary 2-D airfoil boundary layer, the viscous action and the pressure gradient or chordwise distribution of pressure over the airfoil. In the case of an airfoil on a rotor the following actions exist. First the flow components exist both in the chordwise and spanwise directions. The magnitude of the total velocity vector varies during each revolution. The direction of the velocity varies during a revolution. Because of the increasing velocity from root to tip, a very strong spanwise pressure gradient exists even in the absence of any tip vortex effects. This gradient also occurs even with a fixed local angle of attack. Because the boundary layer is effectively attached to the surface, it experiences both a centrifugal force component and a coriolis component. There are also large changes in flow fields due to periodic compressibility and reversed flow. In addition to all these coupled actions, the ordinary chordwise airfoil pressure distribution and viscous actions remain. It is rather surprising, therefore, that the past use of two dimensional theory has worked as well as it has.

From a physical viewpoint the boundary layer on a rotor (and the related stall and drag actions) provides the following approximate picture. As the advance ratio increases and the retreating blade experiences higher angles of attack a point is reached where two dimensional theory would predict separation of the boundary layer in the chordwise direction and based upon an ordinary flow situation this would imply that stall had occured. However, closer examination would reveal that the boundary layer due to spanwise flow may not have yet reached the conditions for separation. Consequently, a true "stall" as known in a two dimensional sense may not occur. It may be possible that when the chordwise component approaches incipient separation, an increased spanwise flow in the boundary layer takes place; --a virtual pumping of the lower speed inboard boundary layer out towards the outboard region of the blade. If this does indeed occur, then it is possible that the flow, boundary layer, and airfoil characteristics of portions of the blade may be modified and increased power and changed pitching moments may result. The actual increased control loads and the sharp power increases at high advance ratio are of course experienced by any helicopter. These increases have generally been attributed to ordinary stall, but in light of the foregoing discussion may not be the proper explanation. Another important contributing factor is the $\dot{\alpha}$ effect and the boundary layer separation which may be strongly affected by the nature of the boundary layer.

DISCUSSION OF PAST RELATED BOUNDARY LAYER WORK

Only a relatively limited amount of work has been accomplished which

is directly applicable to the helicopter rotor. Work on propellers and some work on turbine compressors is generally applicable. Propeller data are not directly applicable because of three main factors; operation near stall is not an important condition in ordinary propellers, steady flow exists through the propeller, and the propellers generally use very thin airfoil sections in the main working region of the blade. With thin sections the ordinary boundary assumptions are more nearly valid. Some limited data from the dissertation by Himmelscamp, however, do show large increases in $C_{L_{max}}$ in the inboard area of a test propeller. Radial flow and centrifugal effects could possibly be important in this case.

A thorough study of the references listed at the rear of this paper indicated that there was strong evidence to support the contention that interactions within a boundary layer could greatly modify its behavior. Secondary flows within turbine and compressor cascades were found to exist which greatly modified both the principal boundary layers as well as the primary flow stream through the cascades. These secondary flows tended to cross the walls of the channels normal to the primary stream direction and then rolled up into trailing vortices which extended downstream of the passage. In the case of swept wings large distortions of the ordinary two dimensional patterns are found. Likewise because of the induced spanwise flow, the lift and drag characteristics of swept wings are greatly modified. Many other indications are found that a "spanwise" flow can greatly modify the characteristics of an airfoil boundary layer, and hence the characteristics of the airfoil itself.

Review of prior analytical work revealed that only limited effort had

been applied. The hovering cases accomplished under Sears at Cornell had concentrated on the hovering case without any gradient or cross flow effects. More extensive work by Moore, Hansen, and Mager of NASA had been directed towards the boundary layers for turbines, but relatively little useful information was available. All analytical investigators pointed out the complexity of the problem. In the rotor blade case, it is believed that the predominant effect will come from the large spanwise pressure gradients, the associated induced spanwise flows, and the spanwise flows due to the periodic yaw. In the case of the rotor the added coupling due to rotational effects, centripetal and coriolis acceleration, could be particularly significant.

It is believed that one very significant action in the boundary layer on a rotor would occur as a result of the spanwise variation of pressure which exists on the retreating blade of a helicopter rotor. A typical variation in the negative pressures on the upper surface of a blade at a fixed chordwise location is shown schematically in Figure 2. As can be seen a rapidly increasing region of negative pressure exists on the surface of the retreating blade. Such a pressure gradient gives rise to a term of the form, $(-\frac{\partial p}{\partial r})$, which represents a negative spanwise pressure gradient on the upper surface. Because of this gradient the fluid particles within the boundary layer may tend to drift outward and then couple with the chordwise boundary layer flow. Possible boundary layer profiles in the chordwise and spanwise directions are shown schematically in Figure 3.

The approach used in the analysis is to start with the Navier Stokes

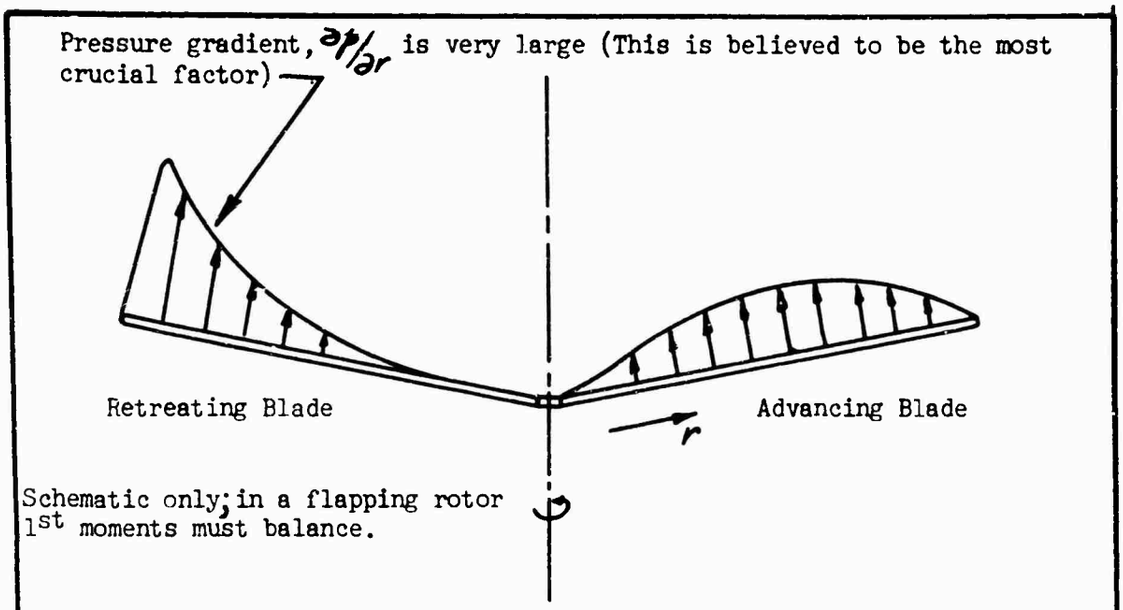

Figure #2, Variations of Pressure on a Rotor

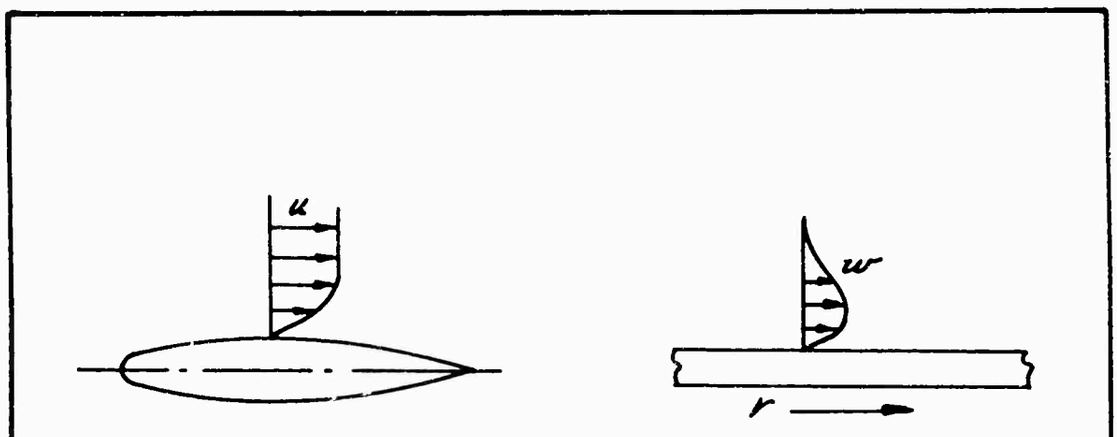

Normal chordwise boundary layer profile (exaggerated scale)

Possible spanwise boundary layer--

Figure #3, Boundary Layer Schematics

equation for viscous flow written in cylindrical coordinates. The equations are then transformed to the rotating coordinate system moving with the rotor. This transformation gives rise to the "coriolis" terms which appear to the observer located in the non-inertial rotating system. In order to get a feel for the possible interactions and their magnitudes, the integral techniques of Von Karman are applied. The Navier Stokes equations are integrated across the boundary layers and profiles are assumed in both chordwise and spanwise directions. In the process the usual boundary layer assumptions are made, and the procedures for reduction of the Navier Stokes are similar to those found in "Boundary layer Theory" by Schlichting. Although it must be recognized that the integral techniques cannot give any information on the actual detailed structure of the boundary layer, they can lead to very useful trends. Particularly they can show gross effects of coupling and gradients and can even provide estimates of the boundary layer thickness.

ANALYTICAL APPROACH

The analysis begins with the Navier Stokes equations written in cylindrical coordinates:

$$\rho\left(\frac{\partial w}{\partial t}+w\frac{\partial w}{\partial r}+\frac{u}{r}\frac{\partial w}{\partial \phi}-\frac{u^2}{r}+v\frac{\partial w}{\partial y}\right)= \qquad 1$$
$$-\frac{\partial p}{\partial r}+\mu\left(\frac{\partial^2 w}{\partial r^2}-\frac{1}{r}\frac{\partial w}{\partial r}-\frac{w}{r^2}\frac{\partial^2 w}{\partial \phi^2}-\frac{2}{r^2}\frac{\partial u}{\partial \phi}+\frac{\partial^2 u}{\partial y^2}\right)$$

$$\rho\left(\frac{\partial u}{\partial t}+w\frac{\partial u}{\partial r}+\frac{u}{r}\frac{\partial u}{\partial \phi}+\frac{wu}{r}+v\frac{\partial u}{\partial y}\right)= \qquad 2$$
$$-\frac{1}{r}\frac{\partial p}{\partial \phi}+\mu\left(\frac{\partial^2 u}{\partial r^2}+\frac{1}{r}\frac{\partial u}{\partial r}-\frac{u}{r^2}+\frac{1}{r^2}\frac{\partial^2 u}{\partial \phi^2}+\frac{2}{r^2}\frac{\partial w}{\partial \phi}+\frac{\partial^2 u}{\partial y^2}\right)$$

$$\rho\left(\frac{\partial w}{\partial t}+w\frac{\partial w}{\partial r}+\frac{u}{r}\frac{\partial w}{\partial \phi}+v\frac{\partial w}{\partial y}\right)= -\frac{\partial p}{\partial y}+\mu\left(\frac{\partial^2 w}{\partial r^2}+\frac{1}{r}\frac{\partial w}{\partial r}+\frac{1}{r^2}\frac{\partial^2 w}{\partial \phi^2}+\frac{\partial^2 w}{\partial y^2}\right) \quad 3$$

and the continuity equation:

$$\frac{\partial w}{\partial r}+\frac{w}{r}+\frac{1}{r}\frac{\partial u}{\partial \phi}+\frac{\partial v}{\partial y}=0 \quad 4$$

Making the usual boundary layer assumptions, and transforming the above equation into the rotating coordinate frame, we obtain the equation along the blade span:

$$\frac{\partial w}{\partial t}+w\frac{\partial w}{\partial r}+\frac{u}{r}\frac{\partial w}{\partial \phi}+v\frac{\partial w}{\partial y}-\frac{(u+\Omega r)^2}{r}=-\frac{1}{\rho}\frac{\partial p}{\partial r}+\nu\frac{\partial^2 w}{\partial y^2} \quad 5$$

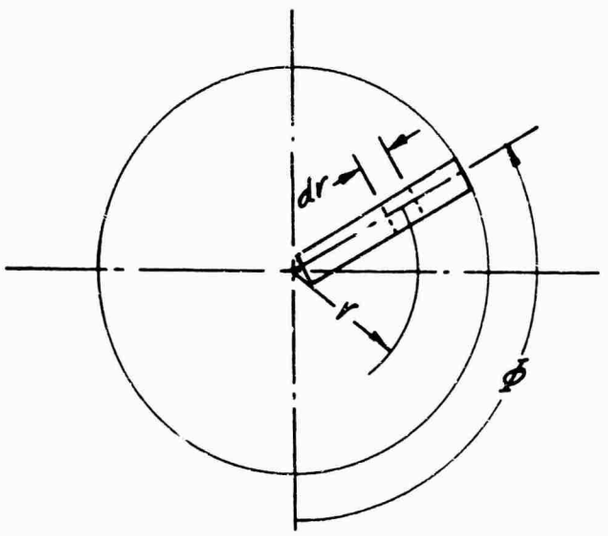

Figure #4 Coordinates of Rotor Blade Segment

and the equation along the chord direction:

$$\frac{\partial u}{\partial t}+\frac{u}{r}\frac{\partial u}{\partial \phi}+w\frac{\partial u}{\partial r}+v\frac{\partial u}{\partial y}+\frac{w}{r}(u+2\Omega r)=-\frac{1}{\rho r}\frac{\partial p}{\partial \phi}+\nu\frac{\partial^2 u}{\partial y^2} \quad 6$$

Continuity:

$$\frac{\partial w}{\partial r}+\frac{w}{r}+\frac{1}{r}\frac{\partial u}{\partial \phi}+\frac{\partial v}{\partial y}=0 \quad 7$$

The usual method of determining the pressure gradient term is to utilize the Bernoulli relation. In this case we must use the full equation above and proceed to the values of the various terms outside the boundary layer. Typically for the hovering case, outside the boundary layer we would find for the spanwise equation,

$$\frac{1}{\rho}\frac{\partial p}{\partial r} = \frac{(V+\Omega r)^2}{r} - W\frac{\partial W}{\partial r} \qquad 8$$

where $u \to V$, $w \to W$ outside the boundary layer. In a hovering case with a flat plate $V = -\Omega r$ and it can be seen that the centrifugal force effects cancel out entirely from the radial flow equation outside the boundary layer as they should. Likewise in the chordwise direction, hovering with a flat plate, $\frac{\partial V}{\partial \phi} = 0$, $v = 0$, $\frac{\partial u}{\partial t} = 0$, $V = -\Omega r$,

$$-\frac{1}{\rho r}\frac{\partial p}{\partial \phi} = W\frac{\partial V}{\partial r} + \frac{W}{r}(V + 2\Omega r) = 0 \qquad 9$$

Hence with the flat plate, there can be no pressure gradient in the chordwise direction in the free stream.

If we integrate the above equations across the boundary layer we get the following spanwise equation:

$$\frac{\partial}{\partial t}\left\{W\int\frac{w}{W}dy\right\} + \frac{1}{2}\frac{\partial}{\partial r}W^2\left\{\int\frac{w}{W}dy\right\} - \frac{\partial \theta_r W^2}{\partial r} - \frac{\theta_r W^2}{r} \qquad 10$$

$$+ \frac{V}{r}\frac{\partial W}{\partial \phi}\left\{\int\frac{u}{V}dy\right\} - \frac{\partial VW\theta_{\phi r}}{r\partial \phi} - \int\frac{(u+\Omega r)^2}{r}dy = -\frac{1}{\rho}\frac{\partial p}{\partial r}\delta_r - \frac{\tau_{w_r}}{\rho}$$

Chordwise equation:

$$\frac{\partial}{\partial t}\left[V\int\frac{u}{U}dy\right]+\frac{\partial V}{\partial r}\int w\,dy-\frac{\partial \bar{v}W\theta_{r\phi}}{\partial r}-\frac{VW\theta_{r\phi}}{r}+\frac{\partial V}{r\partial\phi}\left\{\int u\,dy\right\} \quad 11$$

$$-\frac{\partial\theta_{\phi}V^{2}}{r\partial\phi}+\int\frac{w}{r}(u+2\Omega r)dy=-\frac{1}{\rho r}\frac{\partial p}{\partial\phi}\delta_{\phi}-\frac{\tau_{w\phi}}{\rho}$$

where:

$$\theta_{\phi}\equiv\int\frac{u}{U}\left(1-\frac{u}{U}\right)dy \quad 12$$

$$\theta_{r}\equiv\int\frac{w}{W}\left(1-\frac{w}{W}\right)dy \quad 13$$

$$\theta_{r\phi}\equiv\int\frac{w}{W}\left(1-\frac{u}{U}\right)dy \quad 14$$

$$\theta_{\phi r}\equiv\int\frac{u}{U}\left(1-\frac{w}{W}\right)dy \quad 15$$

Since it is believed that the most important parameter is the spanwise flow associated with the very strong spanwise pressure gradient on the retreating blade (or that resulting from effective yaw), it was decided to investigate the effects of spanwise flow on the rotating blade. The case considered is that of a flat plate blade. If coupling is found to take place in this basic case, it is believed that even greater actions could occur in a case of a surface with a chordwise pressure distribution. To

simulate the spanwise pressure and flow effects, the spanwise flow was assumed to be of the form $W = W_t (r/R)^n$ 16

and n was chosen as 0,1, and 2. The variation of the form $W = W_t (r/R)^2$ 17 gives rise to a spanwise pressure gradient of the form $p = f(r^4)$ which is considered steep enough to represent the gradient observed on the retreating blade.

It should be noted, however, that an equation of the form $W = W_t (r/R)^n$ may cause one of the usual boundary layer assumptions to be questionable, since the terms of the Navier-Stokes equation in the y direction (eqn. 3) may not be negligible. In order to obtain some estimate of the actions within the boundary layer, just equations 4 and 5 were considered as is common in much boundary layer analysis

In order to facilitate the calculations the two velocity profiles were assumed as

$$w = W \eta^* \quad \text{(a linear variation)} \qquad 18$$

$$u = U(2\eta^* - \eta^{*2}) \quad \text{(a parabolic variation)} \qquad 19$$

where $\eta^* = y/\delta$ and δ is the boundary layer thickness. With the integral technique it is possible to assume any other profiles which meet the boundary conditions at the surface and at the free stream. Changing profiles will change the constants in the equations but rarely will change the trends indicated. It is believed that the elementary shapes chosen will be adequate to indicate some of the actions of the boundary layers.

Since the time delay for boundary layer development is very short, the

boundary layer in a non-steady case reaches its final value in about one chord length for an impulsive start case. Hence, the boundary layer picture can be considered as a quasi-steady situation and first order effects can be obtained by making this assumption. To get an estimate of the spanwise gradient effects, a psuedo-hovering case is considered in wh which $\frac{\partial}{\partial t}=0$, $U=-\Omega r$ (the hovering local velocity distribution) and that $W=W_t'(\frac{r}{R})^p$ Under these assumptions the equations for the boundary layer become

$r^{\underline{th}}$ or spanwise equation

$$\frac{\partial \delta_r^2}{\partial r}+\frac{3}{2}\frac{U}{W}\frac{\partial \delta_r^2}{r\partial\phi}-\delta_r^2\left(\frac{1}{W^2}\frac{\partial W^2}{\partial r}-\frac{2}{r}-\frac{32}{5}\frac{U^2}{W^2 r}-16\frac{\Omega U}{W^2}-\frac{12\Omega^2 r}{W^2}+\frac{12}{\rho W^2}\frac{\partial p}{\partial r}\right)=\frac{12\mu}{\rho W} \qquad 20$$

the ϕ^{th} or chordwise equation

$$\frac{\partial \delta_\phi^2}{\partial r}+\frac{8}{5}\frac{U}{Wr}\frac{\partial \delta_\phi^2}{\partial\phi}-\delta_\phi^2\left(\frac{10}{U}\frac{\partial U}{\partial r}-\frac{2}{W}\frac{\partial W}{\partial r}+\frac{8}{r}+\frac{24\Omega}{U}+\frac{24}{\rho UWr}\frac{\partial p}{\partial\phi}\right)=\frac{48\mu}{\rho W} \qquad 21$$

Using a method based upon finding the characteristic lines in the r-ϕ plane each of the above partial differential equations can be transformed into a pair of ordinary differential equations. The one equation gives the characteristic line in the r-ϕ plane, and the other equation is the ordinary equation for δ^2 along the characteristic line. Since the effects on the ϕ equation are of greatest interest and since its solution is more straight forward a few steps will be indicated.

Under the assumptions of

$$U=-\Omega r,\quad W=W_t(r/R)^2,\quad \eta=r/R,\quad \delta\equiv\delta_r\equiv\delta_\phi$$

then the r equation and the ϕ equation are redundant.

Picking the chordwise equation to solve

$$\frac{\partial \delta^2}{\partial \eta} - \frac{8}{5}\,\frac{\Omega R}{W_t}\,\frac{\partial \delta^2}{\eta^2 \partial \phi} = -\frac{10\delta^2}{\eta} + \frac{48\mu R}{\rho W_t \eta^2} \qquad 22$$

and using characteristics:

$$a \equiv \frac{5}{8}\frac{W_t}{\Omega R}$$

$$\frac{d\eta}{1} = \frac{d\phi}{(-1/\eta a)} = d\delta^2 \Big/ \left(-\frac{10\delta^2}{\eta} + \frac{30\nu}{a\Omega}\,\frac{1}{\eta^2}\right) \qquad 23$$

$$\frac{d\eta}{\eta^2} + a\,d\phi = 0$$

$$C_1 = a\phi - \frac{1}{\eta}$$

and $$\eta = \frac{1}{a\phi - C_1} \qquad 24$$

$$\frac{d\delta^2}{d\eta} + 10\frac{\delta^2}{\eta} = \frac{30\nu}{a\Omega\eta^2} \qquad 25$$

$$\delta^2 = \frac{10\nu}{3a\Omega}\eta^{-1} - C_2\eta^{-10} \qquad 26$$

$$C_2 = \delta^2\eta^{10} - \frac{10\nu}{3a\Omega}\eta^9$$

$$C_2 = \delta^2\,\frac{1}{(a\phi - C_1)^{10}} - \frac{10\nu}{3a\Omega}\,\frac{1}{(a\phi - C_1)^9} \qquad 27$$

using the boundary condition

$$\delta^2 = 0 \quad @ \quad \phi = 0$$

$$C_2 = \frac{10\nu}{3a\Omega}\left(\frac{1}{C_1^9}\right) \qquad 28$$

and

$$\delta^2 = \frac{10\nu}{3a\Omega}\,\frac{1}{\eta}\left\{1 - \frac{1}{(1 - a\phi\eta)^9}\right\} \qquad 29$$

for $a\phi\eta << 1$

$$\delta^2 \cong -\frac{30\nu}{\Omega}\phi\left\{1 + 3.125\left(\frac{W_t}{\Omega R}\right)\phi\eta + 7.17\left(\frac{W_t}{\Omega R}\right)^2\phi^2\eta^2 + ----\right\} \qquad 30$$

where ϕ is inherently negative as we move from the leading edge of the blade to the trailing edge.

Letting $\theta = -\phi$ 31

$$\delta^2 \cong \frac{30\nu}{\Omega}\theta\left\{1 - 3.125\left(\frac{W_t}{\Omega R}\right)\theta\eta + ----\right\} \qquad 32$$

The equation for an ordinary flat plate boundary layer (with a parabolic profile) is

$$\delta^2 = \frac{30\nu x}{U} \qquad 33$$

Writing the previous equation in the form

$$\delta^2 = 30\nu\left(\frac{r\theta}{\Omega r}\right)\left\{1 - 3.125\left(\frac{W_t}{\Omega R}\right)\theta\eta + ----\right\} \qquad 34$$

reveals that the forms of the two equations for ordinary flat plate and gradient case are similar. When the spanwise flow goes to zero, i.e. $W_t \to 0$, then the form for the equations are identical.

Thus the equation for the boundary layer in terms of δ^2 indicates that the thickness in the chordwise direction decreases with a spanwise pressure gradient. A radial outflow condequently leads to the condition where δ is decreased over the case with no outflow. This result indicates

a stabilizing action in the boundary layer.

The solution for the spanwise boundary layer growth is much more complex and the solution is difficult to interpret. It does, however, show coupling effects as did the chordwise equation.

Generally similar results are found with spanwise variations of the type

$$W = \text{constant} \qquad 35$$

$$W = W_t\,(r/R) \qquad 36$$

The solution for W = constant is representative of the spanwise flow at the most upwind and most downwind position of the rotor blades (fore and aft). It indicates the same general thinning of the boundary layer if the flow is from the root to tip, and a thickening if the flow is from the tip to the root.

The linear variation, $W = W_t\, r/R$ indicates a similar trend, and it also predicts a constant thickness in the spanwise direction.

DISCUSSION OF RESULTS

From a consideration of the analysis conducted with the flat plate and a spanwise pressure variation, or a spanwise flow, it appears that the predominant influence is that of a general thinning of the boundary layer in the chordwise direction if W is directed outwardly. Conversely a thickening takes place if a radial inflow takes place. The actions of centrifugal force do not seem to be of prime importance, but the action of the coriolis acceleration appears to be the important coupling agent between the spanwise flow and the chordwise boundary layer.

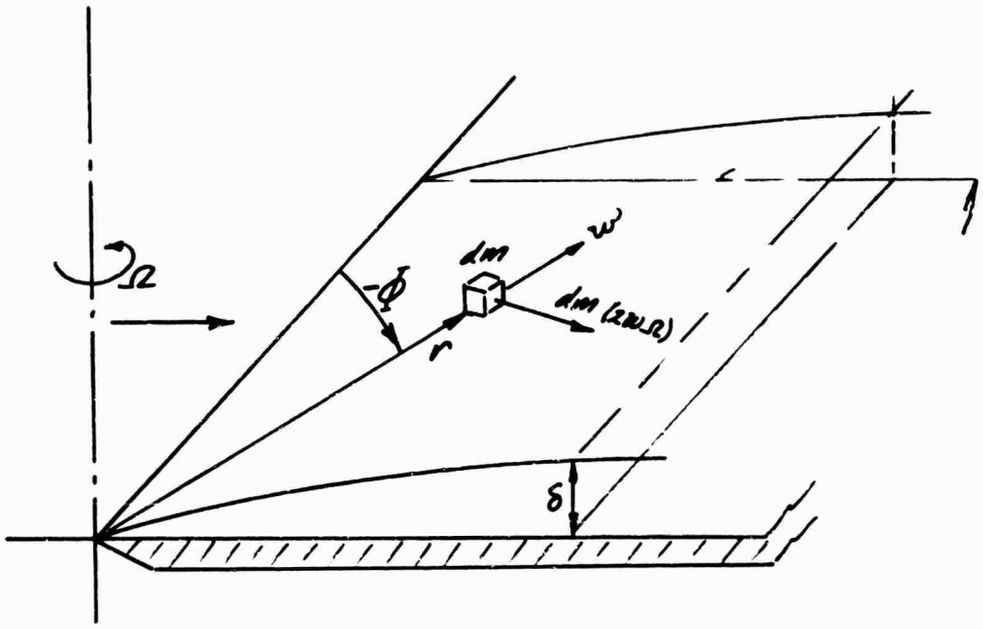

Figure #5 Chordwise Force in Boundary Layer

The action of the cross flow on the flat plate can be visualized as shown in the above sketch. As an air particle moves outward along the rotating flat surface blade, it tends to experience an accelerating force component towards the rear of the airfoil. This action tends to be analogous to a favorable pressure gradient, and should act to stabilize the boundary layer. This action takes place for any outward spanwise flow of the general form $W = W_t \eta^n$.

On the other hand if W were directed inward from the tip to the root, the action would be reversed. One can readily see that the particle would tend to move forward against the normal chordwise boundary layer flow. This would slow down and thicken the boundary layer and act as an adverse pressure gradient.

These same conclusions are borne out by study of the equation for δ^2

particularly

$$\delta^2 = \frac{30\nu}{\Omega}\theta\left\{1 - 3.125\left(\frac{W_t}{\Omega R}\right)\theta\eta + 7.17\left(\frac{W_t}{\Omega R}\right)^2\theta^2\eta^2 + \cdots\right\} \qquad 34$$

For W positive outwards along the blade, and small values of θ usually encountered, thinning is possible as the first term $\theta\eta$ predominates. Thus the coriolis action would tend to stabilize the flow. For W negative moving inwards, it can be seen that <u>all</u> the terms are positive and a very rapid thickening takes place. One would expect this behavior to cause a very thick wake and it could be destabilizing. For the case of $W = W_t =$ constant, similar comments can be made as for the case of $W = W_4\eta^2$ above.

The solution for δ_ϕ^2 reveals that as:

(1) $W_t \longrightarrow 0$, $\delta_\phi^2 \longrightarrow \delta^2$ flat plate

(2) $\phi \longrightarrow 0$, $\delta_\phi^2 \longrightarrow \delta^2 \longrightarrow 0$, flat plate

(3) $\eta \longrightarrow 0$, $\delta_\phi^2 \longrightarrow \delta^2$ flat plate

(4) $\phi\eta W_4 \longrightarrow 0$, $\delta_\phi^2 \longrightarrow \delta^2$ flat plate

(5) $\phi \longrightarrow$ large $\delta_\phi^2 = \frac{16\nu R}{3W_t\eta}$; $\delta_\phi = \frac{4}{\sqrt{3}}\frac{r}{\sqrt{N_{Re_r}}}$

where $N_{Re_r} = \frac{\rho W_t r}{\mu}$

Since the quantities and W_t and ΩR always appear together, their ratio is of importance. That is, either one can be changed to achieve a result. A change in Ω however can have a different result, since the first order term $\delta^2 = 30\nu/\Omega$ will predominate. That is, for small W_t and low rotational speeds, δ_ϕ^2 will be large. For large rotational speeds δ_ϕ^2 will be smaller and the boundary layer will be thinner independent

of radius. The limiting value of δ_ϕ as ϕ gets large, however, indicates that the boundary layer thickness aft on the surface will get thicker with increasing rotor radius.

Since the shear stress is a function of the boundary layer thickness, we can also get a feel for the effects on airfoil drag using

$$\tau = \mu \frac{\partial u}{\partial y}\Big|_{y=0} \qquad 38$$

For the assumed profile,

$$\tau_\phi = \frac{2\mu U}{\delta} \qquad 39$$

where τ_ϕ is + in the $+\phi$ or forward direction

Hence

$$\tau_\phi = \frac{2\mu U}{\delta} = 2\mu(-\Omega r)\left\{\frac{30\nu\theta r}{\Omega r}\left(1 - 3.125\left(\frac{W_t}{\Omega R}\right)\theta\eta + \cdots\right)^{-1/2}\right. \qquad 40$$

$$\tau_3 = -2\mu\Omega r\left(\frac{\Omega}{30\nu\theta}\right)^{1/2} \Big/ \left\{1 - 3.125\left(\frac{W_t}{\Omega R}\right)\theta\eta + \cdots\right\}^{1/2} \qquad 41$$

As the boundary layer thins down to $-3.125\left(\frac{W_t}{\Omega R}\right)\theta\eta$, τ_ϕ increases.

Examination of the equation for δ_ϕ^2 reveals that at a fixed value of W_t and η the thickness of the boundary layer is relatively flat in the θ direction.

$$\delta_\phi^2 = \frac{10\nu}{3a\Omega}\,\frac{1}{\eta}\left\{1 - \frac{1}{(1+a\theta\eta)^9}\right\} \qquad 42$$

Assuming, $\eta = 1$, a = Constant

$$\delta^2 = \frac{10\nu}{3a\Omega}\left\{1 - \frac{1}{(1+a\theta)^9}\right\} \qquad 43$$

For values of $\theta > 0$, the function $(1 + a\theta)^9$ rises rapidly, so that $(1 + a\theta)^{-9}$ becomes essentially equal to zero after some increase in θ. Hence, only in the region of small θ will δ^2 vary significantly with θ. A general trend can be seen from a sketch which presents δ^2 versus θ where the asymptotic value of δ^2 as θ gets large is $\delta^2 \rightarrow \frac{4}{\sqrt{3}} \frac{R}{\sqrt{N_{Re_r}}}$.

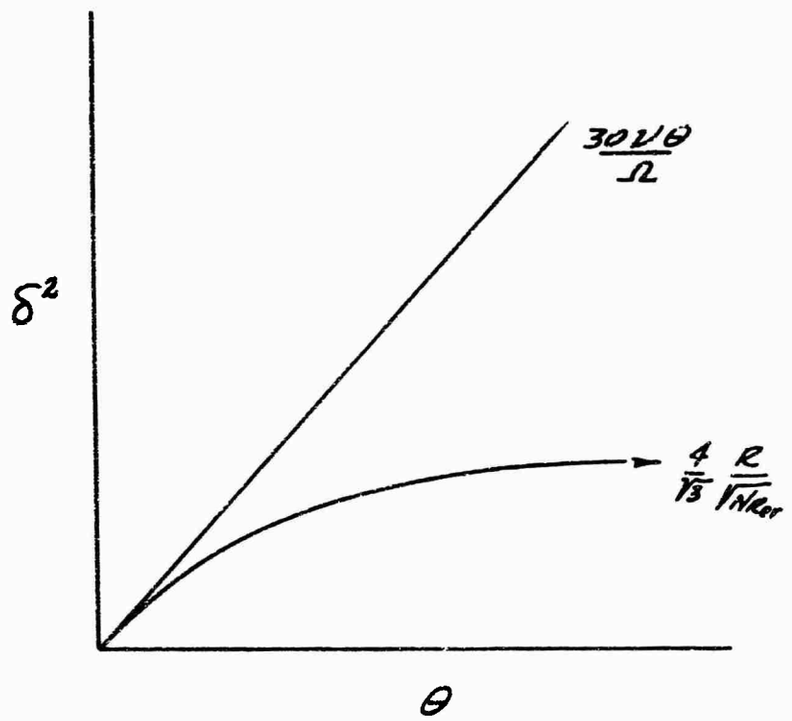

Although lack of time precluded calculation of actual values, the trends are evident in the foregoing sketch. If $W_t = 0$, then an ordinary boundary layer develops. If $W_t > 0$ then the boundary layer thickness tends to approach a constant thickness as θ increases, and a thickness that decreases from the root value outward.

Such thinning could lead to a stabilization of the boundary layer. The approximately constant δ^2 for larger values of θ is similar to that found in stagnation flow. In stagnation flow, $\delta^2 = \text{const}$, an accelerating flow exists in the region of the stagnation point, and a favorable pressure gradient exists. Consequently it can be surmised that a spanwise outward flow on a rotating blade (flat plate) gives rise to a strong chordwise coupling which acts similarly to stagnation flow. Since stagnation flow has very stable boundary layers, it can be tentatively concluded that a more stable boundary layer exists in regions where a velocity of the form $W = W_t \frac{r^2}{l}$ occurs.

In summary the overall trends indicated by the preliminary analysis based upon consideration of a steep spanwise pressure variation has led to the following possible actions within the boundary layer.

(a) An "apparent pressure gradient" term in the θ direction on a flat plate.

(b) A stabilizing influence on the boundary layer which accompanies a thinning boundary layer.

(c) A tendency for an increased C_f drag even though the effect is stabilizing.

I would also like to acknowledge the support given by the Vertol Division of Boeing which allowed this study to be conducted and to the assistance given in portions of the analysis by Mr. B. Sunstein.

BIBLIOGRAPHY

1. Himmelskamp, H., Profiluntersuchungen on einem umla..lenden Propeller -Die vorliegende Schrift ist eine etwas gekurzte Wiedergabe der Dissertation des Verfassers (Gottingen 1945; Referent: Prof Dr. Alb. Betz) Mitt. Max - Planck - Inst. 2, (1950)

2. Sears, W. R., "Potential Flow Around a Rotating Cylindrical Blade", Journal of Aeronautical Sciences, March 1950. pp. 183-184

3.Tan, H. S., "On Laminar Boundary Layer over a Rotating Blade", Journal of The Aeronautical Sciences, 1953 or 1954 pp. 780-781

4. Mager, H., "Three-Dimensional Laminar Boundary Layer with Small Cross-Flow", Journal of The Aeronautical Sciences, Dec. 1954. pp 835-845

5. Rott and Smith, "Some Examples of Laminar Boundary-Layer Flow on Rotating Blades", Journal of The Aeronautical Sciences, Nov. 1956, pp. 991 -996

6. Hawthorne, W. R., "Some Aerodynamic Problems of Aircraft Engines", Journal of The Aeronautical Sciences, Oct. 1957. pp. 713-729

7. Harris, F. D., "Some Thoughts About Blade Stall", Inter-Office Memorandum 8-7003-3-328, Vertol Division, The Boeing Company, 22 October 1962

8. Banks and Gadd, "Delaying Effect of Rotation on Laminar Separation", AIAA Journal, April, 1963. pp. 941-942

9. Jeffrey, A., "Nonlinear Waves", International Science and Technology, July 1964. pp. 37-44

10. Corson, B. W., Jr., "A Review of Propeller Theory", NACA Technical Note TN-1850G, Langley Aeronautical Laboratory, Langley Field, Va., June 21-23 1948. pp. 71-125

11. Becker, J. V., "Characteristics of Wing Sections at Transonic Speeds" of NACA Technical Note TN-1850F, Langley Aeronautical Laboratory, Langley Field, Va., June 21-23,1948.

12. Dannenberg, R. E., "Measurements of Section Characteristics of a 45° Swept Wing Spanning a Rectangular Low-Speed Wing Tunnel as Affected by the Tunnel Walls",NACA Technical Note TN-2160, Ames Aeronautical Laboratory Moffett Field, California, August 1950

13. Mager, A., "Generalization of Boundary-Layer Momentum-Integral Equations to Three-Dimensional Flows Including Those of Rotating System", NACA Technical Note TN-2310, Lewis Flight Propulsion Laboratory, Cleveland, Ohio, March, 1951

14. Moore, F. K , "Unsteady Laminar Boundary-Layer Flow", NACA Technical Note, TN-2471, Lewis Flight Propulsion Laboratory, Cleveland, Ohio,Sept 1951

15. Altman and Hayler, "An Comparison of the Turbulent Boundary-Layer Growth on an Unswept and a Swept Wing", NACA Technical Note TN-2500, Ames Aeronautical Laboratory, Moffett Field, California, Sept. 1951

16. Hunton, L. W., "Effects of Finite Span on the Section Characteristics of Two 45° Sweptback Wings of Aspect Ratio 6",NACA Technical Note TN-3008, Ames Aeronautical Laboratory, Moffett Field, California, Sept. 1953

17. Kofskey and Allen, "Smoke Study of Nozzle Secondary Flows in a Low-Speed Turbine", NACA Technical Note TN-3260, Lewis Flight Propulsion Laboratory, Cleveland, Ohio, Nov. 1954

18. Chapman, Kuehn, and Larson, "Preliminary Report on a Study of Separated Flows in Supersonic and Subsonic Streams",NASA Research Memorandum RM-A55L14 Ames Aeronautical Laboratory, Moffett Field, California, 12 June 1956

19. Hansen and Herzig, "On Possible Similarity Solutions for Three-Dimensional Incompressible Laminar Boundary Layers. I-Similarity with respect to Stationary Rectangular Coordinates", NACA Technical Note TN-3766, Lewis Flight Propulsion Laboratory, Cleveland, Ohio, Oct. 1956

20. Mair, W. A., "The Distribution of Pressure on an Aerofoil, in a stream with a Spanwise Velocity Gradient", Aeronautical Research Council, F. M. 2093 (16,937), NASA N-36625, Cambridge University Aeronautics Laboratory, 3 July 1954

21. Liu, S. W , "The Laminar Boundary-Layer Flow on Rotating Cylinders. Part I, Flat Plate", AFOSR TN57-298, ASTIA 132369, Cornell University, Graduate School of Aeronautical Engineering, Ithaca, New York, June 1957

22. Liu, S. W., "The Laminar Boundary-Layer Flow on Rotating Cylinder, Part II, Cylinders", AFOSR TN57-298, AD 132 369, Cornell University, Graduate School of Aeronautical Engineering, Ithaca, New York, June 1957

23. Ostrowski, J., "Wlasciwosci Opxywu Ptatow Skos'nych W Zakresie Krytycznyc Katow Natarcia", Archiwum Budowy Maszyn, Tom VII, 4 Zeszyt 1960

24. Stain, W. C., "The Three-Dimensional Turbulent Boundary Layer on a Rotating Disk", Research Report No. 35 (Navy Contract NONR 978 (01)), Aerophysics Department of Mississippi State University, 8 August 1962

25. Sweet and Jenkins, Jr. "Results of Wing-Tunnel Measurements On a Helicopter Rotor Operating at Extreme Thrust Coefficients and High-Tip-Speed Ratios". Journal of the American Helicopter Society, Vol. 8, No. 3 July 1963, pp. 4-7

26. Hains, F D , "Comparison of the Stability of Poiseuille Flow and the Blasius Profile for Flexible Walls", Flight Sciences Laboratory Report No. 75 (DI-82-0264), Boeing Scientific Research Laboratories, June, 1963

27. Hains, F. D., "On the Stability of MHD Channel Flow", Flight Sciences Laboratory Report No. 88, (DI-82-0331), Boeing Scientific Research Laboratories March 1964

28. Schlichting, H., Boundary Layer Theory, fourth edition, translated by J. Keston, McGraw-Hill, 1960

29. Lackmann, G. V., (editor), Boundary Layer and Flow Control, two volumes, Pergamon, 1961

30. Hildebrand, F. B., Advanced Calculus for Applications, Prentice-Hall, 1963

31. Hildebrand, F. B., Methods of Applied Mathematics, Prentice-Hall, 1963

32. Scarborough, J. B., Numerical Mathematical Analysis, Johns Hopkins Press, 1950

33. Kennedy, Earnest D., "Application of a New Method of Approximation in the Solution of Ordinary Differential Equations to the Blasius Equation" Journal of Applied Mechanics, March 1964, pp. 112-113

REFERENCES:

1. Legrand, F. L., "Structural Behavior of the Super Frelon in High Speed Flight". Proceedings of the American Helicopter Society, May 1964, Washington, D. C.

2. Gessow, A., and Meyers, G. C., "Aerodynamics of the Helicopter", Macmillan, New York, 1953.

3. Sweet, G., and Jenkins, J., Jr., "Results of Wind Tunnel Measurements on a Helicopter Rotor Operating at Extreme Thrust Coefficients and High Tip Speed Ratios", Institute of Aeronautical Sciences Preprint, January, 1963.

LIST OF SYMBOLS

a	$a = 5W_t/8\Omega R$
C	Speed of sound
C_2	Constant
C_f	Skin friction coefficient
$C_{L_{max}}$	Maximum list coefficient
C.P.	Center of pressure
c_1	Parameter in method of characteristics
c_2	Parameter in method of characteristics
M	Mach number
N_{Rer}	Reynolds number - spanwise
n	Exponent
p	Pressure
R	Rotor radius
r	Dimension along radius
t	Time
$\bar{U}$	Free stream velocity in ϕ direction
u	Local velocity in ϕ direction
V	Reference velocity of helicopter
v	Local velocity in y direction
W	Free stream velocity in r direction
W_t	Reference free stream velocity in r direction
w	Local velocity in r direction
y	Dimension perpendicular to the plane of rotation

$\dot{\alpha}$	Rate of change of angle of attack
δ	Boundary layer thickness
δ_r	r direction boundary layer thickness
δ_ϕ	ϕ direction boundary layer thickness
η	$\eta = r/R$
η^*	$\eta^* = y/\delta$
θ	$\theta = -\phi$
θ_ϕ	Defined by equation 12
θ_r	Defined by equation 13
$\theta_{r\phi}$	Defined by equation 14
$\theta_{\phi r}$	Defined by equation 15
μ	Viscosity
ρ	Density
τ	Shear stress
τ_ϕ	Shear stress in ϕ direction
τ_{w_o}	Shear stress in r or w direction at surface
τ_{u_o}	Shear stress in ϕ or u direction at surface
ϕ	coordinate in cylindrical coordinate system
Ω	Rotational speed $\Omega = \dot{\phi}$.

THE BOUNDARY LAYER OF THE HOVERING ROTOR

by

W. H. TANNER, AERODYNAMICS ENGINEER

Bell Helicopter Company
Fort Worth, Texas

P. BUETTIKER, ASSISTANT PROFESSOR

Aerospace Engineering
Arlington State College
Arlington, Texas

SUMMARY

Extensive experimental studies have been carried out on the boundary layer of a hovering rotor. The techniques employed involved flow visualization by means of evaporative chemical films. Also, data are presented from use of pressure and hot wire instrumentation in the boundary layer.

Summarized results from these investigations show location of transition from laminar to turbulent boundary layer flow in a centrifugal force field, the formation of tip vortices, the direction of flow in the boundary layer, and other aerodynamic features. The tests show that even with conventional production type profiles with relatively rough leading edges, appreciable laminar flow can be obtained. A laminar flow section was built and tested on a rotor with good results. Correlation with wind tunnel information on this section is shown.

In conjunction with the results of the experiments, theoretical analysis is presented to explain the observed lack of centrifugal outflow in the boundary layer and the apparent angle of attack change occurring over the outboard portion of the blade. This theory takes into account the flow field of the contracting slipstream and the effects of the individual velocity components due to discrete vortices in the wake of the rotor.

INTRODUCTION

This paper is the second report on boundary layer studies and presents results from Bell Helicopter's continuing study to develop a better understanding of the real aerodynamic environment of a rotor for prediction purposes and to improve the efficiency of rotary wing aircraft. More specifically, the objects of this phase of the study are:

1. Define the direction of flow in the boundary layer, especially near the tip and offer explanations for the findings (continuation of work from Reference 1).

2. Measure boundary layer velocity profiles in a high centrifugal force field (continuation of work from Reference 1).

3. In conjunction with the experimental studies, develop a mathematical model based on vortex theory for the flow field and boundary layer of a hovering rotor.

4. Conduct experiments with laminar flow profiles operating in a high centrifugal force field.

5. Extend the hovering study into forward flight.

Reference 1 presented results from the initial studies of the boundary layer in a high centrifugal force field and proposed qualitative explanations for the experimental findings. Since Reference 1 was published, some theoretical work has been accomplished and as yet portions of the theoretical work are not complete. A simplified mathematical model for the hovering rotor, based on vortex theory, has been developed and explanations for experimentally observed phenomena such as the lack of centrifugal outflow and the angle of attack change near the tip of a hovering rotor are offered.

In addition to the theoretical information, further experimental studies have been carried out. A laminar flow profile designed for helicopter use has been tested and measurements in the boundary layer in both hover and forward flight have been made using pressure probe and hot wire techniques. Results from these tests are presented.

The tests have been conducted using the UH-1 main, tail, and model rotors for a range of test conditions for angles of attack from zero to above stall, tip centrifugal forces to 4000 g's and Reynolds numbers up to 8.0×10^6.

SUMMARY OF EARLIER TEST RESULTS

Reference 1 has shown that the chemical film technique offers the aerodynamicists a convenient tool for studying the boundary layer and flow field of a hovering rotor. The most significant results obtained from the earlier study are summarized in the following paragraphs.

Surface Condition

Results from main and tail rotor tests show that erosion on the leading edge of the airfoil had little effect on the airfoil's ability to maintain laminar flow over a considerable portion of the chord. The tail rotor photograph, Figure 1, shows the blade lower surface on which erosion is evident on the leading edge. Actually, the aircraft on which this rotor was mounted was engaged in a 100-hour sand test when this picture was taken. The main rotor, Figure 1, was a standard production blade with many hours of service and was able to maintain better than 80 percent of the laminar flow which would exist on a blade with no erosion.

Boundary Layer Transition

The chemical film technique can be used to determine the transition of laminar to turbulent flow in the boundary layer. Figure 2a shows that transition on the hovering rotor follows trends identical to those of fixed wings. On the upper surface, the transition point moves forward with increased incidence and on the lower surface it moves aft. The dashed line on this figure is from two-dimensional results, Reference 2. Figure 2b (data from the studies conducted by the U. S. Army Aeronautical Activity at Ames Research Center) gives typical results from wind tunnel tests of a production UH-1 tail rotor blade (non-rotating) compared with rotating test data. In both figures, the angles of attack were calculated using the conventional blade element-momentum balance method which does not include contraction of the wake. Good correlation is shown in both these figures.

Boundary Layer Flow Direction

Another significant result from Reference 1 is that there is no evidence of outward flow or centrifugal pumping of the boundary layer for a hovering rotor. Similar results were reported for the fan tests of Reference 3. Figure 3 shows flow patterns on the upper and lower blade surfaces for several values of root collective pitch angles. On Figure 3, the undisturbed flow (constant angular velocity) is indicated by the circular arc about the center of rotation. The arrows represent the actual boundary layer flow direction, which over much of the blade surface is inward, and the shaded areas are the very turbulent regions due to the tip vortex. The boundary between laminar (L) and turbulent (T) flow (transition region) is also shown.

Angle of Attack Shift Near the Blade Tip

It was observed that the transition point on the outboard 20 percent of the blade is shifted forward on the upper side and aft on the lower side (Figure 4). This effect cannot be explained by Reynolds number influence because tip speed did not affect this phenomenon. The explanation is sought in an angle of attack change: near the blade tip in hovering, the angle of attack of the untwisted test blades increased by from 1 to 2 degrees. A theoretical explanation for this phenomenon is given in a later section of this paper.

Pressure Probe Tests

Figure 5 is a photograph of a pressure probe device (total and static) installed in a UH-1 tail rotor blade. Results obtained with this test equipment are presented in Figures 6a and 6b for rotating and non-rotating cases. These figures show comparable boundary layer profiles and dimensions for the rotating and non-rotating cases and that there is no apparent change in boundary layer thickness with rotation. These tests have shown that it is possible to obtain boundary layer profiles with simple pressure measuring equipment. A discussion of a pressure probe for forward flight is in a later section.

RADIAL FLOW EFFECTS

A significant result from the earlier tests was that there was no evidence of centrifugal outflow of the boundary layer. In fact, as shown in Figure 3, a slight inward flow prevails. To define the direction of flow of the boundary layer of a hovering rotor, four effects must be taken into account.

1. Inboard flow due to wake contraction
2. Spanwise pressure gradient

3. Centrifugal pumping due to viscous effects
4. Undeveloped tip vortex

Wake Contraction Effects

In an effort to gain a better understanding of the inward flow due to wake contraction, a very simple mathematical model of the hovering flow field has been developed to determine first order effects. A sketch of the model is shown in Figure 7. The model can be best visualized in the following manner. Beginning with the right-hand blade, a vortex is generated (solid line) which moves rearward in the tip path plane to a point 90 degrees from the blade. At that point, it drops down vertically a distance, Z, then remains in that plane for 180 degrees (ring 1), then is displaced vertically again to a lower plane (ring 2). This process is repeated for any desired number of steps. The left-hand vortex follows a similar pattern (dashed lines). The result is that the wake with this system is represented by two partial ring vortices in the tip path plane and a series of rings of constant vortex strength beneath the rotor. With this model, the induced and horizontal velocity components in the tip path plane can be computed using lifting line theory, assuming constant circulation which results in a triangular lift distribution as follows.

1. Reference 4 gives the relationship for the incremental velocity induced by an element of a straight vortex line of circulation Γ at a point A.

$$dW_A = \frac{\Gamma r dr \sin\phi}{4\pi r^2} \qquad (1)$$

2. With this equation and Figure 8, the velocity dW_A can be resolved into the vertically induced velocity v_i and the radial component v_ρ at a point A on the rotor. The equations are:

$$v_i = \frac{\Gamma r}{4\pi} \int_0^{2\pi} \frac{(r - \rho \sin\psi)\, d\psi}{[(r - \rho\cos\psi)^2 + (\rho \sin\psi)^2 + Z^2]^{3/2}} \qquad (2)$$

and

$$v_\rho = \frac{\Gamma r}{4\pi} \int_0^{2\pi} \frac{\cos\psi\, d\psi}{[(r - \rho\cos\psi)^2 + (\rho \sin\psi)^2 + Z^2]^{3/2}} \qquad (3)$$

Equations 2 and 3 are for a vortex of strength Γ and radius r, a distance Z below the rotor. The total solution for n rings plus the two partial rings is obtained by summing the contributions of all vortices in the rotor plane. Integration of the two partial rings required some special treatment. If the velocities due to these partial rings are integrated from 0 to $\pi/2$ and π to $3\pi/2$ excessive velocities result at the blade tip. This is not a new problem. References 5 to 7 suggest that the calculation of induced velocities at points with distances from the vortex core of the order of the vortex core dimension should be done by employing real rather than potential vortices. If this procedure for some reason becomes too involved, it is better to ignore the contribution to the total induced velocity of that relatively small region in which potential vortex theory would yield excessive values for the induced velocity. In this simple analysis, the latter was chosen and the partial rings were integrated from 2 degrees to $\pi/2$ and 272 degrees to $3\pi/2$. These limits were determined by trial and error. The criteria was that the final thrust distribution have the triangular shape which would be consistent with the initially assumed uniform circulation.

A second feature of this model is that the wake shape (contraction as a function of distance below the rotor) may be determined from momentum theory or by iteration procedures which are under development for a flexible wake or any specified wake

shape desired. For convenience in the present analysis, the wake shape was fixed by scaling the shape from smoke flow pictures of Reference 8. The following relationship was obtained.

$$r = \frac{R}{2}\left(1 + \frac{1}{1 + Z^{.4}}\right) \tag{4}$$

With the wake shape specified and an average induced velocity obtained from momentum theory, the vortex ring spacing can be calculated. The calculation begins with starting values from simple momentum theory. Then an iteration process is used until the values of velocity calculated in the rotor plane yield the desired thrust. The thrust is calculated using the momentum theory with the inclusion of the radial flow component. In the analysis, normally 20 vortex rings are used.

Results from this analysis, showing the radial velocity component, v_ρ, are presented in Figure 9a. These radial velocities near the 80 percent radius station are almost equal in magnitude to the axial velocity components which will be shown in a later figure.

Figure 9b shows the resultant boundary layer flow angle considering only the angular velocity and the axial velocity due to wake contraction. It is shown that a 2 to 3 degree inward flow must be expected to exist due to the axial velocity which is about 30 percent of the measured flow angle near the blade tip at the higher collective pitches (see Figure 3).

Centrifugal Force Field Effect

Another problem area in rotating machinery which has received very little attention by the theoretical aerodynamicists is the centrifugal force field effects on the boundary layer in three-dimensional flow. For a long time the only solution of a three-dimensional boundary layer problem was the rotating disc treated by von Karman (Reference 9). More recent solutions are

presented in References 10 and 11, treating rotating rotor and turbine-compressor blades, respectively, for laminar flow. Figure 10 shows a comparison between the rotating disc and a hovering rotor blade (UH-1 main rotor) of finite thickness (from Reference 10). The rotating disc solution yields rotational velocities within the boundary layer in excess of 130 ft/sec while the rotating rectangular flat plate of finite aspect ratio gives a maximum outward velocity of about 30 ft/sec. The difference between these two solutions is due to the increased boundary layer thickness as a function of radius in the case of the disc. This buildup cannot occur for the rectangular plate since the boundary layer is shed at the trailing edge of the plate.

For the case of the rotor blade with a weak pressure gradient, Figure 10 shows that a small inward velocity component exists. Reference 10 points out that if an analogy with yawed wings exists this solution may not be correct for strong pressure gradients. It must also be noted that the information of Reference 10 is only for the laminar portion of the boundary layer. The corresponding flow angles in the boundary layer for the case of a flat plate according to Reference 10 is about 1.5 degrees outward, indicating a very small effect of the centrifugal outflow in the laminar boundary layer.

Much theoretical work is needed in this area of centrifugal force effects on the boundary layer of rotating blades, but from what has been done it appears that the effects are small in the laminar boundary layer. In the turbulent boundary, especially when part of the blade is operating in a stalled condition, it is possible that large amounts of centrifuging of the boundary layer may be present. No theoretical work in this area seems to exist. Some experimental information on stall is given in a later section of this paper.

Effect of Radial Pressure Gradients

Figure 11 is a graph of lines of constant pressure coefficients for the UH-1 tail rotor (NACA 0015 profile pressure data from Reference 12) for 12 degrees of collective pitch and 805 rpm. In these data, the tip Mach number is 0.7 and ΔP is defined as the local minus the free stream static pressure divided by the tip dynamic pressure. The graph shows that for this condition the spanwise pressure gradient will cause an outward acceleration of the boundary layer on both surfaces. However, the upper surface gradient is about 10 times that on the lower surface. To obtain inward acceleration from the pressure gradient it was found that the angle of attack near the root must be negative, then the lower surface only will have an inboard acceleration.

Judging from the experimental evidence presented in this paper, it appears that the magnitude of the velocities are of the order of 0 and 50 ft/sec. The actual value depends, of course, on the angle of attack and possibly some other parameters.

Undeveloped Tip Vortex Effects

Little or no theoretical work exists on undeveloped tip vortices; however, experimental work using the chemical film technique gives some insight into the effects. Figure 12 gives photographs and sketches from the UH-1 tail rotor tests where the outer white line shown is at 87 percent radius. On the upper surface, several phenomena are visible. Very near the blade tip, there is a region of low velocity (line A on sketch) where the flow is essentially parallel to the chord. Inboard there is a higher velocity region (hashed lines) where the flow is directed outward (arrows). Further inboard the velocity must decrease since the chemical film remains and the flow direction is inboard as shown by the arrows on the sketch.

On the lower surface near the tip, as would be expected, the flow is outward and with decreasing radius it develops an inward component as shown in the sketch.

An interpretation of these experimental observations is offered in the upper sketch of Figure 12 which is a view of the blade in the plane of the chord. Air from the lower surface flows around the blade tip to the forming vortex, as illustrated. However, in forming the vortex a region (A) is left where the velocities are low (compared to the forming vortex) at the blade tip. The region outside the forming vortex also has lower velocities which are directed inward. This inward velocity component is believed caused by air coming from the lower surface, but instead of being shed with the vortex, strikes the blade surface, as shown by the outside arrow. This velocity from the forming vortex would oppose any tendency for the boundary layer to centrifuge.

Further information on the forming of tip vortices is shown in Figure 13 from the oil film tests. At the blade tip, it was noticed that there was a change in the flow angle of the oil film which is an indication of increased aerodynamic forces at the tip. These markings corresponded to the tip vortex marking found in the chemical film tests and Figure 14 is a sketch to aid in understanding the significance of these tests. The top sketch shows a particle of oil (square block) in and out of the forming tip vortex, and the velocity direction in the boundary layer from the chemical film test is shown by arrows. Centrifugal forces (C.F.) act on the oil and an aerodynamic viscous drag force (D) yielding a resultant force (R) with the flow direction of the oil along the resultant force. If the aerodynamic force within the tip vortex was less than outside the vortex, the flow angle would decrease within the vortex as shown in the upper figure. However, the oil film tests show that

the opposite is true and that the flow angle of the oil increases within the vortex as illustrated by the lower sketch indicating that the aerodynamic friction force must be larger than the centrifugal force.

Considering that the centrifugal force at the tip of a tail rotor can be 4000 g's, it follows from the above that the drag force in the forming vortex must be very large and is undoubtedly absorbing a significant percentage of the hovering power required. This leads one to speculate that if the size and/or velocities in the vortex could be decreased with special tip shapes, considerable hovering power savings may be attainable.

AXIAL FLOW

Results from the analysis giving the axial velocity component for a constant correlation are shown in Figure 15. The induced velocity distribution is essentially constant to 60 percent radius. From 60 to 85 percent radius, there is a steady reduction in the induced velocity. Outward of 85 percent there is an increase in velocity to 95 percent, then the velocity drops to zero at the tip. Due to this change in induced velocity outward of 80 percent radius, an angle of attack change of 1 degree results as illustrated in the lower graph of Figure 15. This figure shows the calculated inflow angle distribution. Th dashed curve was obtained by assuming a uniform induced velocity (momentum theory), while with the simple vortex theory thrust is calculated using the resultant of the radial and axial velocity components. It is interesting to note that with the new method a slightly lower angle of attack over the entire blade is obtained. Figure 4, from the tail rotor tests using the chemical film technique, shows this almost step angle of attack change near the tip. The vertical line shown in Figure 15 is the position of the first vortex below the rotor. It is evident that this vortex

must have a strong influence on the local angle of attack. Note that the position of the vortex core is directly below the apex of the induced velocity curve.

This information has interesting implications when applied practically to the hovering rotor. At high tip speeds, a one degree change in angle of attack on the outward 20 percent of the blade can produce a considerable increase in the profile drag. This suggests that the optimum twist for a hovering rotor would be one with a near step change in twist distribution at about the 80 percent radius station.

LAMINAR FLOW PROFILE EXPERIMENTS

Improved airfoil profile theories have been developed by Dr. Wortmann in Germany. Results for a laminar flow profile designed for helicopter rotors (FX05-H-126) have been published in Reference 13. Figure 16 shows a comparison of the two-dimensional characteristics for the FX05-H-126 with a NACA 8-H-12 profile tested in the same low turbulence wind tunnel and indicates that the FX05-H-126 is an improvement over the NACA profile. To test this airfoil under rotating conditions, a section of the profile was built around a UH-1 tail rotor blade. The two airfoil chord lines were so oriented as to operate at about the same lift coefficient. A result from the flow visualization tests with this profile is seen in Figure 17. A comparison of boundary layer transition for the laminar flow profile with the NACA 0015 profile of the UH-1 tail rotor blade is shown in Figure 18a. Figure 18b gives the length of the total turbulent boundary layer for the standard 0015 and laminar flow profiles and illustrates the existence of a drag bucket for the FX05-H-126 under rotating conditions. The importance of maximizing the laminar flow area is seen in Figure 19 (data from Reference 14). These data point out that both the position of transition point and Reynolds number are first order effects on airfoil profile drag.

Reference 13 gives two-dimensional lift-drag ratios for several airfoils. The variation of profile drag with Reynolds numbers for many airfoil profiles is given in Reference 14, and it is well known that lift curve slope also increases with Reynolds number, to a point. This information leads to an interesting speculation about hovering rotors. It appears from the available data that best efficiency (maximum L/D, minimum C_{d_o}, etc.) will be obtained with the NACA four digit (00XX) profiles at a Reynolds number of about 3×10^6 and with laminar flow profile at about 10^7. Assuming a hovering tip speed of 750 ft/sec, the variation of blade chord keeping constant Reynolds number is shown in Figure 20 and illustrates that laminar flow blades should have significantly more chord than conventional profiles. Integrating all the available information, it appears that there will be appreciable benefits in efficiency if wide chord laminar flow blades (low aspect ratios) are used. Of course, if wide chord blades are to be successful, the tip section will require special treatment to minimize any adverse aspect ratio effects. This is yet another area where more study is needed.

The effects of leading edge roughness were investigated on the FX05-H-126 profile and results from these tests are seen in Figure 21. Figure 21a shows the leading edge of the test specimen which is badly eroded. The wooden blade was eroded by throwing sand into the rotor while operating it at 1200 rpm. Figures 21b and 21c are photographs of the rough blade from the flow visualization tests showing transition on the upper surface. The flow was completely laminar on the lower surface. Operating at the low end of the drag bucket, $\theta_o = 8°$ (compare with X on Figure 16) roughness had no significant effect on the extent of laminar flow on either surface. Figure 21c is for an angle of attack at the high lift portion of the drag bucket (circle on Figure 16) and demonstrates that to a large extent laminar flow

is still maintained. These results are very encouraging and more study with true laminar flow profiles is underway at Bell.

STALL INVESTIGATION

The use of hot wires for accurate boundary layer measurements in hovering is being investigated and Figure 22 gives some results from model tests. The hot wire was located 0.04 inches above the blade surface at 65 percent chord on the upper surface of the blade. These data show, as would be expected, that with increased incidence (forward movement of transition point) the velocity decreases and the turbulence level builds up. The curves have a sharp knee at about 20 degrees of pitch and an associated increase in turbulence level; this point may be stall onset (point X on C_L versus insert). Another change in curvature and increased turbulence level is seen at about 22 degrees which is thought to represent complete separation, or stall (circle an insert on figure).

Stall was also encountered on the UH-1 tail rotor at 20 degrees of collective pitch during the tuft tests. The blade shown in Figure 23 was sprayed with the chemical film and the areas around the tufts exhibit the classical circular motion of tufts in an area of stall.

These data bring up an interesting point which is that clear evidence of stall is shown at very low Reynolds, especially for the 3-inch chord model blades on which the hot wire was mounted. Many investigators have shown that rotating blades at low Reynolds numbers do not show the classical stall brake when thrust is graphed versus horsepower. This effect has been attributed to centrifugal outflow of the boundary layer which gave the blades built-in boundary layer control. The results of this study have shown this concept to be false since the general boundary layer flow direction is inboard and clear indications

of stall have been measured. More refined studies of the properties of stalled flow under rotating conditions is strongly recommended.

FORWARD FLIGHT

Some first results from the effort to extend the boundary layer measurements into forward flight are shown in Figure 24. These data were obtained with a hot wire mounted on a model rotor blade in the Bell wind generator. The advance ratio is 1.0 at the wire location and effects of the reverse flow region can readily be seen. At ψ = 270 degrees, there is a reverse in the velocity curve where the flow at the wire is coming from trailing edge to leading edge.

Efforts are continuing to extend both the experimental and theoretical boundary layer studies into forward flight and the necessary test instrumentation is under development. In addition to the hot wire equipment, a directional pressure probe has been built and a sketch of this instrument is shown in Figure 25. Wind tunnel tests have shown that velocity magnitudes and angles of ±22 degrees from the center line can be read. Rotating tests will be conducted in the future with the probe to determine if it has the necessary frequency for forward flight.

CONCLUDING REMARKS

Extensive experimental studies have been carried out on the boundary layer of a hovering rotor using the chemical film, pressure probe, and hot wire techniques. In conjunction with the experimental work, theoretical analysis has been accomplished to explain some of the experimentally observed phenomena. The following results have been obtained.

1. In hovering, there is no evidence of an outboard flow of the boundary; in fact, a slight inward flow prevails. The theory shows that the vortex field beneath the rotor gives an inward velocity component on the blade lower surface. Experimental evidence gives indication that the forming tip vortex gives an inward velocity on the blade upper surface. The pressure gradient along the span gives an outward acceleration to the boundary layer. Theory for thin airfoils with weak pressure gradients show that pumping effects due to centrifugal force are small.

2. The studies in the boundary layer of a hovering rotor have shown that extensive laminar flow can be maintained, especially with properly designed airfoil profiles. Profiles such as the FX05-H-126 should provide significant improvements in the hovering efficiency of rotors.

3. Clear indications of blade stall have been found experimentally even at very low Reynolds numbers.

4. Initial results have shown that the experimental study of the boundary of a rotor can be extended to forward flight using both hot wire and pressure measuring techniques.

REFERENCES

1. Tanner, W. H., and Yaggy, P. F., Experimental Boundary Layer Study on Hovering Rotors, paper presented before the 22nd Annual National Forum of the American Helicopter Society, May 11-13, 1966.

2. Silverstine, A., and Becker, J. V., Determination of Boundary Layer Transition on Three Symmetrical Airfoils in the NACA Full Scale Wind Tunnel, NACA Report 637, 1938.

3. Hegnett, E. T., and Gibson, M. M., Surface Flow Patterns as Visualized by Dust Deposits on the Blades of a Fan, Journal of the Royal Aeronautical Society, Vol. 67, No. 633, September 1963.

4. Tietjens, O. G., Applied Hydro and Aerodynamics, Dover Publications Inc., New York, 1934.

5. Newman, B. G., Flow in a Viscous Trailing Vortex, The Aeronautical Quarterly, May 1959.

6. Earnshaw, P. B., An Experimental Investigation of the Structure of a Leading Edge Vortex, Aerodynamics Research Committee, London, Report No. 22.876.

7. Hall, M. G., A Theory for the Core of a Leading Edge Vortex, Fluid Mechanics, Vol. 11, pp. 209 to 228, 1961.

8. Fradenburgh, E. A., Flow Field Measurements for a Hovering Rotor Near the Ground, paper presented before the 5th Annual Western Forum of the American Helicopter Society, Los Angeles, September 25-26, 1958.

9. Von Karman, T., Uber Laminare and Turbulente Reibung, Zeitschr.f.angew, Math u. Mech., Vol. 1, pp. 244-247, 1921.

10. Fogarty, L. E., The Laminar Boundary Layer on a Rotating Blade, Journal of Aeronautical Sciences, Vol. 18, 1951.

11. Horlock, J. H., and Wardsworth, J., The Three-Dimensional Laminar Boundary Layer on a Rotating Helical Blade, Journal of Fluid Mechanics, Vol. 23, 1965.

12. Graham, D. J., Nitzberg, G. E., and Olsen, R. N., A Systematic Investigation of Pressure Distributions at High Speeds Over Five Representative NACA Low-Drag and Conventional Airfoil Section, NACA Report No. 832, 1945.

13. Wortmann, F. X., Experimentelle Untersuchungen an neuen Laminar profilen für Segelflugzeuge und Hubschrauber, Z. Flugwiss. 5, 1957.

14. Schlichting, Hermann, Boundary Layer Theory, McGraw-Hill Book Company, New York, 1960.

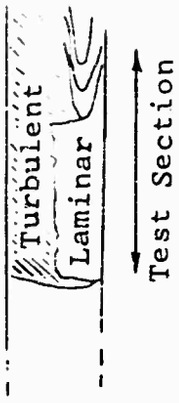

TAIL ROTOR LOWER SURFACE

MAIN ROTOR UPPER SURFACE

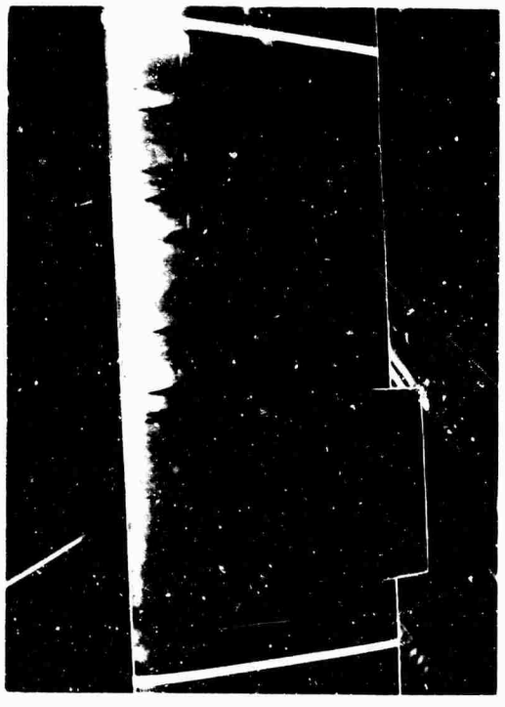

MAIN ROTOR LOWER SURFACE

FIGURE 1. EFFECT OF SURFACE EROSION ON TAIL AND MAIN ROTORS

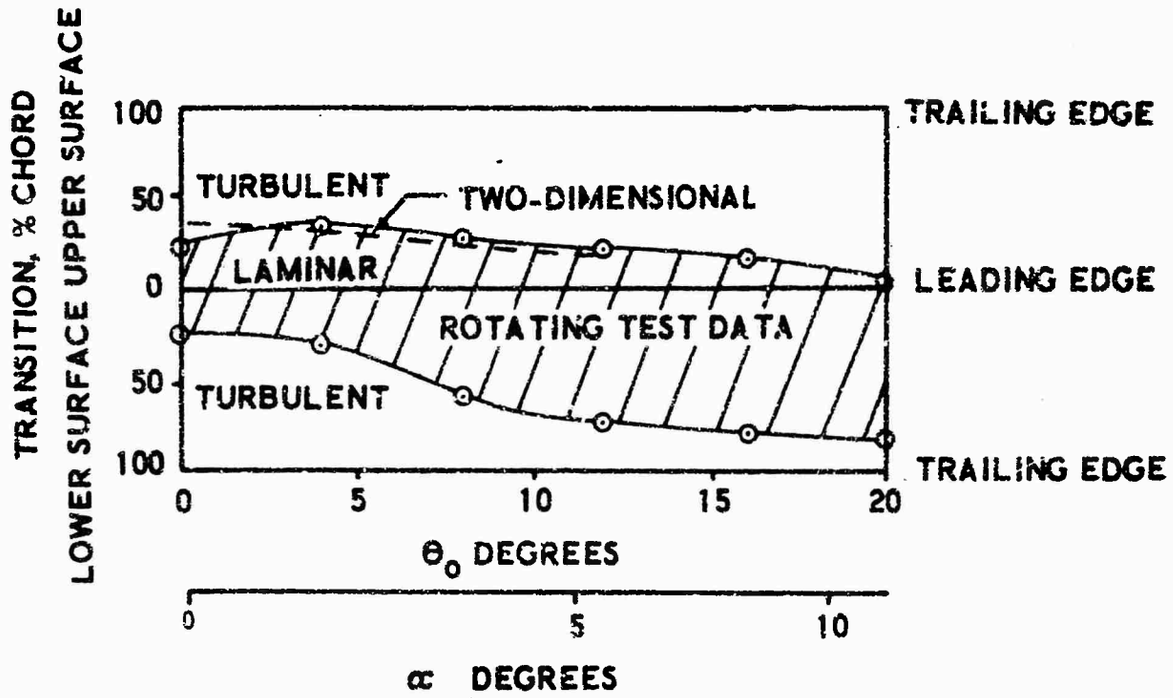

FIGURE 2a. POSITION OF TRANSITION POINT ON UH-1 TAIL ROTOR

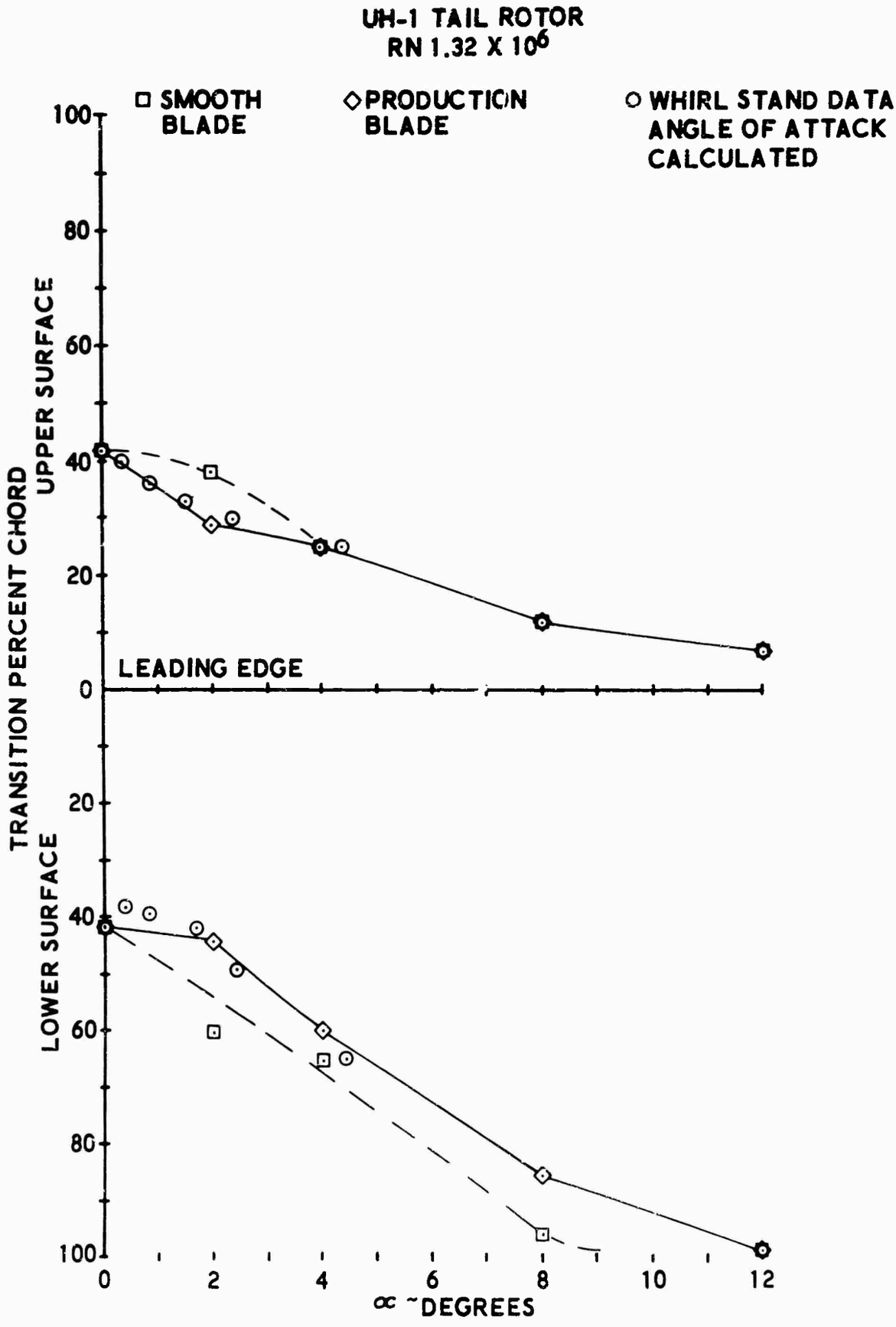

FIGURE 2b. COMPARISON OF WIND TUNNEL AND ROTATING TEST DATA

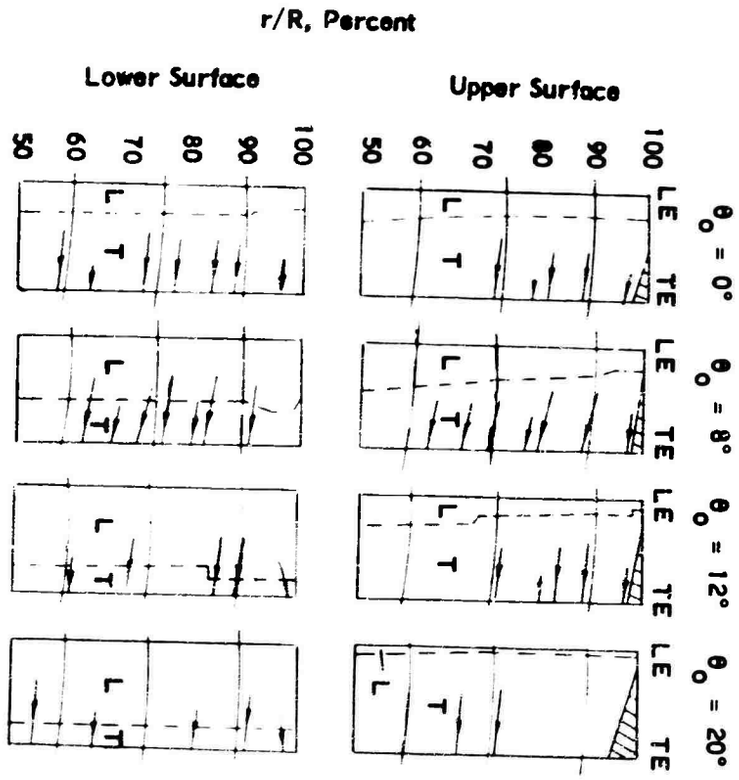

FIGURE 3. BOUNDARY LAYER FLOW PATTERNS AND TRANSITION LINE FROM UH-1 TAIL ROTOR TESTS

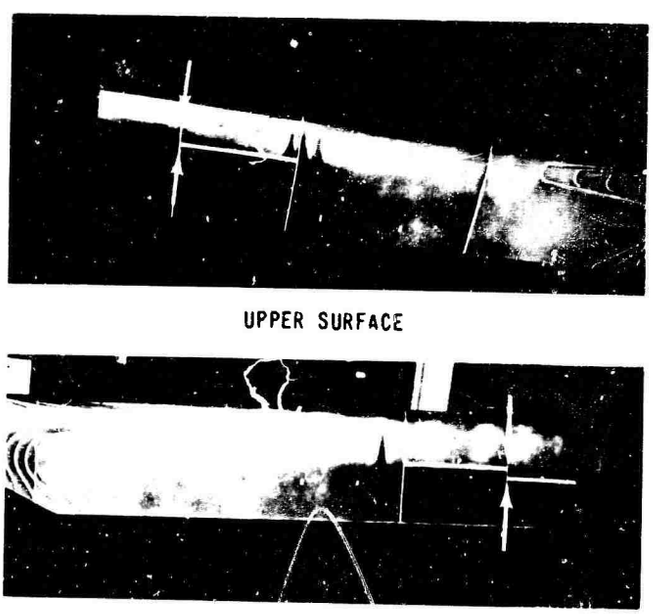

FIGURE 4. SHIFT IN TRANSITION POINT OUTBOARD OF 80 PERCENT RADIUS

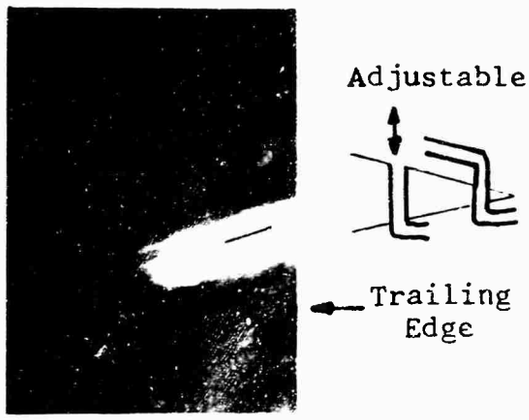

FIGURE 5. PRESSURE PROBE ON UH-1B TAIL ROTOR BLADE

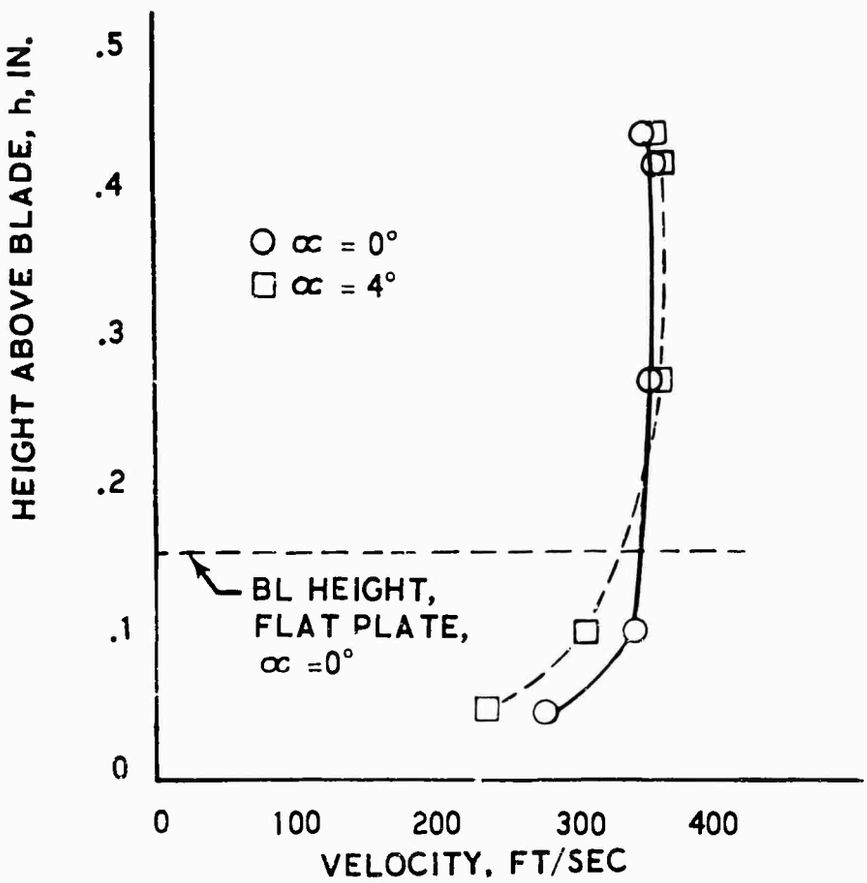

FIGURE 6. BOUNDARY LAYER VELOCITY PROFILES MEASURED WITH PRESSURE INSTRUMENTATION IN WIND TUNNEL

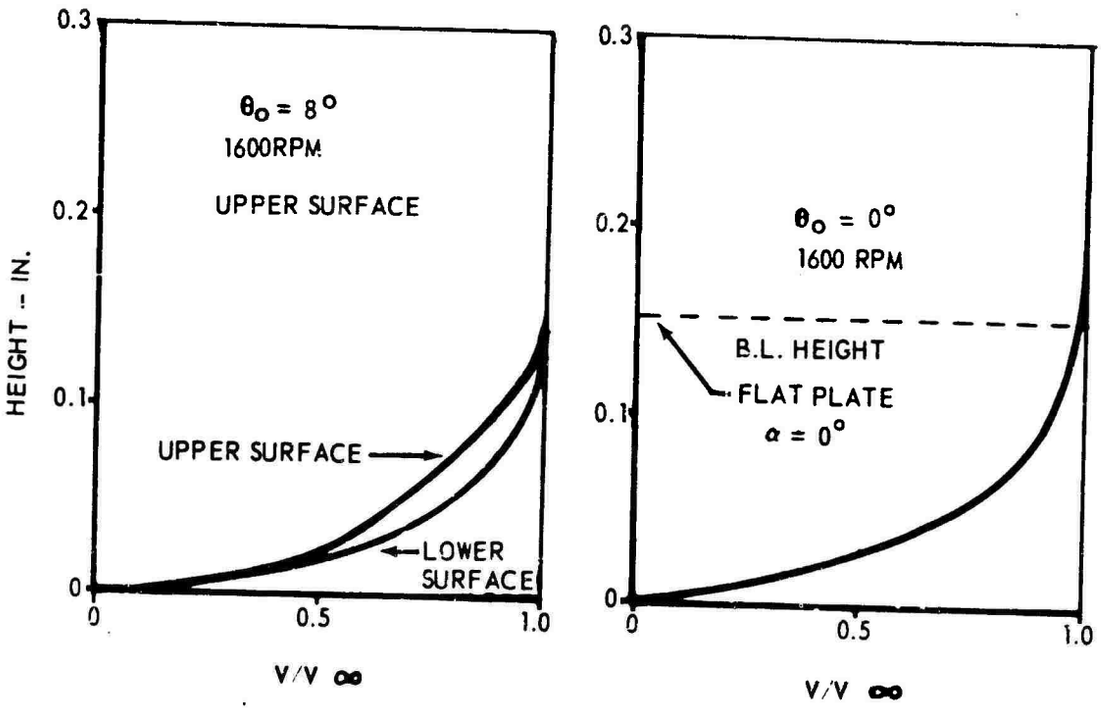

FIGURE 6a BOUNDARY LAYER VELOCITY PROFILES MEASURED WITH PRESSURE INSTRUMENTATION ON ROTATING BLADE

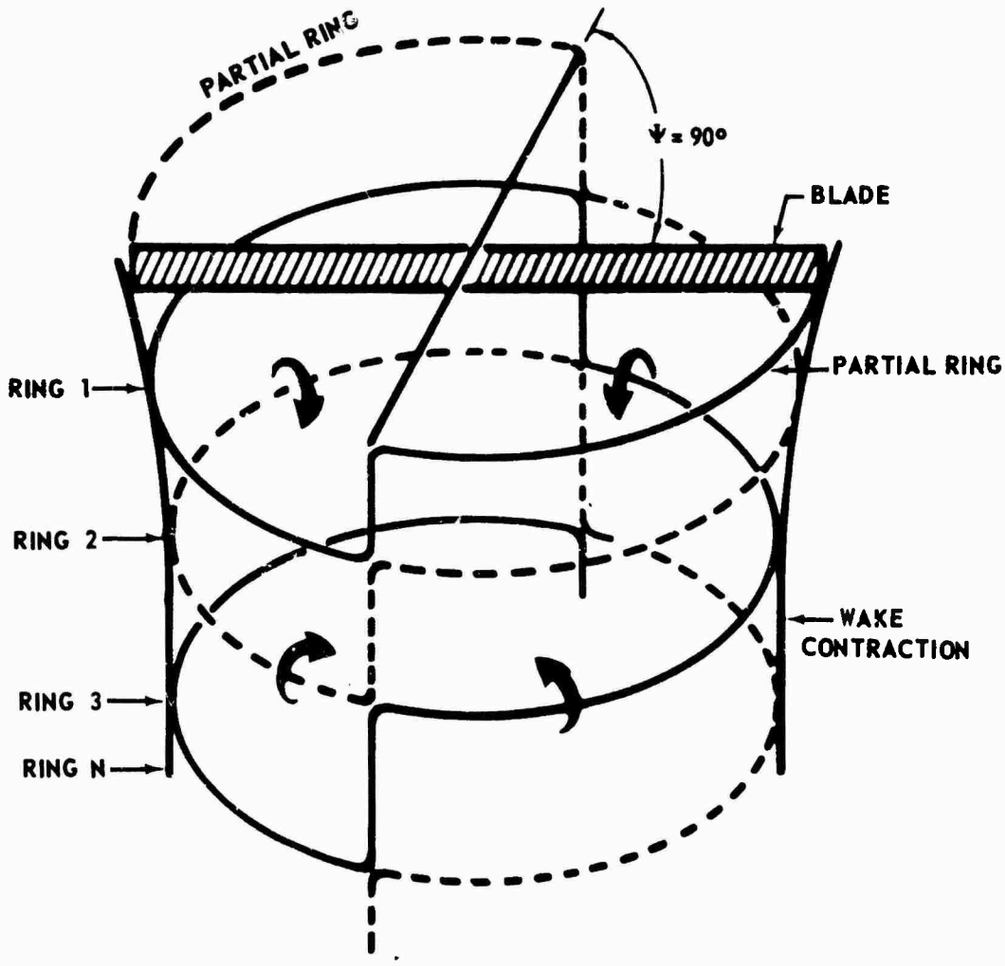

FIGURE 7. SKETCH OF MATHEMATICAL WAKE MODEL

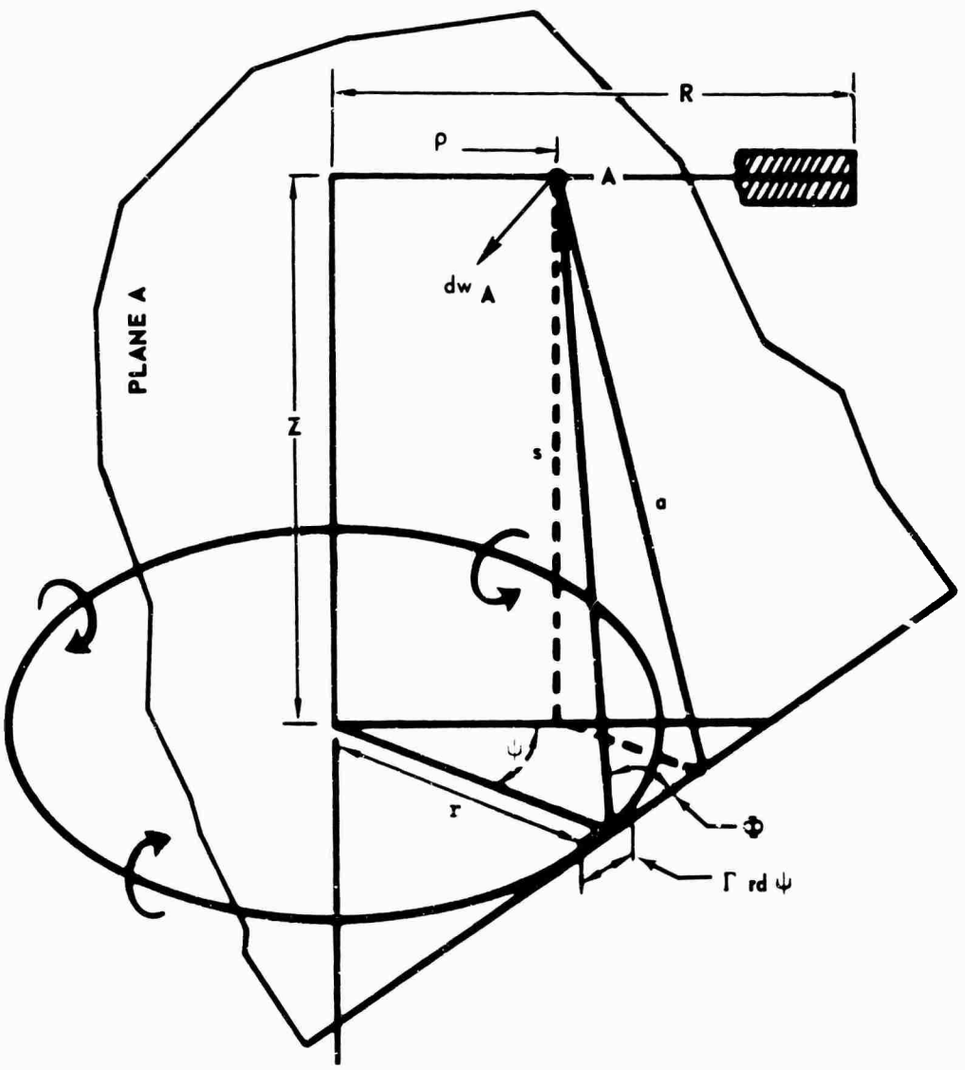

FIGURE 8. RESOLUTION OF AN ELEMENT OF A VORTEX BELOW THE ROTOR INTO THE TIP PATH PLANE

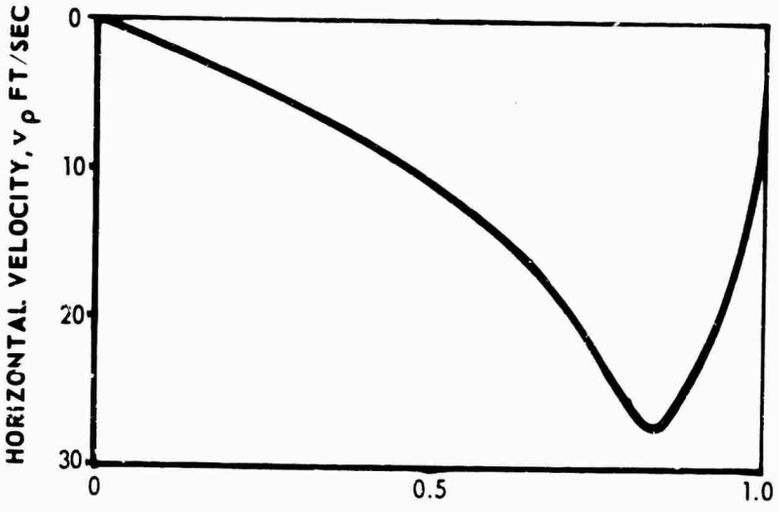

9a

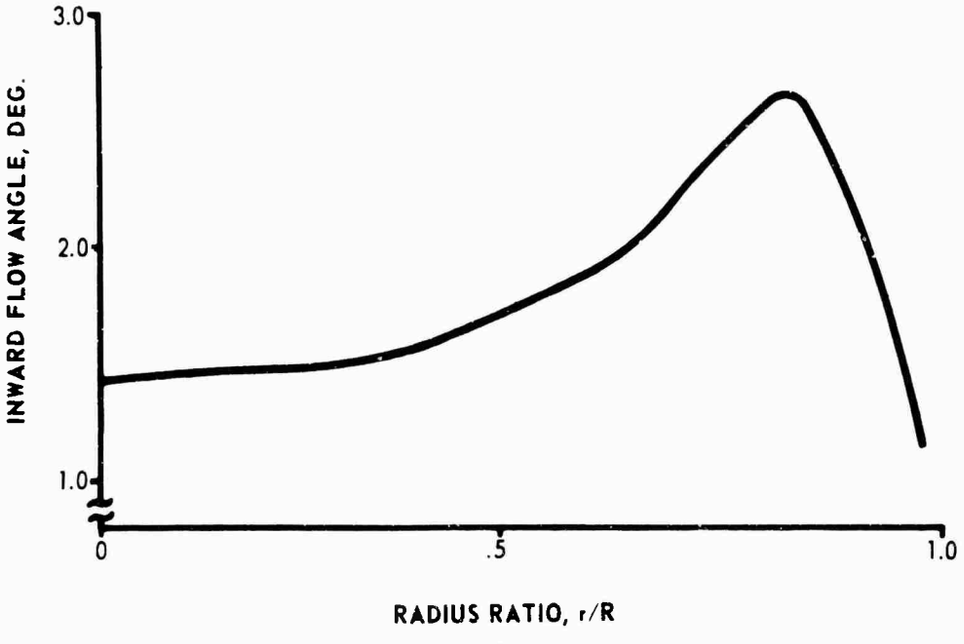

9b

FIGURE 9. THEORETICAL RADIAL VELOCITY AND INWARD FLOW ANGLE

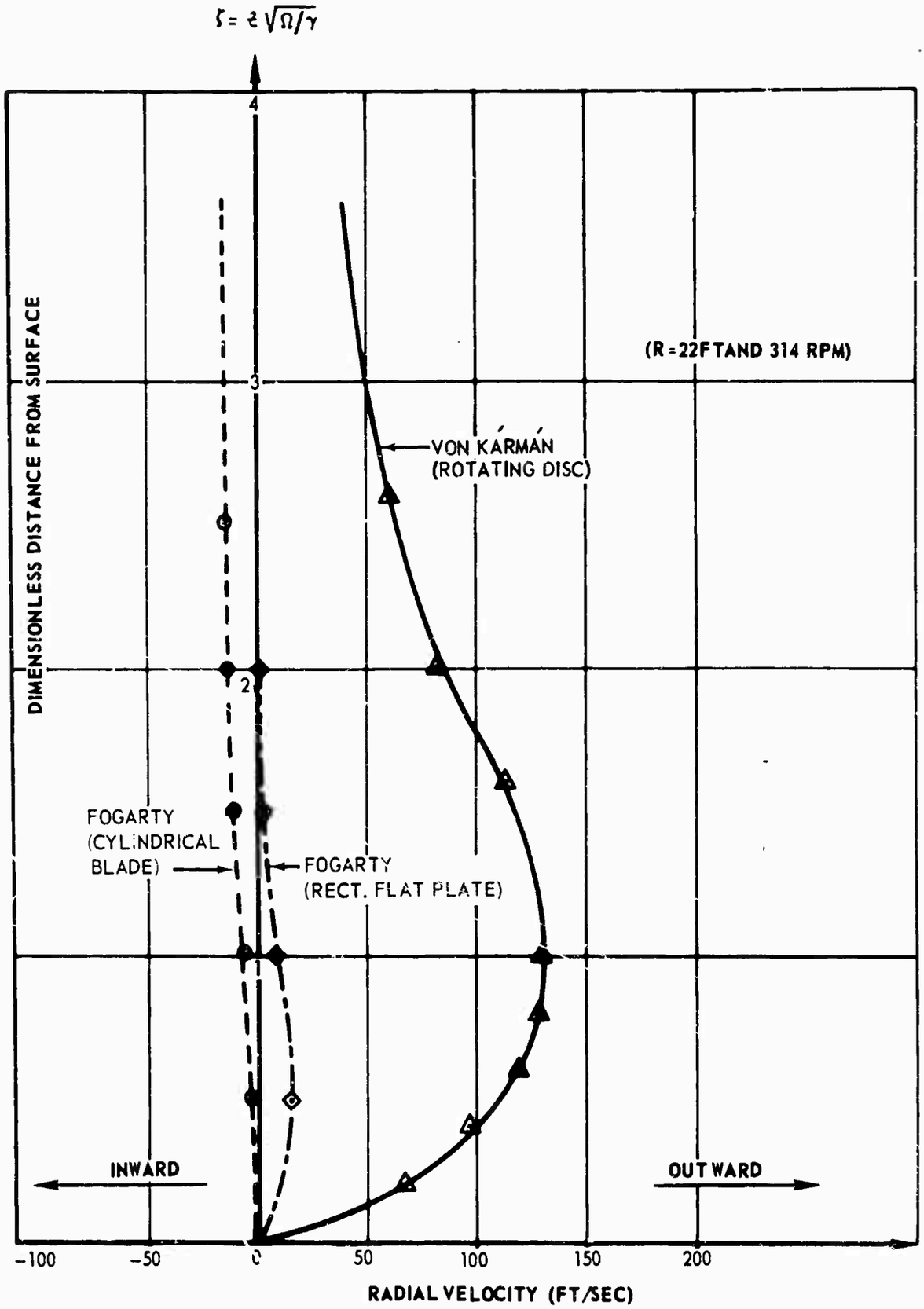

FIGURE 10. CALCULATED RADIAL VELOCITIES DUE TO CENTRIFUGAL FORCE

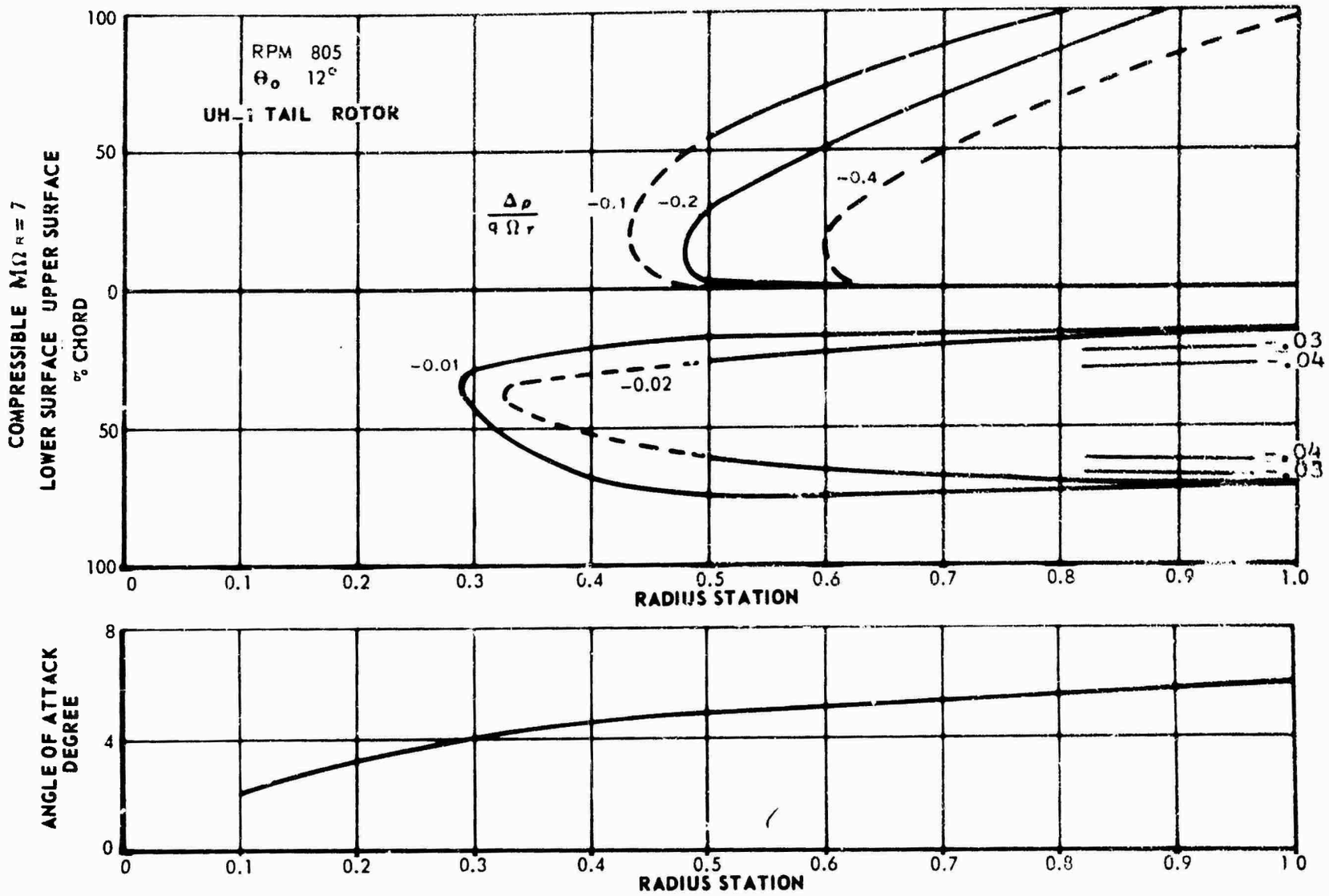

FIGURE 11. SURFACE PRESSURE DISTRIBUTION ON UH-1 TAIL ROTOR

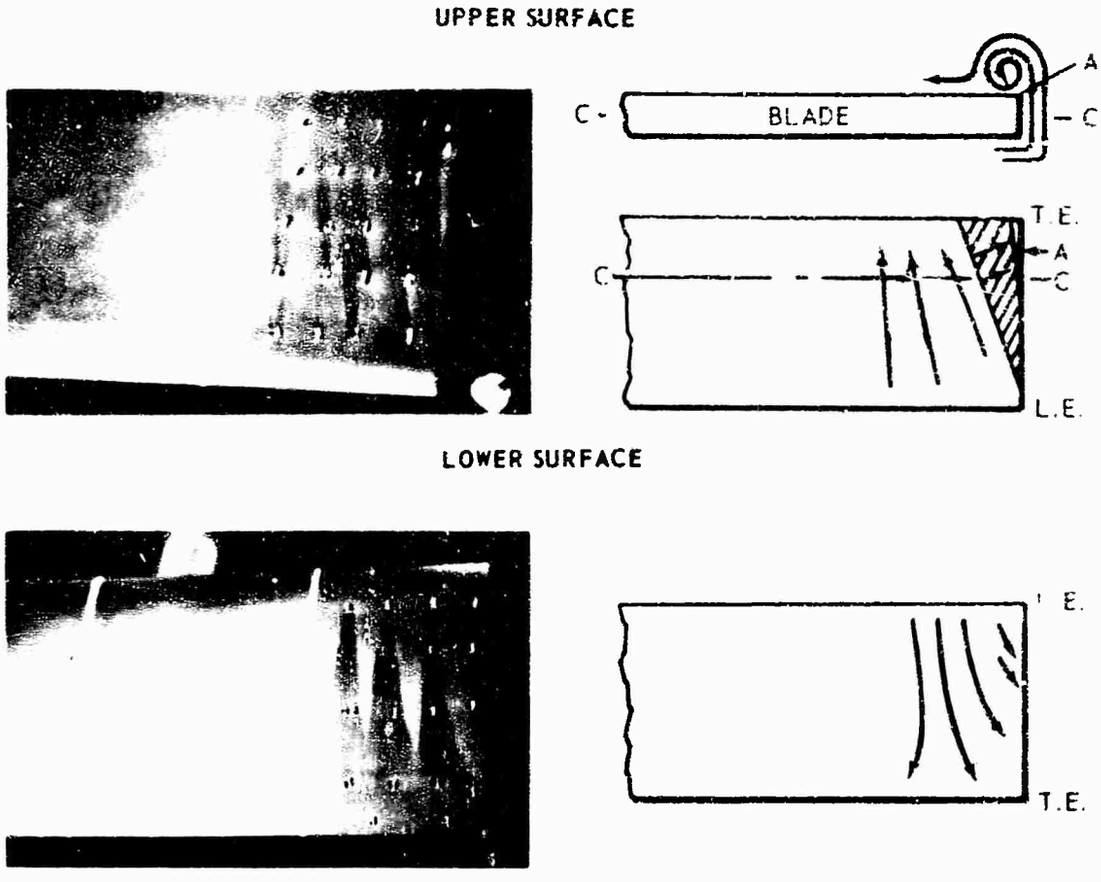

FIGURE 12. FLOW VISUALIZATION OF TIP VORTEX

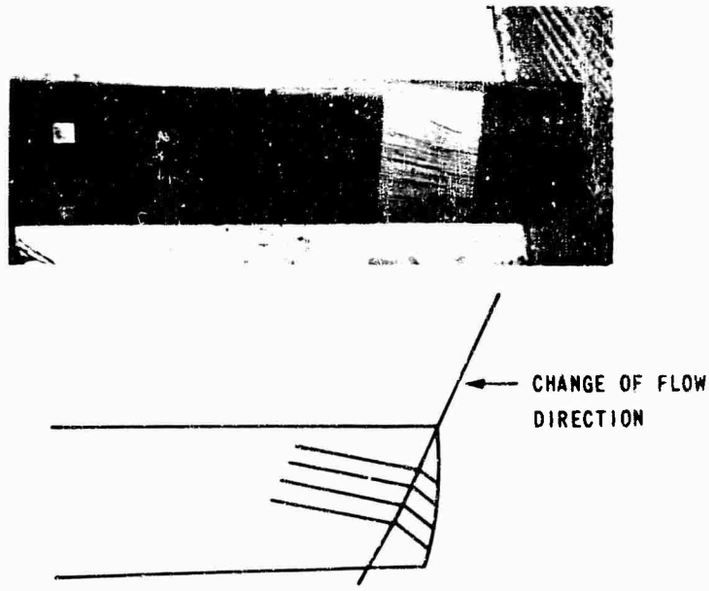

FIGURE 13. OIL FILM SHOWING TIP VORTEX EFFECT

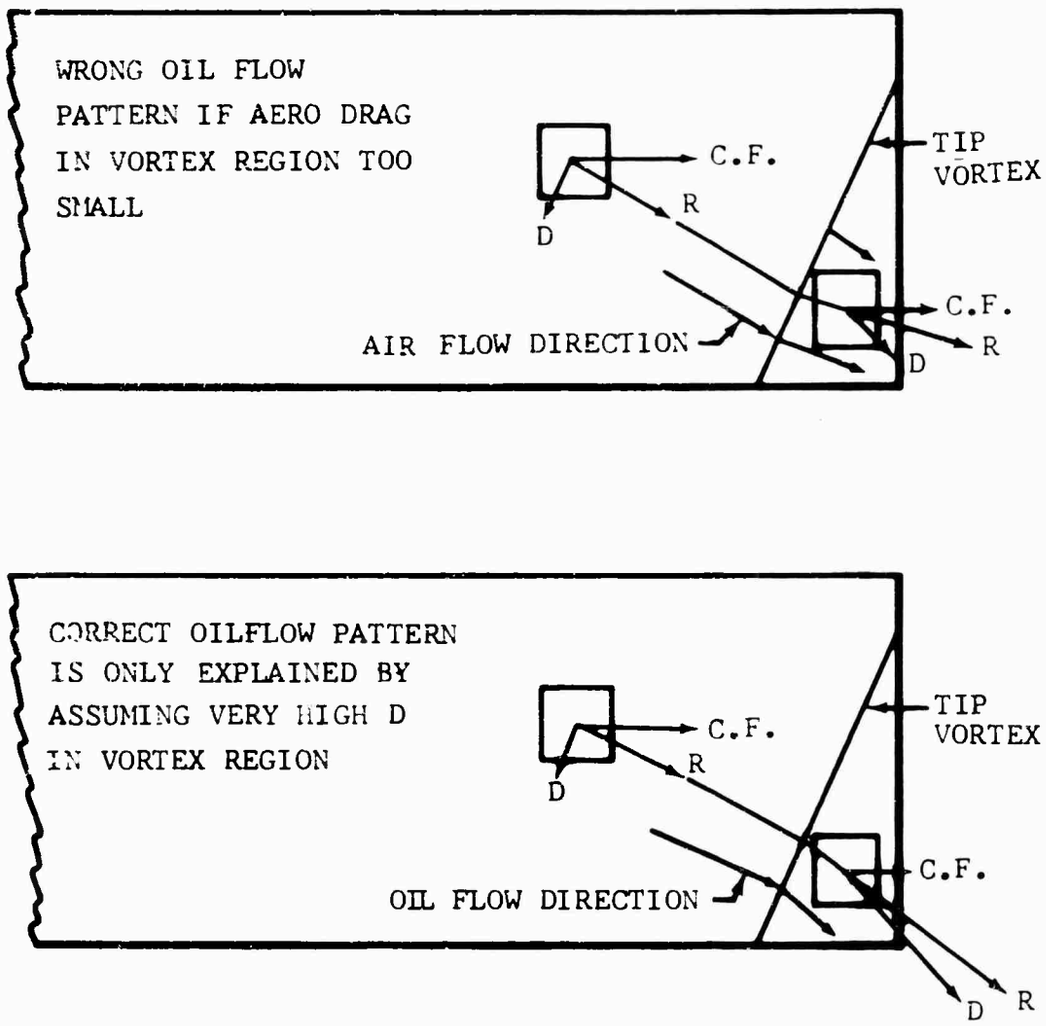

FIGURE 14. SKETCH OF FLOW DIRECTION AND FORCES AT TIP OF BLADE

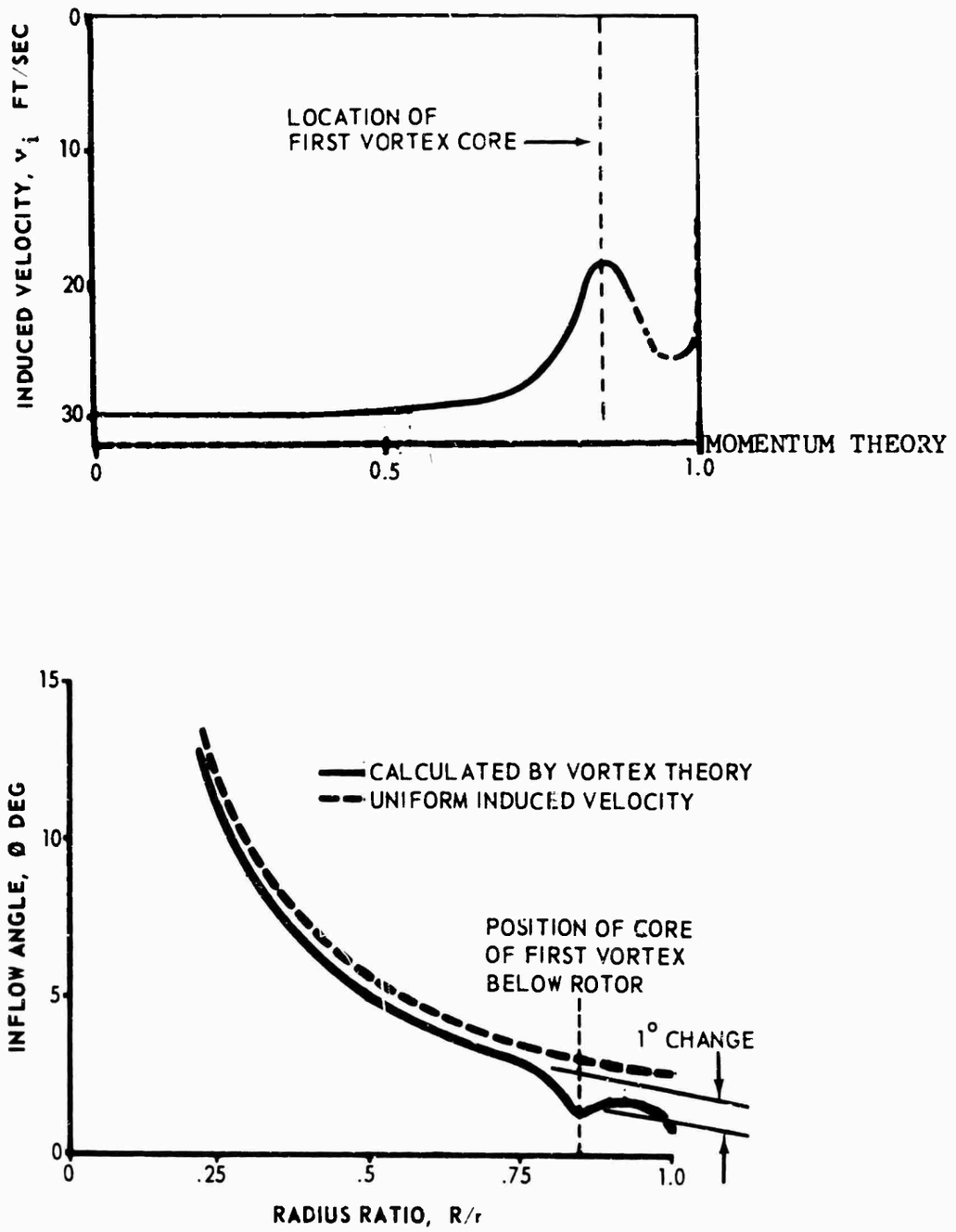

FIGURE 15. THEORETICAL AXIAL FLOW VELOCITY AND INFLOW ANGLE

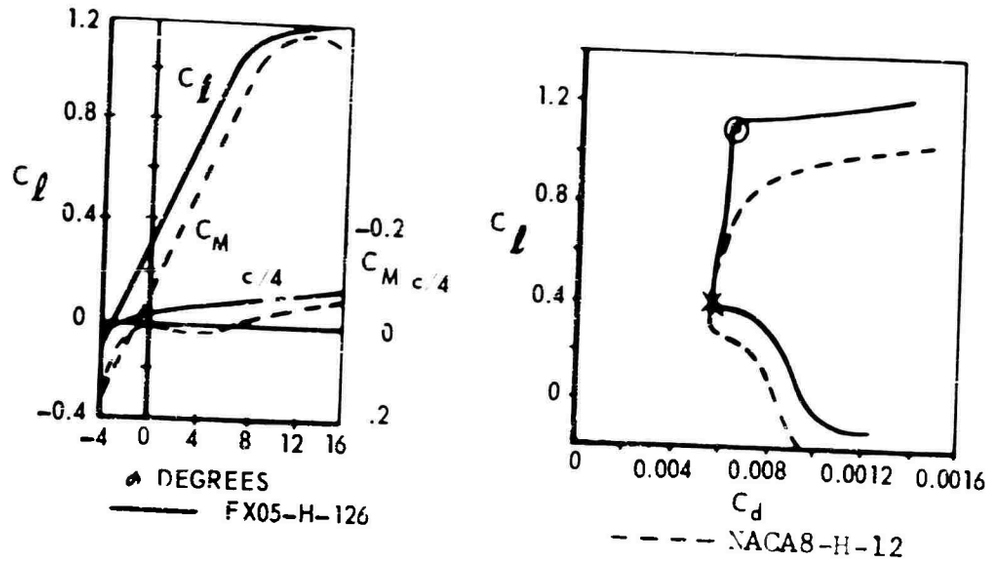

FIGURE 16. COMPARISON OF LAMINAR FLOW PROFILE TWO-DIMENSIONAL CHARACTERISTICS

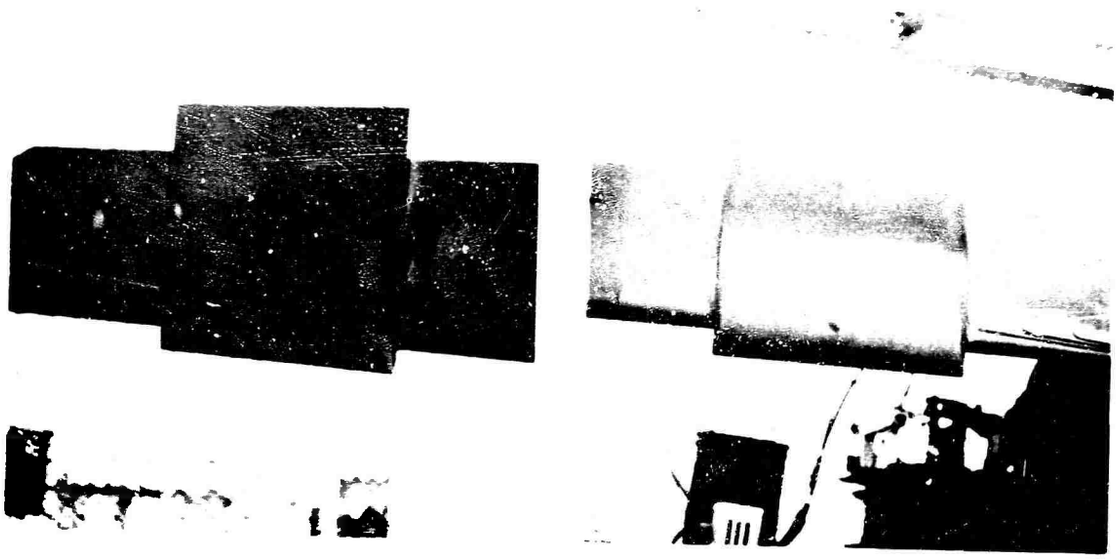

Re . . . . . 1.0 x 10^6
Centrifugal Accel. . 520 g's
Chord . . . . . 11.75 in.
C_l 0.6

FIGURE 17. LAMINAR FLOW PROFILE ON A TAIL ROTOR BLADE

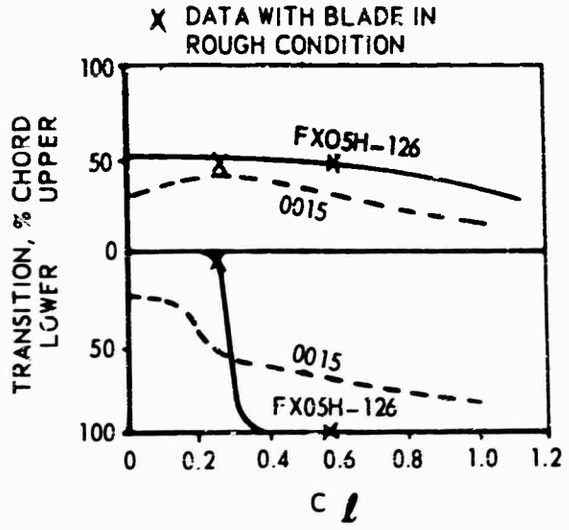

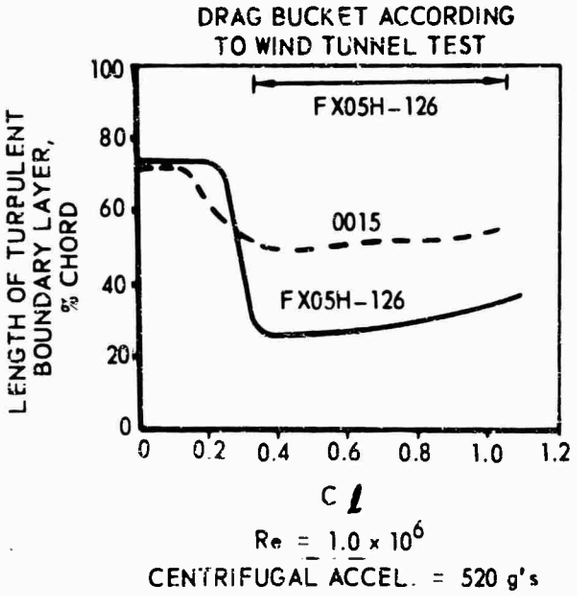

FIGURE 18. COMPARISON OF 0015 AND FX05H-126 TRANSITION CHARACTERISTICS

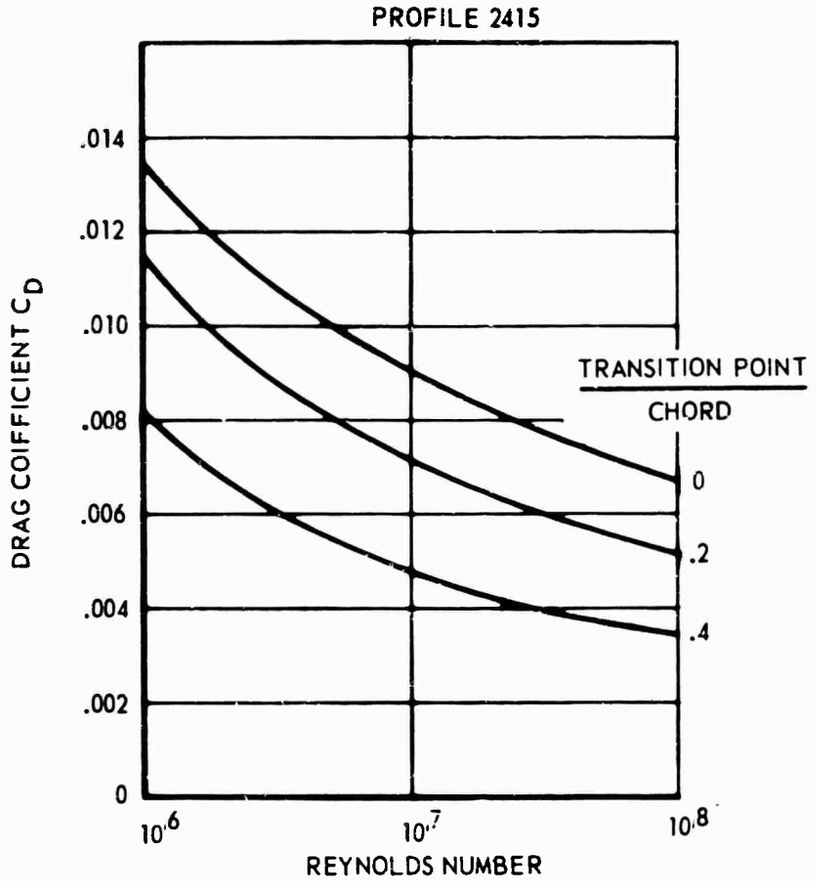

FIGURE 19. INFLUENCE OF TRANSITION POINT WITH REYNOLDS NUMBER, ONE SURFACE

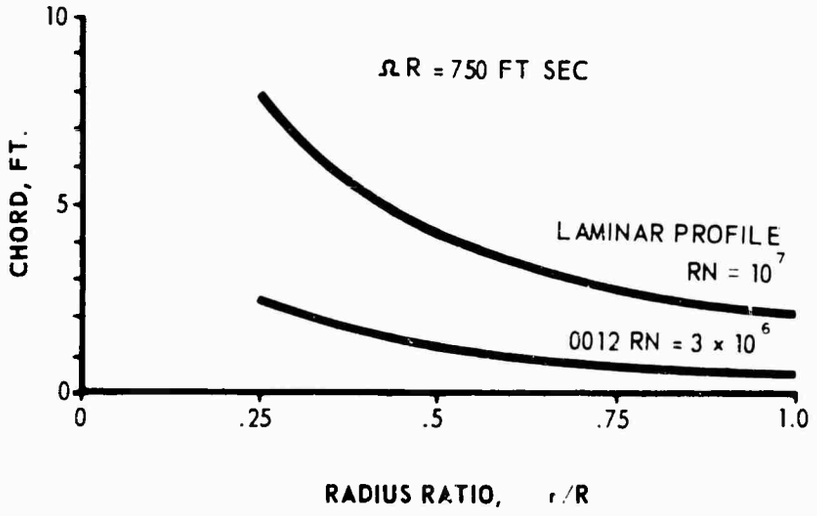

FIGURE 20. COMPARISON OF IDEAL CHORD FOR CONVENTIONAL AND LAMINAR FLOW PROFILES

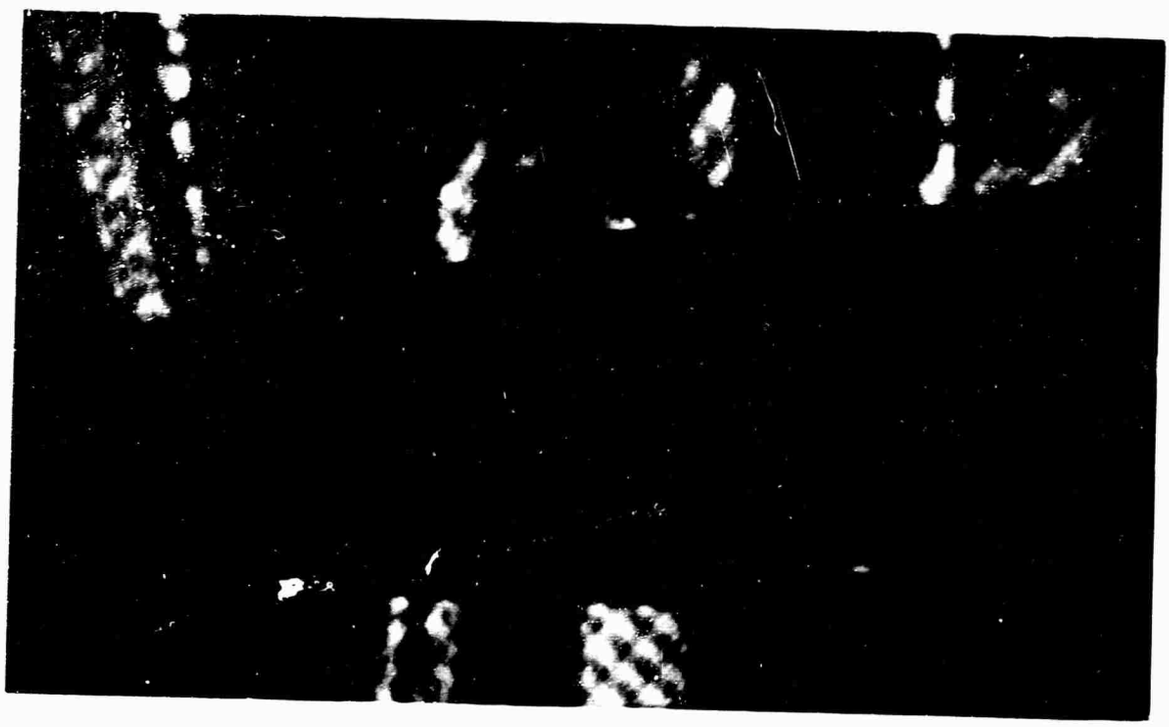

LEADING EDGE

A

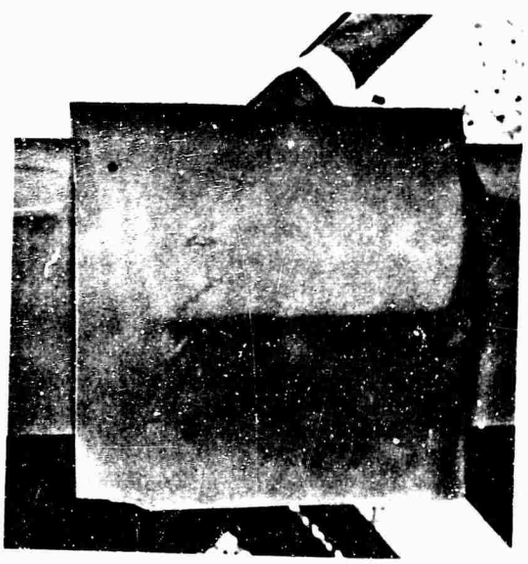

θ_o = 8

B

θ_o = 16°

C

FIGURE 21. CHEMICAL FILM RESULTS FROM ROUGHNESS TESTS WITH LAMINAR FLOW PROFILE

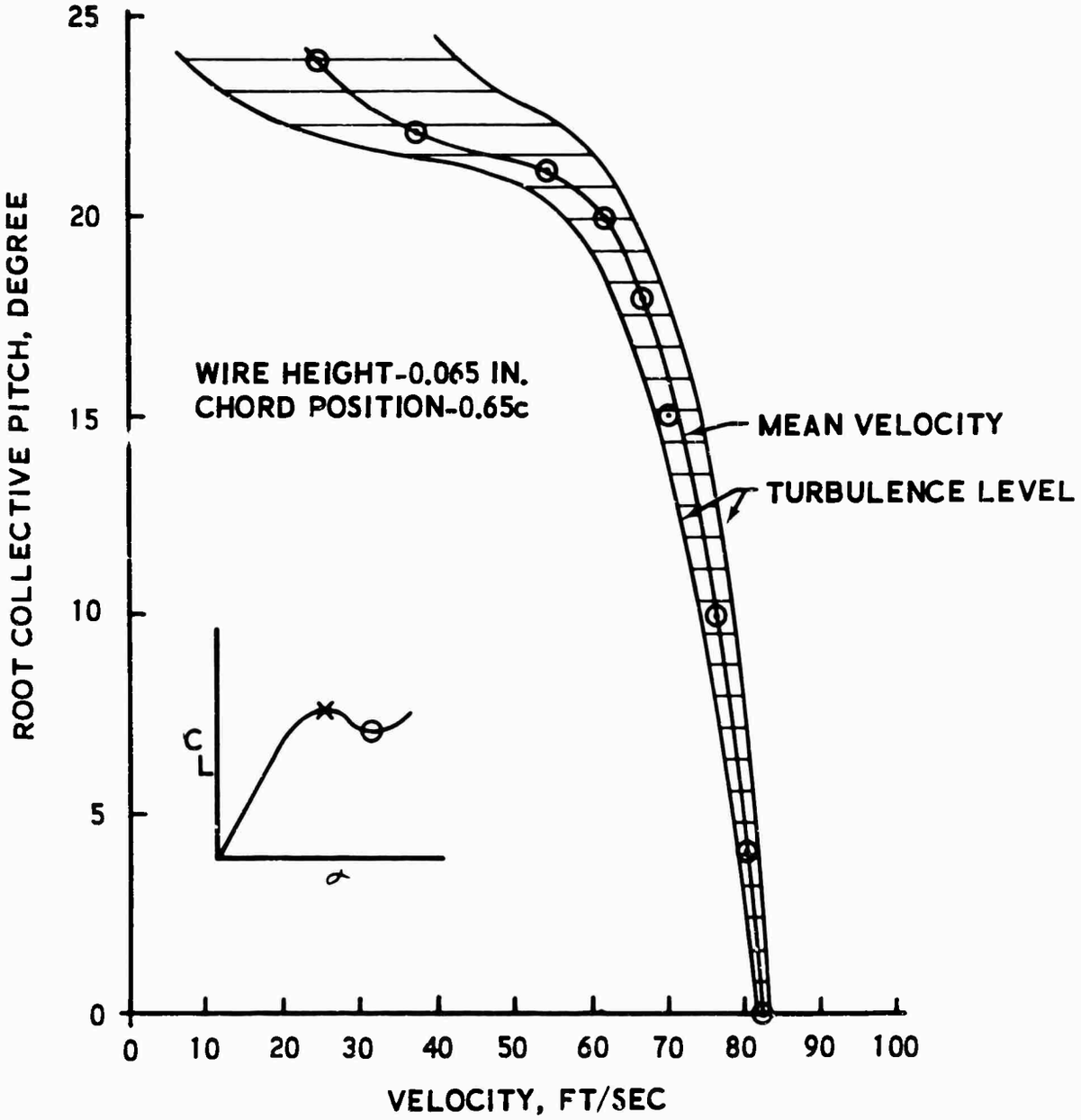

FIGURE 22. FLOW VELOCITY AND TURBULENCE MEASUREMENTS USING HOT WIRE TECHNIQUE

FIGURE 23. STALL EVIDENCE FROM TUFT TESTS

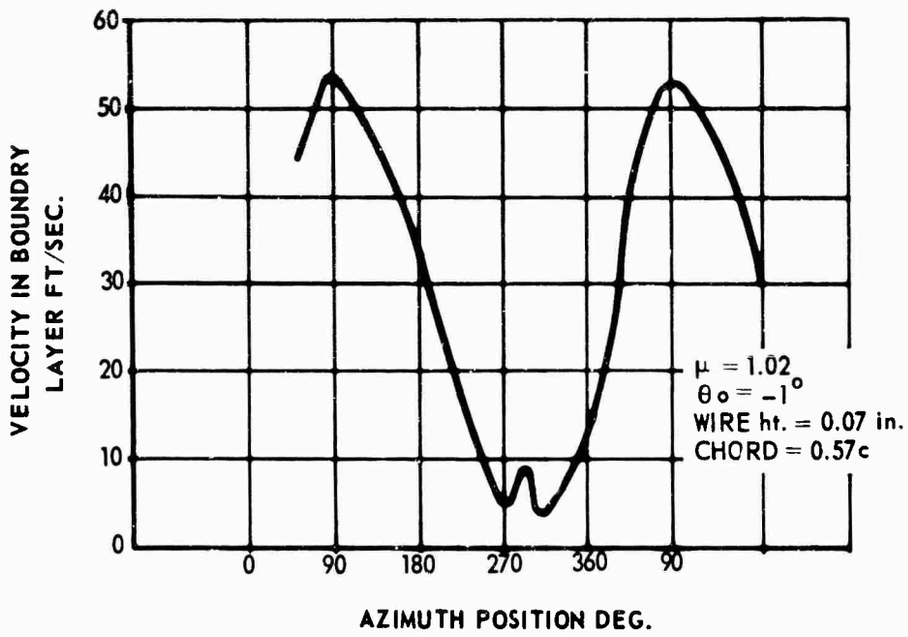

FIGURE 24. BOUNDARY LAYER MEASUREMENTS USING HOT WIRE IN FORWARD FLIGHT

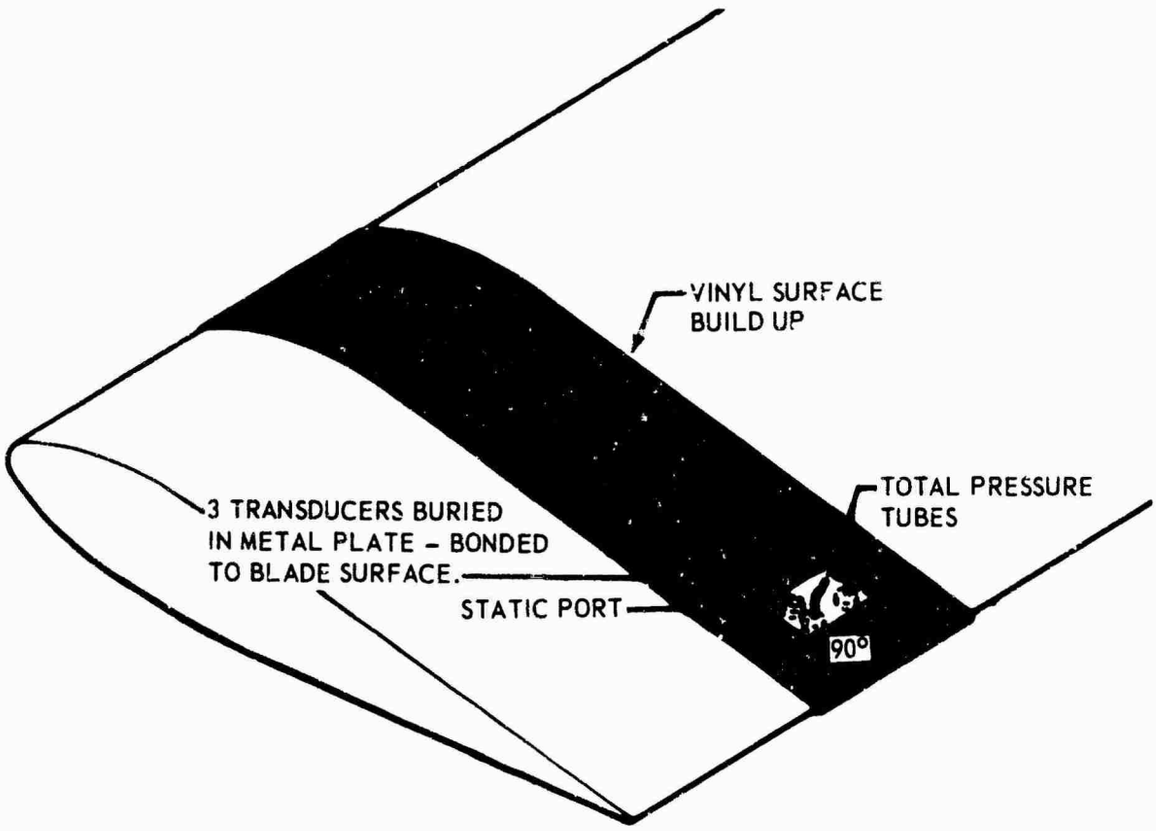

FIGURE 25. SKETCH OF DIRECTIONAL PRESSURE PROBE

AN INVESTIGATION OF THE FEASIBILITY OF A COMMON BOUNDARY LAYER CONTROL SYSTEM FOR HIGH-LIFT AND LOW-DRAG ON AN AIRFOIL SECTION

by

SEÁN C. ROBERTS

Mississippi State University
Aerophysics Department
State College, Mississippi, U.S.A.

INTRODUCTION

For a considerable number of years, boundary layer control has been successfully applied to aircraft wings to increase their lifting capability. This boundary layer control has been suction through discrete or distributed orifices or tangential blowing to maintain an attached turbulent boundary layer in severe adverse pressure gradients. Distributed suction high-lift aircraft have successfully flown in England, Holland, and in the United States where aircraft lift coefficients greater than 5.0 have been achieved on light aircraft. Blown flaps have been successfully used on high-speed strike aircraft such as the British Buchaneer and the U.S.A. Phantom to enable them to successfully land on aircraft carriers.

However, even though boundary layer control has been used in the low-speed, high-lift case, very little attempt has been made to use this installed system to improve the cruise conditions. Boundary layer control used to decrease the drag of bodies by means of the stabilization of the laminar boundary layer has been considered for a number of years. Head, Lachmann, and Pfenninger (References 13, 14, and 15) have successfully flight tested test sections where a 100-percent chord laminar boundary layer

was achieved. Pfenninger has successfully applied laminar boundary layer control to a large jet aircraft through suction slots resulting in a reduction of the aircraft drag thereby extending the aircraft range; however, the cost of obtaining laminar flow is high, not only in engineering and construction costs but also in considerable maintenance costs. Airfoil and slot cleaning between flights and in-flight leading edge cleaning to remove insects account for the high cost of maintenance. In the particular case of STOL aircraft where a slow flying capability is important, the low-drag boundary layer suction laminar boundary layer control system must be compatible with the high-lift boundary layer control system. At the present time, it is not possible to effectively have both a high-lift and a low-drag laminar suction boundary layer control system on a single wing. Eppler's (Reference 3) explanation for this consists essentially of two incompatible criteria - porosity distribution and blower requirements.

The attractiveness of having both a high-lift and a low-drag boundary layer control system on a single wing is appreciable as the possible extention in speed range could be considerable and the hardware for the system would be used in all flight modes, thereby reducing the dead weight penalty normally incurred with boundary layer control systems.

When all possible combinations of the high-lift systems and the low-drag systems are considered, it becomes increasingly obvious that the distributed suction approach is probably more compatible than any of the blowing systems, and a quantitative calculation of the boundary layer control system indicates (Reference 16) that continuous distributed suction is more economical than discrete suction. Since distributed suction boundary layer

control for laminar stabilization has also been reasonably successful, it would appear that the combination of the two systems would be the logical choice. Unfortunately, the difficulties, such as close tolerance on section waviness and smoothness, and insect contamination, that arise with laminar boundary layer control make it difficult to incorporate on operational aircraft even though there have been a number of studies on things such as in-flight cleaning and on jettisonable wing covers. Therefore, the need for a low-shear turbulent boundary layer control system which can be incorporated with a high-lift boundary layer control system is obvious.

In 1953 Carmichael (Reference 1) performed some experiments on leading edge blowing in an attempt to artificially thicken the laminar boundary layer so that it would be less sensitive to surface irregularities than the normal thin leading edge boundary layer. It would appear that if this approach were extended to thickening the boundary layer so that the velocity profile would be distorted, then considerable reductions in skin friction could be achieved. The outflow quantities for such effects on the laminar boundary layer would probably promote transition to turbulence and the flow would be of a more natural turbulent nature. Pappas and Okuno (Reference 8) performed significant experiments in 1965 on the measurement of skin friction on a slender cone with air injection which indicated that skin-friction reduction up to 50 percent of the turbulent boundary layer without air injection was possible with reasonable transpiration velocities in the subsonic case. Black and Sarnecki (Reference 2) developed a method of determining the skin friction of a turbulent boundary layer with transpiration from the boundary layer velocity profiles which predicted that zero or

negative skin friction could be obtained in an attached turbulent boundary layer. The concept of the skin-friction reduction of a turbulent boundary layer with transpiration would appear to be worthy of consideration for application to a subsonic wing since the technique is currently being investigated for the reduction of skin friction and the increase of heat transfer on reentry vehicles (References 4, 5, and 6).

The advantages of such a low-shear turbulent boundary layer control system would be that surface irregularities would have less significance than they would with a laminar flow system and, also, structural and surface tolerances would be increased thereby reducing the initial cost of the aircraft. Maintenance costs would be reduced by the elimination of special leading edge and slot cleaning between flights, thereby indicating that such a low-shear system would be preferable to a laminar flow system. Another major advantage of the low-drag turbulent boundary layer control system over the laminar system is that it would probably lend itself to being used in conjunction with a high-lift boundary layer control system where in both cases the porosity starts very near the leading edge.

The purpose of this paper is to indicate possible solutions to the problem of a combined low-drag and high-lift boundary layer control system and to expose areas where further basic research and development work still needs to be performed prior to the development of a practical system.

DISTRIBUTED SUCTION HIGH LIFT BOUNDARY LAYER CONTROL

To prove effective a boundary layer control system must not only increase the lift of the wings but also utilize sufficiently low horsepower that a net gain in takeoff performance must result when the power for the

system is taken from the main power plant. Also, the system must be mechanically simple, light, reliable and easily maintained. A distributed suction high-lift boundary layer control system employs the use of suction through a porous material or perforations distributed in the upper surface of the airfoil in a manner which closely approximates continuous distributed suction. Since the same airfoil section is to be used for distributed fluid injection, it is essential that a porous material is used on the surface rather than discrete perforations. Discrete perforations perform satisfactorily in the suction case since the three-dimensional discontinuity of the jet through the hole is inside the wing, and the entrained flow outside the wing closely approximates distributed suction. However, if discrete holes are used in the fluid injection case, the discontinuity of the jet through the hole would be outside the surface and the result would not approximate distributed injection.

In designing a high-lift boundary layer control system, the amount and distribution of the required suction can be computed from the von Kármán momentum equation

$$V_w = \theta' + \frac{\theta U'}{U}(H+2) - \frac{1}{2} C_f U$$

The above equation can be used to obtain V_w if all the unknowns can be computed from theoretical considerations. The pressure distribution around an airfoil can be closely approximated by using the potential flow methods of Theodorsen and Pinkerton so that the unknowns U and U' can be found if the angle of attack of the airfoil and the anticipated value of local lift coefficient are known. The value of H is reasonably constant for

an attached turbulent boundary layer, and the final inflow velocity results are very insensitive to small variations in H. θ' can be approximated by either assuming θ or R_θ as a constant and C_f can be found from the impervious skin-friction relationship developed by Ludwieg and Tillmann (Reference 10)

$$\left(\frac{U_I}{U}\right)^2 = 0.123\left(\frac{U\theta}{\nu}\right)^{-.268} 10^{-.678H}$$

The remaining unknown is the value of θ_i at the position on the airfoil where suction begins. The values of θ_i can be calculated from the equation developed by Tani when the local velocity distribution around the airfoil is known.

$$\frac{\theta_i^2}{\nu} = 0.44\, U_i^{-6} \int_0^x U^5\, dx.$$

The total flow requirements are found by an integration process of the local suction velocity over the entire wing and together with the pressure differentials required for suction which are found from the external pressure distribution, a suction pump can be designed for the system.

Practical Application of Distributed Suction High-Lift Boundary Layer Control

TG-3

As a preliminary test the porosity distributions calculated above were applied to a TG-3 sailplane as shown in Figure 1. With the result that the maximum lift coefficient of the unflapped wing was increased from 1.4 to 2.1, although obviously not an STOL vehicle, the system clearly demonstrated

the gains that could be achieved by distributed suction boundary layer control systems. The power required for the operation of the axial flow pumps was supplied by a 24-volt battery. A diagram of the boundary layer control system used on this aircraft is shown in Figure 2.

L-21

An L-21 aircraft (Figure 3) was later modified to accept a boundary layer control system similar to that in the TG-3 sailplane; however, in this particular case the suction air was passed along the inside of the wing through a double windshield and was used to cool the engine so that additional cooling was not necessary and the intakes were sealed. The pumps were mechanically linked to the engine with the result that full boundary layer control was available for takeoff at high engine r.p.m. but not available for landing. This condition made the aircraft unsuitable for STOL performance although it did demonstrate that aircraft lift coefficients of 4.2 could be obtained with the expenditure of approximately 10 horsepower from the engine.

L-19

A third aircraft used in the STOL research program at Mississippi State University was a modified L-19 (Figure 4). A boundary layer control system similar to those of the TG-3 and the L-21 was installed together with pertinent modifications suggested by the previous research. Two hydraulically driven axial flow pumps were fitted to the airplane, one under each wing, powered by a hydraulic pump at the main engine. In this case the boundary layer control could be varied independently of the engine speed, thereby

making the system suitable both for takeoff and landing modes. In the course of the research on this vehicle, it became necessary to perform certain modifications such as increasing the size and shape of the vertical fin and rudder to give adequate directional control at low forward velocities. The flap was modified to eliminate the slot and the sharp geometric discontinuity normally associated with flaps, so that attached flow could be maintained on the flaps without incurring a penalty of increased suction due to the severe adverse pressure gradient. It is interesting to note that as the turbulent boundary layer separation was suppressed at the trailing edge by distributed suction and higher lift coefficients were achieved, the condition of the laminar boundary layer at the leading edge became increasingly important. Due to the severe pressure gradients and the centrifugal forces involved in rounding a relatively sharp leading edge, local laminar boundary layer separation occurred, and when reattachment failed to occur, the loss of lift was quite abrupt. To overcome this condition the leading edge radius was increased 50 percent which effectively reduced the forces acting on the boundary layer ensuring attached leading edge flow.

The high-lift L-19 had a minimum flying speed of 31.0 miles per hour at maximum gross weights which is equivalent to an aircraft lift coefficient of 5.1 with the expenditure of 12 horsepower from the main engine.

Airfoil Section for High-Lift Boundary Layer Control

The airfoil section most suitable for high-lift boundary layer control is a thick, highly cambered section with a large leading edge radius. The major difficulty associated with using thick, cambered airfoils for high lift is that the drag penalty in the cruise condition is large. To

overcome this problem flaps are generally used to change the effective camber of the airfoil which is designed for the cruise condition. Unfortunately, flaps have associated problems when incorporated with a distributed suction boundary layer control system (Reference 11), and it is more economical and mechanically simpler if conventional flaps are replaced by wing bending or camber changing mechanisms.

The design and feasibility of a variable camber wing has been demonstrated by two vehicles which have successfully flown at Mississippi State University with a variable camber wing, i.e., the XAZ-1 and the XV-11A. The variable camber wing is manufactured from glass fiber materials and the longitudinal members in the wing are joined to the top and bottom airfoil surfaces with piano hinges which allow angular movement of the structural members relative to the skin. A model of the variable camber mechanism is pictured in Figure 5 which shows the two curved arms that rotate on bearings which are used to vary the camber to any position between the limits. Figure 6 shows the variable camber wing on the XV-11A.

The use of the variable camber wing is an excellent means of obtaining two airfoil shapes with a single section which could be used for both high-lift and low-drag when boundary layer control is used in both cases. The use of the variable camber mechanism could be expanded to obtain cruise airfoil shapes other than those shown in Figure 5 by suitable selection of the curved areas.

LOW-SHEAR TURBULENT BOUNDARY LAYER CONTROL SYSTEM

In the field of supersonic aerodynamics, considerable theoretical and experimental work has been performed investigating the effect of fluid

injection into the supersonic boundary layer to reduce the surface shear and increase the heat transfer. Mickley and Davis (Reference 6) predicted considerable decreases in skin friction for the subsonic case, and Pappas and Okuno (Reference 8) performed drag measurements on a slender cone up to Mach numbers of 4.5 with fluid injection. Their results indicate a 50-percent reduction in skin friction due to air injection (Figure 7).

Black and Sarnecki (Reference 2) developed a technique based on the law of the wall in the inner region of the turbulent boundary layer to analyze the turbulent boundary layer velocity profile with suction or injection. Using this technique to analyze boundary layers measured by Mickley (Reference 9), it was found that for the intermediate injection rate, $V_w/U = 0.003$, the result indicated negligible wall shear; and for injection rates higher than that, negative effective wall shear was obtained. The above negative wall shear means that the values obtained satisfy the momentum equation and the bilogarithmic law; for certain surfaces this does not necessarily imply negative velocities near the wall, nor even inflection of the velocity profiles such as occurs near separation on a solid surface. On a porous surface where the transpiration orifices are discrete, the boundary layer condition $U_w = 0$ may not be true with the result that the quantity $\overline{u_w v_w}/\overline{U v_w}$ may be appreciable, so at high injection rates the value of $U_w V_w$ may be greater than $\frac{\tau_w}{\rho}$, resulting in a negative effective wall shear. Black and Sarnecki's hypothesis includes the case of the homogeneous surface where in such a layer the boundary layer velocity in the sublayer and part of the inner region would be negligible so that the law of the wake as developed by Coles (Reference 17) would describe the entire layer which would

behave like a free jet boundary.

To predict the porosity distribution required for low shear, the momentum equation is probably the most logical choice. For the case of the flat plate where $\frac{d\theta}{dx} = 0$ is assumed,

$$U_\tau^2 + V_w U = 0;$$

however, when applied to an airfoil section, the pressure term must be included and attempts could be made between the pressure terms and the transpiration velocity to maintain the condition $\theta' = 0$. The above approach would give a first approximation to a porosity distribution in a manner similar to that mentioned in the previous section.

Current Experiments in Direct Shear Measuring

To date Pappas and Okuno have been the only researchers to determine surface shear with transpiration by a direct measurement technique rather than by using the analysis of the boundary layer velocity profiles. A slender cone was used in these experiments and the drag measurements were corrected for pressure drag.

The author is currently engaged in directly measuring the skin friction of a turbulent boundary layer on a flat-plate in a zero pressure gradient using a porous floating element technique.

The boundary layer research wind tunnel in Figure 8 shows the adjustable wall which can vary the pressure gradient on the 11 inch by 36 inch floating test section. The test section floats on a layer of mercury and the transpiration air passes through three pipes protruding through the mercury into the bottom of the floating element. Flow deflectors

on the top are used to pressure balance the system. The height of the floating element could be raised or lowered by adding or removing mercury, and leveling was accomplished by the addition of small weights in the corners of the element. The surface shear forces were measured by means of a strain gauge balance which was adjustable both in axial and transverse directions to ensure a free-floating element during the test. Boundary layer measurements were obtained by means of a micrometer screw total head tube.

The system was checked out using an impervious surface and the results obtained from the balance and the integrated values of skin friction computed from the boundary layer velocity profiles agreed to within 7 percent. The porous material used was made from a matted fiber glass material bonded on ½-inch honeycomb for stiffness. The results of the boundary layer measurements are shown in Figure 12 indicating the reduction in U_τ along the plate with distributed fluid injection. The direct shear readings were very unpredictable, the effects of the gap around the element, leveling, smoothness, and alignment were appreciable, and the results showed a general increase in measured drag due to fluid injection. These results are probably due to the primitive experimental set-up. Work is currently underway to determine direct shear measurements on a flat-plate in fluid injection from a more sophisticated apparatus where linear transformers are used instead of strain gauges.

SUGGESTIONS FOR A COMMON BOUNDARY LAYER CONTROL SYSTEM

If a combined high-lift and low-drag boundary layer control system were possible, it would appear from the injection velocity requirements in

the high-speed cruise condition that the low-drag turbulent boundary layer control system should be restricted to the upper surface of the wing where the porosity is also required for the high-lift case. This means that laminar flow should be maintained on the bottom surface as far aft as possible in the cruise condition. This could be obtained by smoothing the bottom surface and by means of the camber changing mechanism to ensure a favorable pressure gradient as far aft as possible. The upper surface should be made from an evenly distributed porous material, either metal or glass fiber material, and the porosity could be changed by means of top hat type stringers inside the wing with flapper valves to regulate the flow to each section. The curvature of the upper surface should be such that the pressure distribution in the cruise condition in conjunction with the fluid injection requirements for low drag are as close as possible to the porosity requirements and inflow distribution required for the high-lift case when the wing is cambered. In the cruise condition the injection air could be obtained from the trailing edge of the airfoil through large suction slots thereby reducing the wake component in the trailing edge boundary layer. In the high-lift case, the same suction pump could be used to suck the front compartment of the wing; and from preliminary calculations that would be applicable to a small aircraft of 25 pounds per square foot wing loading, cruising at 250 knots and capable of a lift coefficient of 4.0; the blower suction requirements both for the high-lift case and the low-drag case are of the same order of magnitude. Figure 13 shows a possible approach to the problem of a combined boundary layer control system.

If a gas turbine engine is the main power plant on the aircraft,

the compressor can be used as a suction source for the high-lift boundary layer control as in the case of the XV-11A (Figure 14), and for the cruise condition a by-pass bleed system could be installed behind the compressor to satisfy the low-drag boundary layer control flow requirements.

DISCUSSION

The benefits that would result in a combined high-lift and low-drag boundary layer control system are obvious and research towards attaining this goal should be extended. The distributed suction boundary layer control system has been proven to be an acceptable method of obtaining high lift coefficients with a small outlay of power with a minimum of structural modifications, as has been demonstrated in the L-19 and XV-11A aircraft. However, the present technology still makes it rather difficult to accurately predict the porosity requirements on a distributed suction boundary layer control system. This is due to a failure of the theories to predict the pressure distribution about highly cambered airfoil sections and airfoils at large angles of attack and a breakdown of the turbulent boundary layer theories with transpiration in severe adverse pressure gradients. On the L-19 and XV-11A aircraft, the theories gave a first approximation to the porosity distribution and an experimental iteration process was used to optimize the boundary layer control system. Obviously, further research in turbulent boundary layer theory with transpiration is required.

The low-shear turbulent boundary layer control system appears to be very attractive especially if wing surface imperfections can be tolerated and the cleaning maintenance over the leading edge and the slots or holes could be eliminated. Unfortunately, very little work has been performed in

the reduction of skin friction in a turbulent boundary layer with fluid injection except in the supersonic case on flat-plates and a slender cone. The analysis of the turbulent boundary velocity profile with fluid injection shows considerable decreases in skin friction with reasonably low values of fluid injection; however, it is obvious that further experiments to directly measure the surface shear of a turbulent boundary layer with fluid injection need to be performed with sophisticated experimental arrangements to verify the theoretical prediction and the meager experimental results in the subsonic case.

The variable camber wing, as successfully flight tested in the XAZ-1 and the XV-11A aircraft, indicates considerable potential as a method of compromising between the very different airfoil requirements for high-lift and low-drag. The porous material to be used on the surface must be relatively smooth with evenly distributed porosity; discrete holes for injection are unacceptable. However, if the surface pores are sufficiently small so that the net effect could be considered in a manner similar to surface roughness then with a sufficiently thick boundary layer the surface would be aerodynamically smooth and would conform to the idealized model. The porous glass fiber material used in the experiments mentioned above was found to be acceptable for surface material if fixed to an open honeycomb material for rigidity.

If such a combined system as mentioned above is possible, the cost of wing manufacture should not be much greater than that of the equivalent conventional aircraft. The operational gains in either STOL capability or increased wing loading and in cruise speed and range even with the power

requirements taken from the main power plant should make the idea of a combined boundary layer control system very attractive.

REFERENCES

1. Carmichael, B. H., Unpublished Report, Aerophysics Department, Mississippi State University, State College, Mississippi, 1953.

2. Black, T. J. and Sarnecki, A. T., The Turbulent Boundary Layer with Suction or Injection, A.R.C. R & M 3387, 1965.

3. Eppler, R., Common Boundary Layer Control for High-Lift Devices and High-Speed Flight, Bolbow-Entwicklungen, No. 49, 1962.

4. Czarnecki, K. R., Analytical Investigation of Reduction in Turbulent Skin Friction on a Flat Plate by Means of Air Injection Through Discrete Slots, NASA Tech Note D-2102, 1964.

5. Lavin, M., Mass Injection into a Turbulent Boundary Layer, Research and Advanced Developments Division, RAD-TM-64-28.

6. Mickley, H. S. and Davis, R. S., Momentum Transfer for Flow Over a Flat Plate with Blowing, NACA Tech Note 4017.

7. Ludweig, H., Instruments for Measuring the Wall Shearing Stress of Turbulent Boundary Layers, NACA Tech Memo 1284, 1950.

8. Pappas, C. C. and Okuno, A. F., The Relation Between Skin Friction and Heat Transfer for the Compressible Turbulent Boundary Layer with Gas Injection, NASA TN D-2857, 1965.

9. Mickley, H. S., Ross, R. C., Squyers, A.L. and Stewart, W. E., Heat, Mass and Momentum Transfer for Flow Over a Flat Plate with Blowing or Suction, NACA Tech Note 3208, 1954.

10. Ludwieg, H. and Tillmann, W., Investigation of the Wall Shearing Stress in Turbulent Boundary Layers, NACA Tech Memo 1285, 1950.

11. Roberts, S. C., Development of Distributed Suction High-Lift STOL Aircraft, Presented at the International Congress on Air Technology, Hot Springs, Arkansas, 1965.

12. Roberts, S. C., Smith, M. R., and Clark, D. G., Flight Test Evaluation of a Distributed Suction High-Lift Boundary Layer Control System on a Modified L-19 Liaison Aircraft, Aerophysics Report No. 66, Mississippi State University, State College, Mississippi, 1966.

13. Head, M. R., Johnson, D., and Coxon, M., Flight Experiments on Boundary Layer Control for Low Drag, ARC, R & M No. 3025, 1955.

14. Lachmann, G. V., Laminarization Through Boundary Layer Control, Aero Eng Rev 13, 37919540.

15. Pfenninger, W., Groth, E. E., Carmichael, B. H., and Whites, R. C., Low Drag Boundary Layer Suction Experiments in Flight on the Wing Glove of an F-94A Airplane, Northrop Corp, NAI-55-458 (BLC-77), 1955.

16. Cornish, J. J. III, A Comparison of the Power Requirements of Distributed Suction and Jet Blowing to Increase Lift, Aerophysics Department, Mississippi State University, State College, Mississippi, 1959.

17. Coles, D., The Law of the Wake in the Turbulent Boundary Layer, NACA Tech Note 4017, November 1959.

LIST OF SYMBOLS

C_F	average skin-friction coefficient
C_f	local skin-friction coefficient
F	injection mass flow normal to the surface
H	δ^*/θ
U	local free-stream velocity
U'	$\partial U/\partial x$
U_τ	wall shear velocity
V_w	inflow velocity
x, y	coordinates along and normal to the surface
δ^*	boundary layer displacement thickness
θ	boundary layer momentum thickness
ν	kinematic viscosity
ρ	fluid density
τ	surface shear stress

Subscripts

0	zero injection condition
w	surface conditions
∞	free-stream condition
i	initial condition

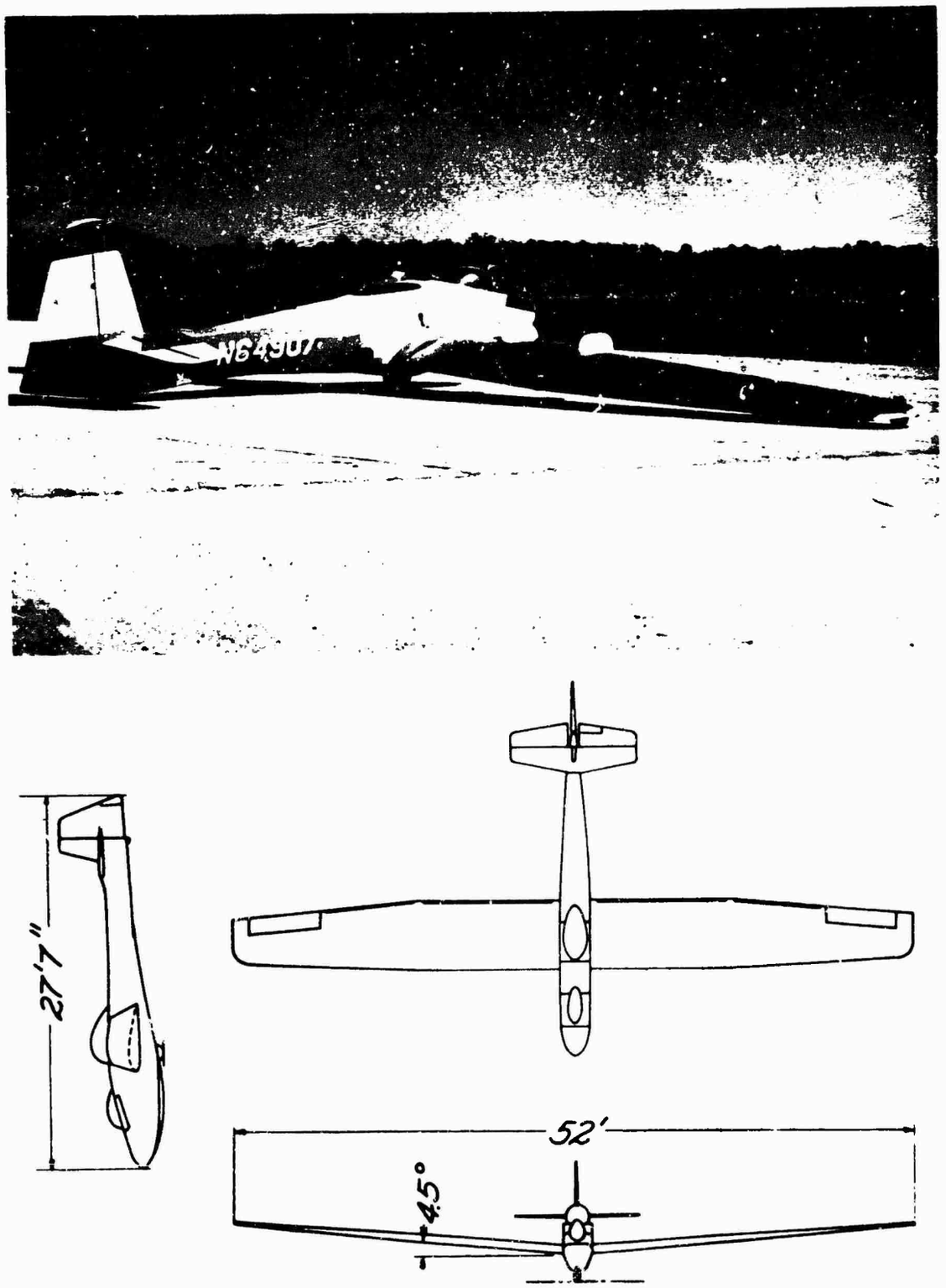

Figure 1. Modified Schweizer TG-3A High-Lift Research Aircraft.

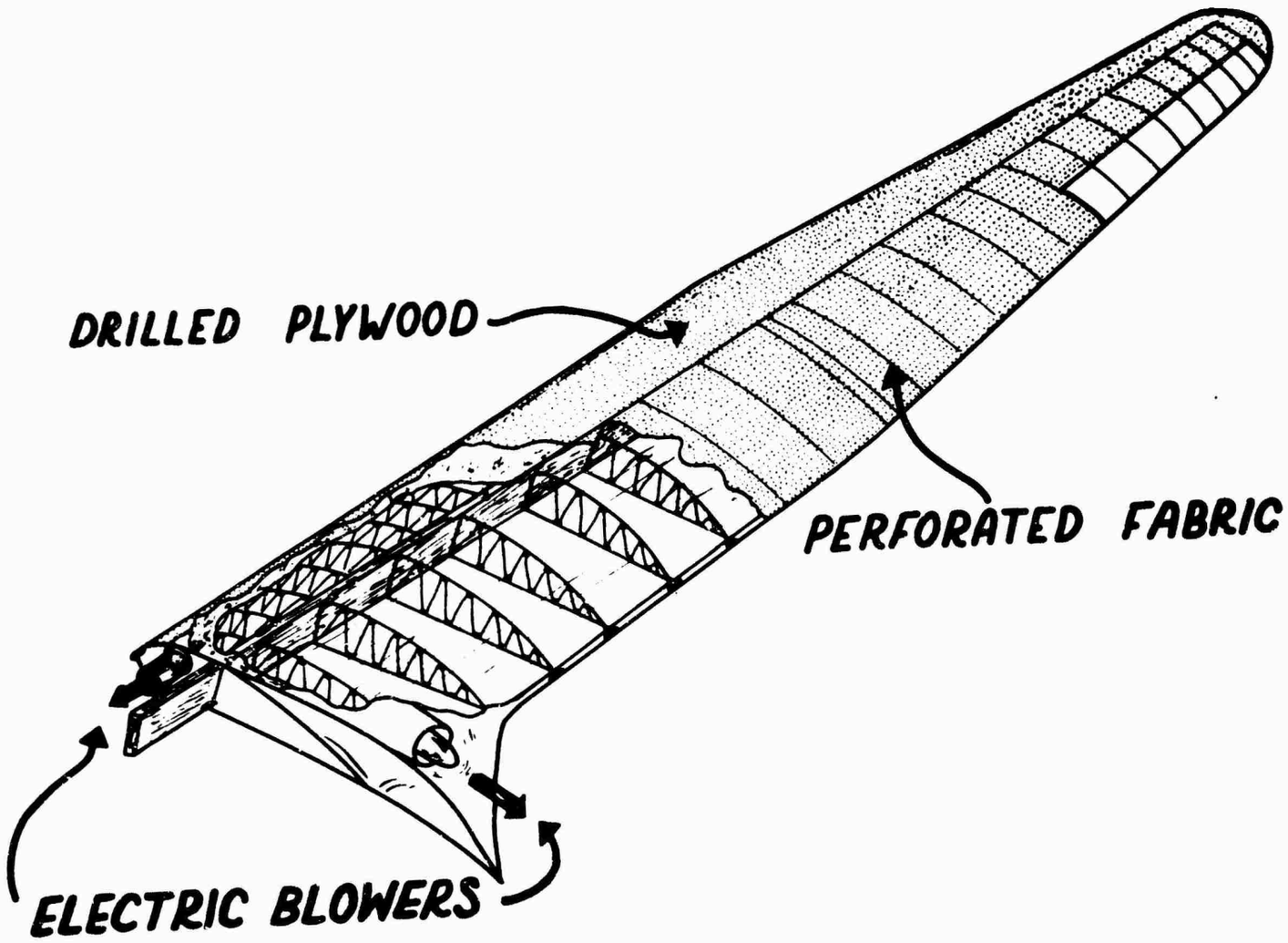

Figure 2. Schematic of High-Lift Boundary Layer Control System in IG-3A Sailplane.

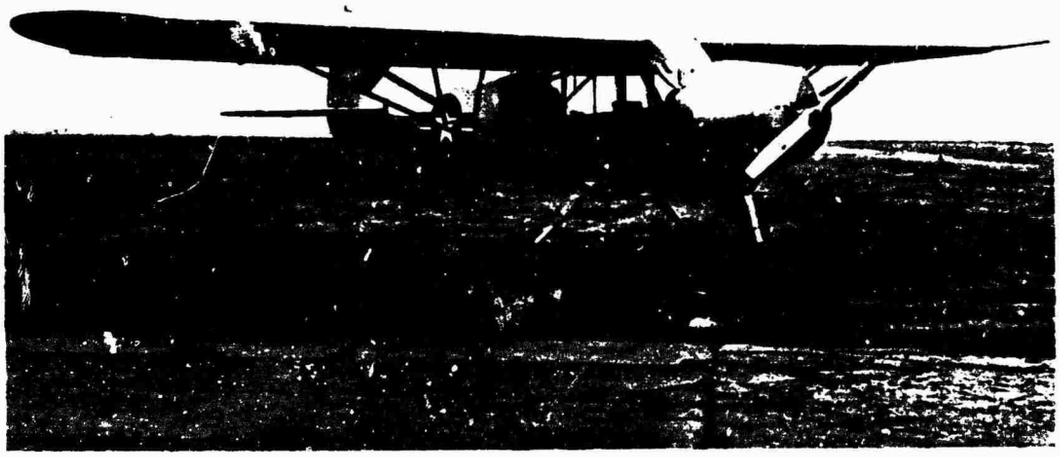

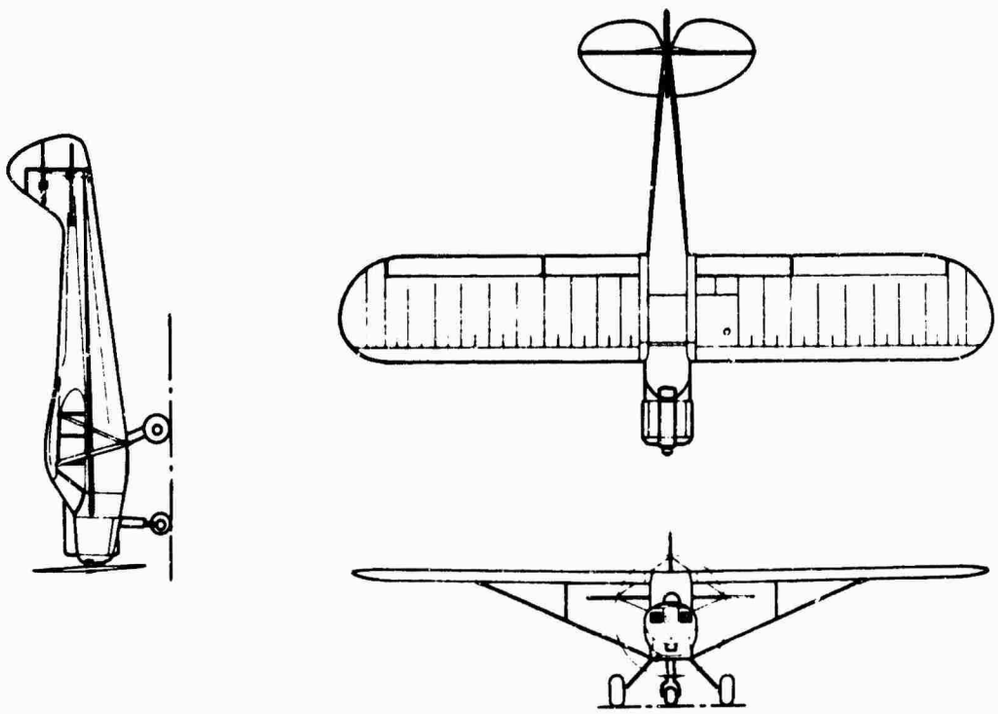

Figure 3a. Modified Piper L-21 High-Lift Research Aircraft.

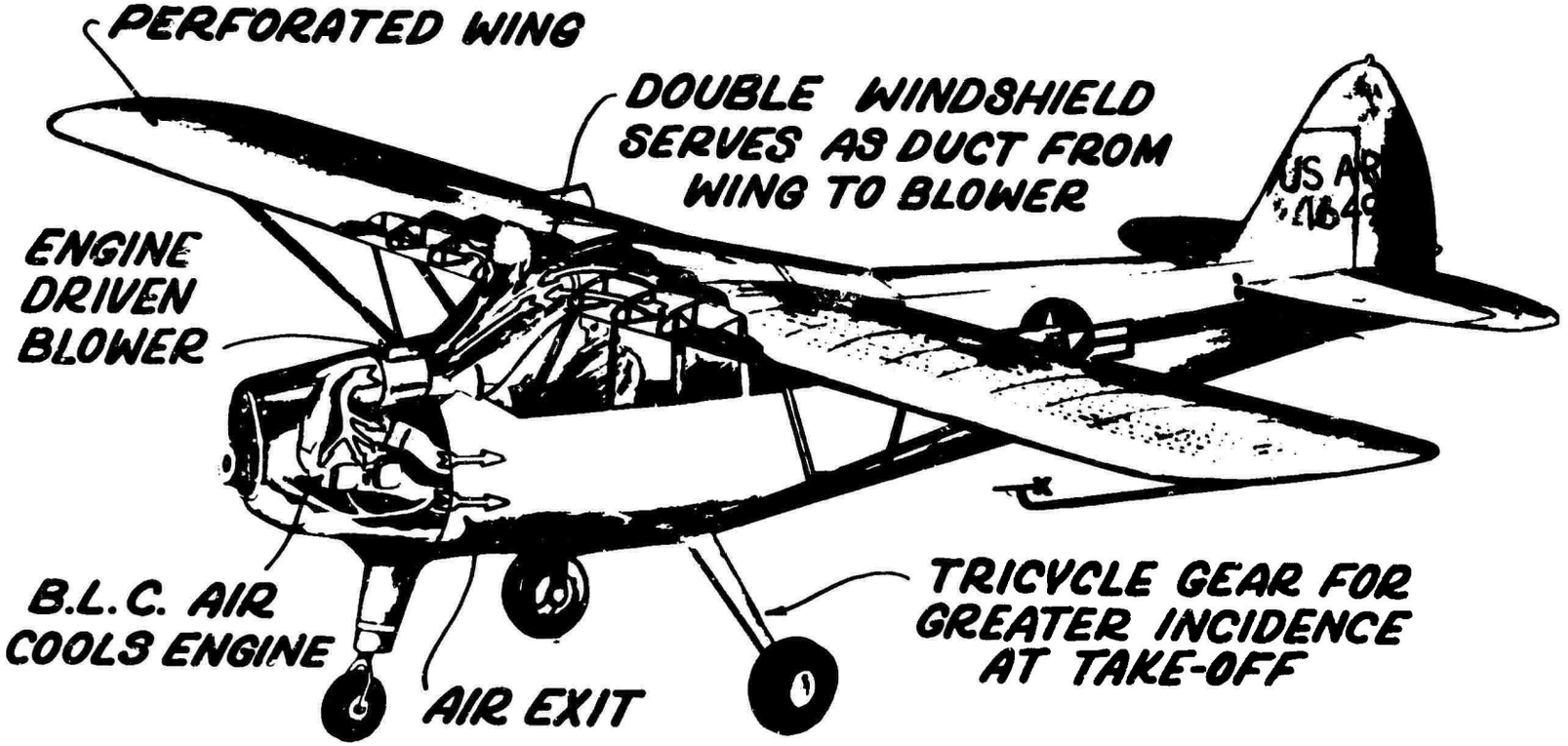

Figure 3b. Schematic of Boundary Layer Control System on L-21.

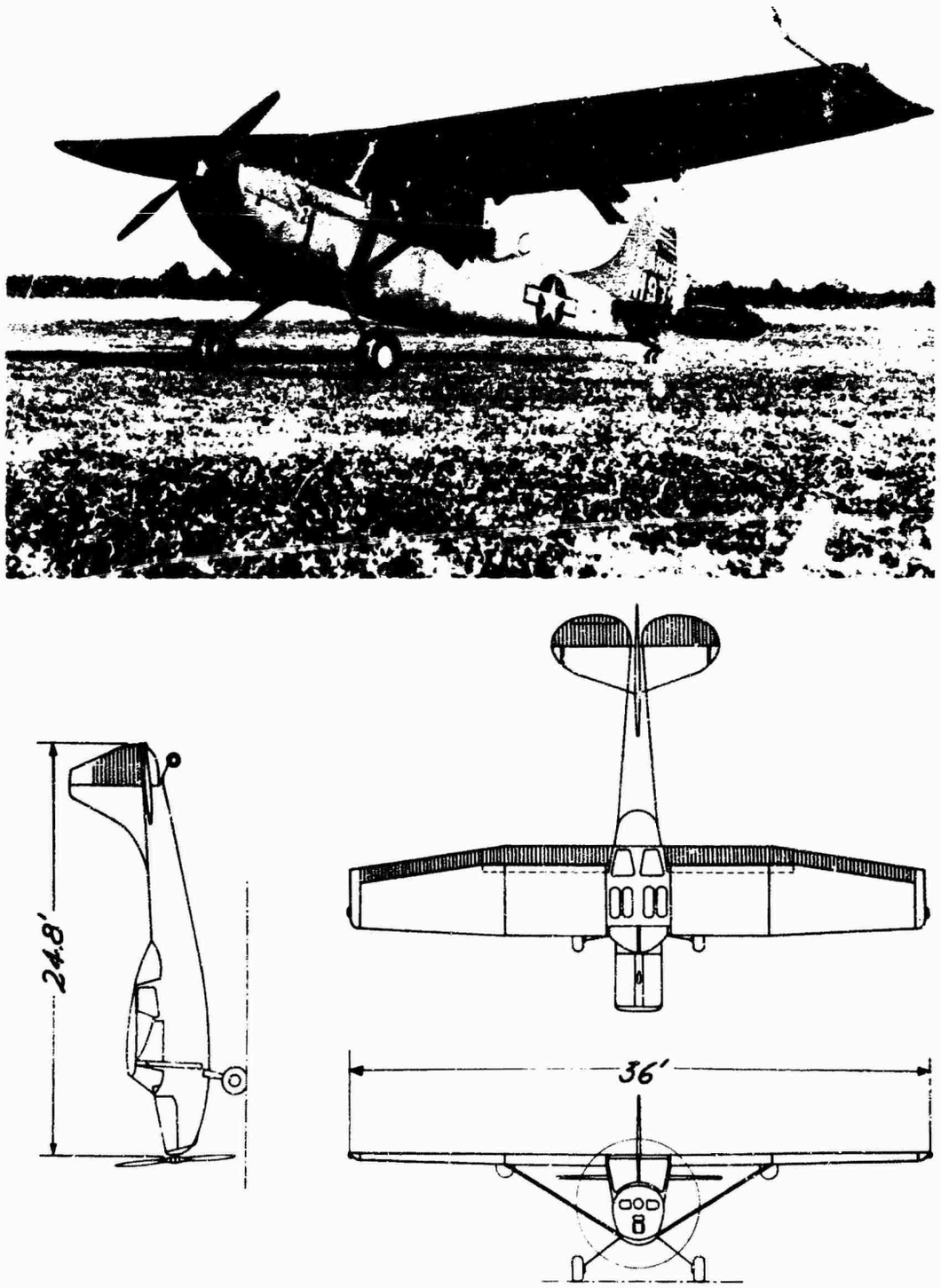

Figure 4a. Modified Cessna L-19 High-Lift Research Aircraft.

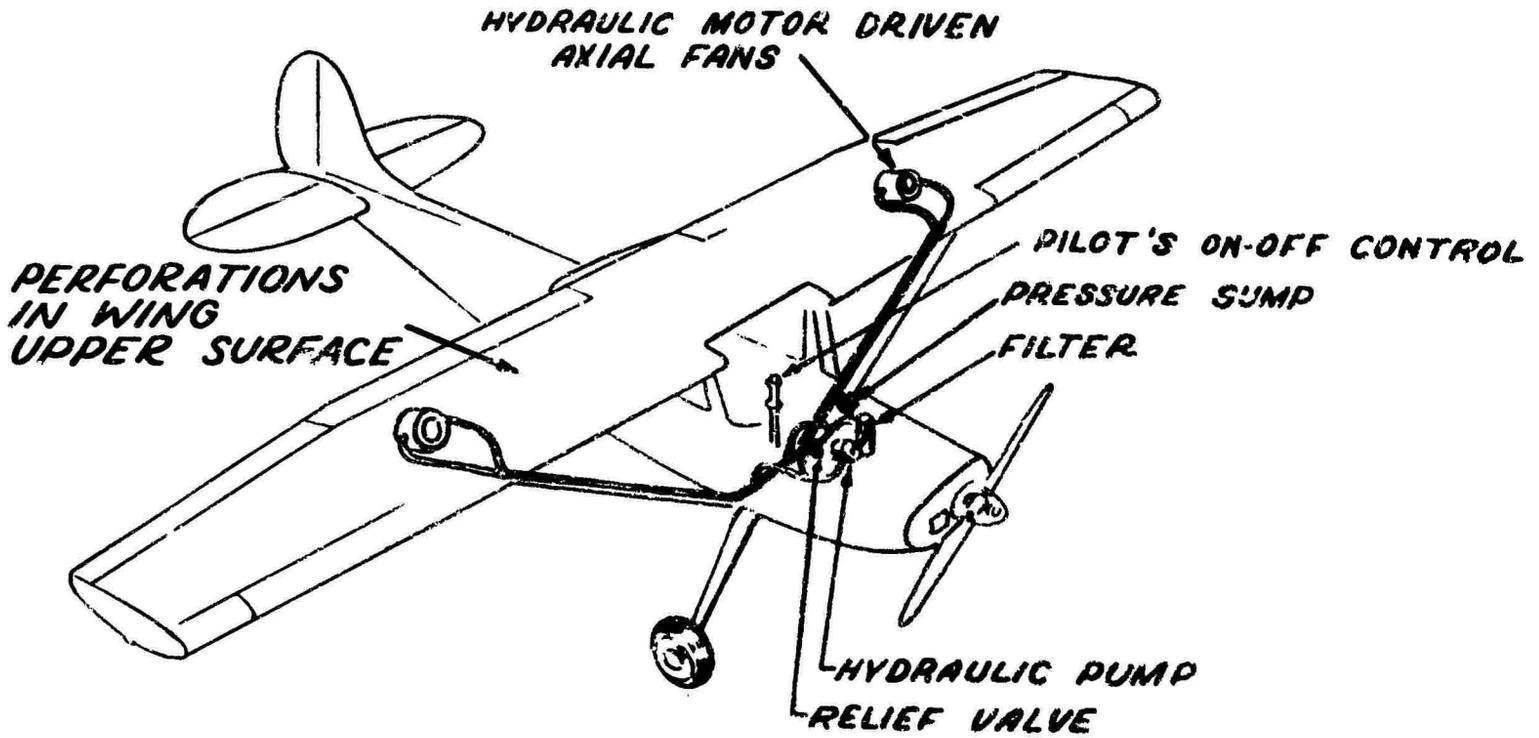

Figure 4b. Schematic of Boundary Layer Control on L-19.

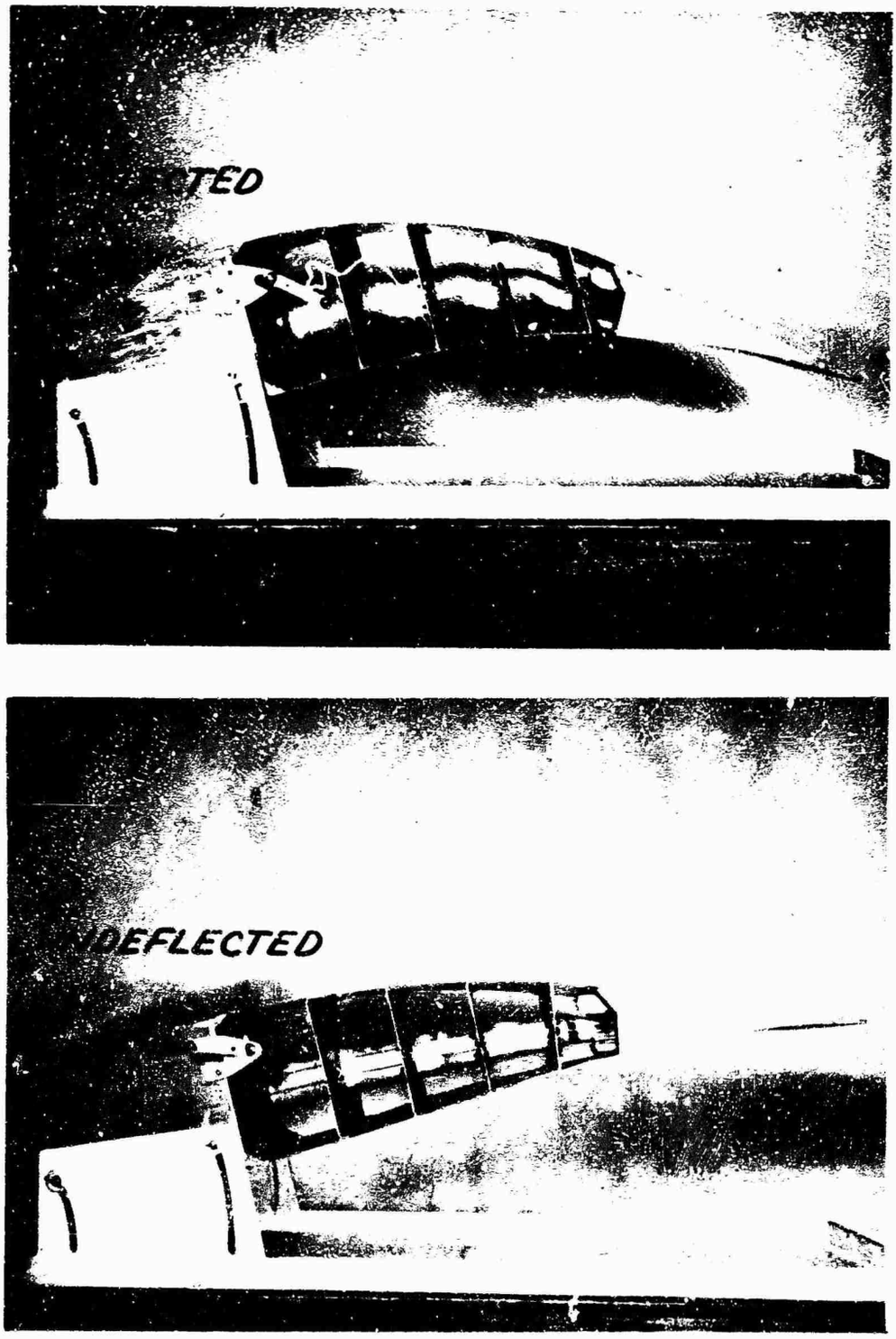

Figure 5. Wing Camber Change Mechanism on XAZ-1.

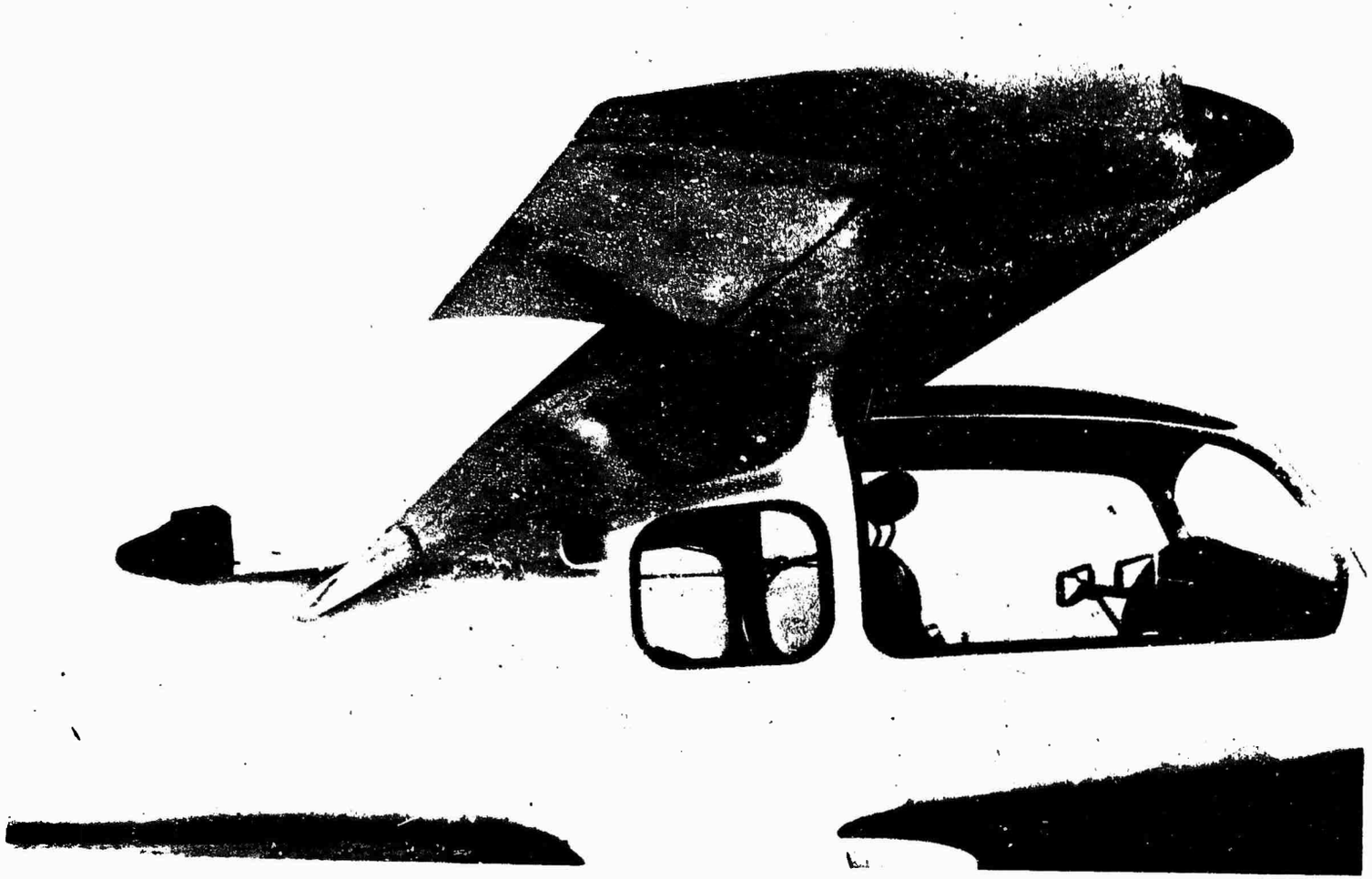

Figure 6. Photograph of the Variable Camber Wing on the XV-11A Aircraft.

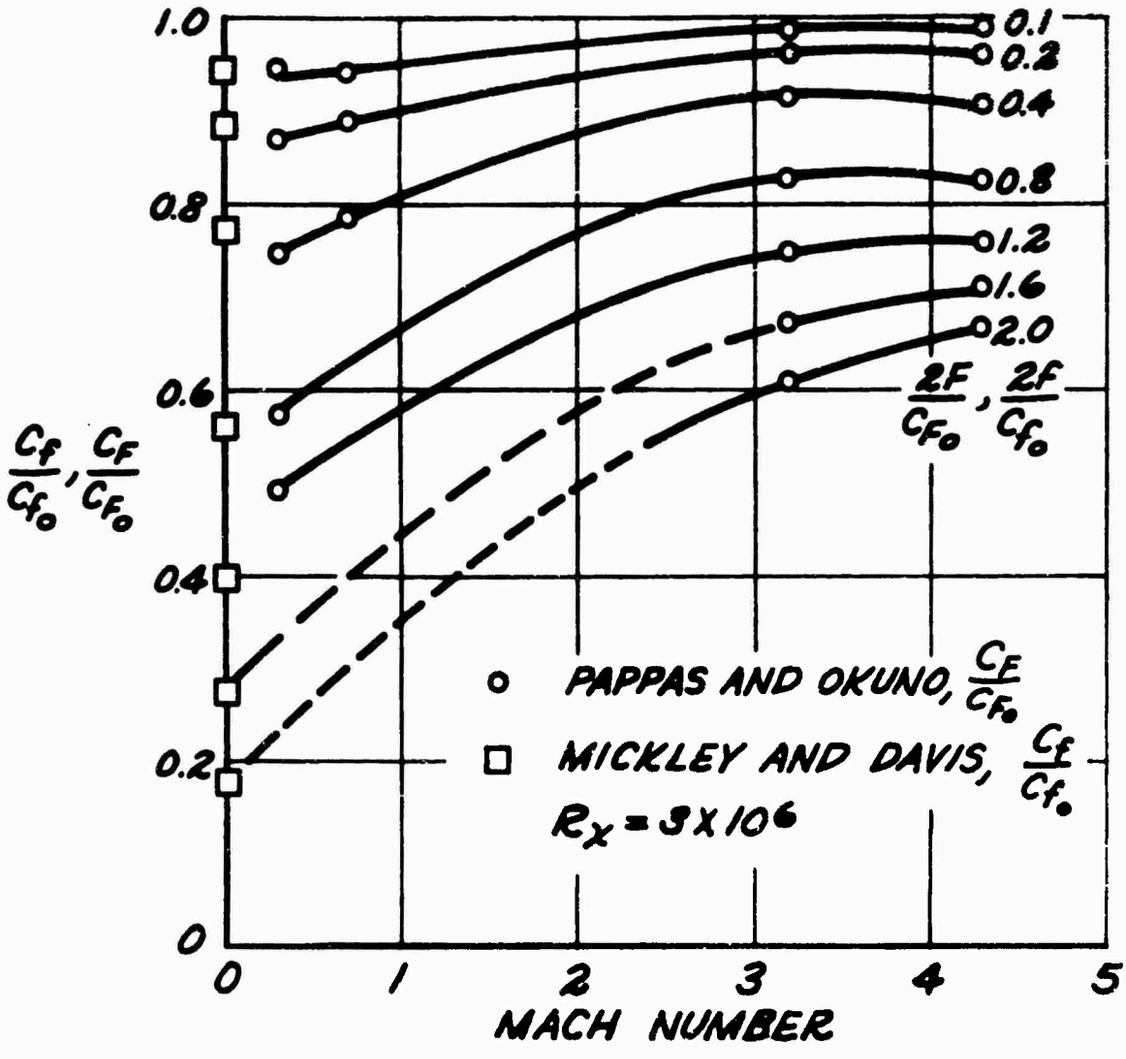

Figure 7. Effect of Mach Number on the Reduction in Skin Friction Due to Air Injection.

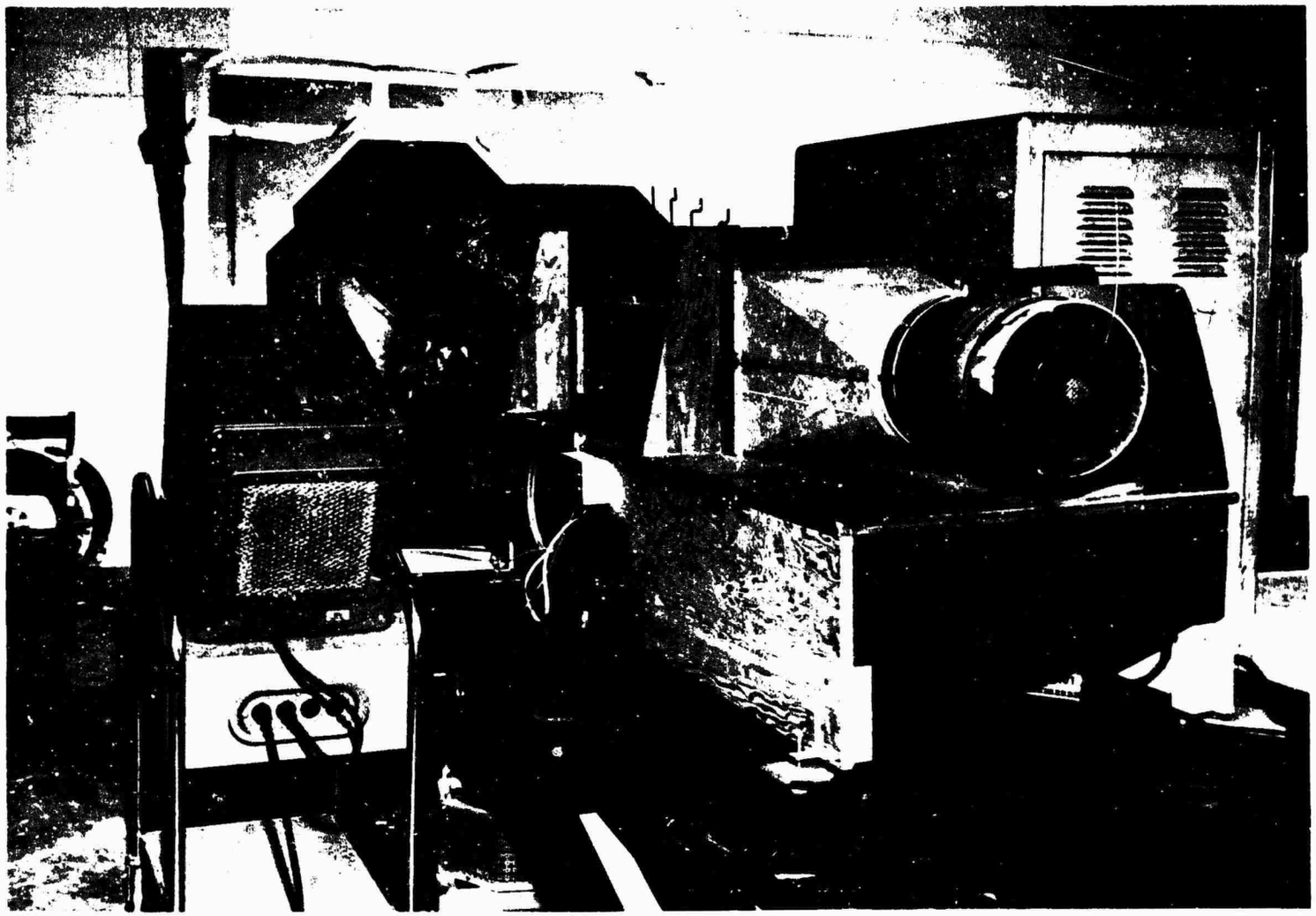

Figure 8. Photograph of the Boundary Layer Research Wind Tunnel Modified for Direct Shear Measurements.

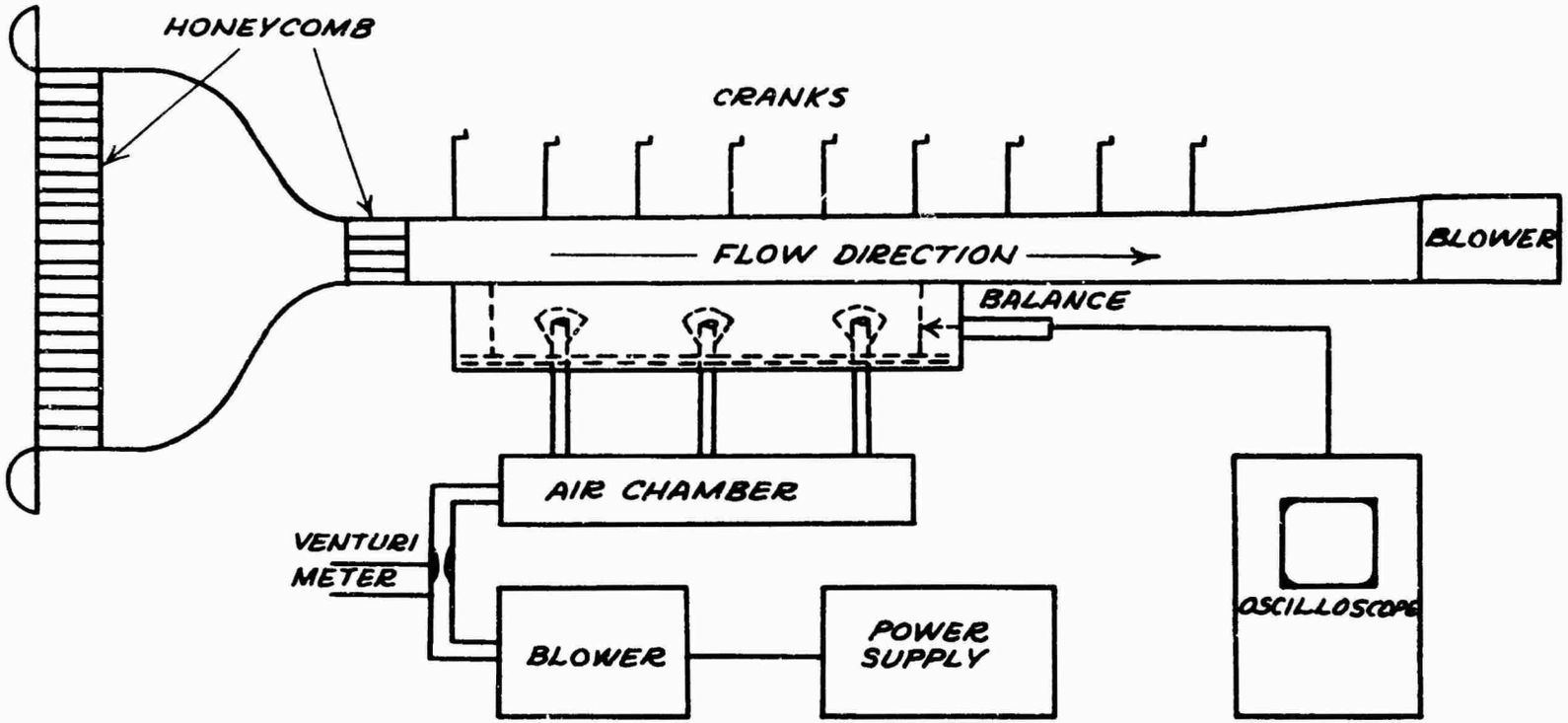

Figure 9. Schematic Drawing of the Modified Wind Tunnel.

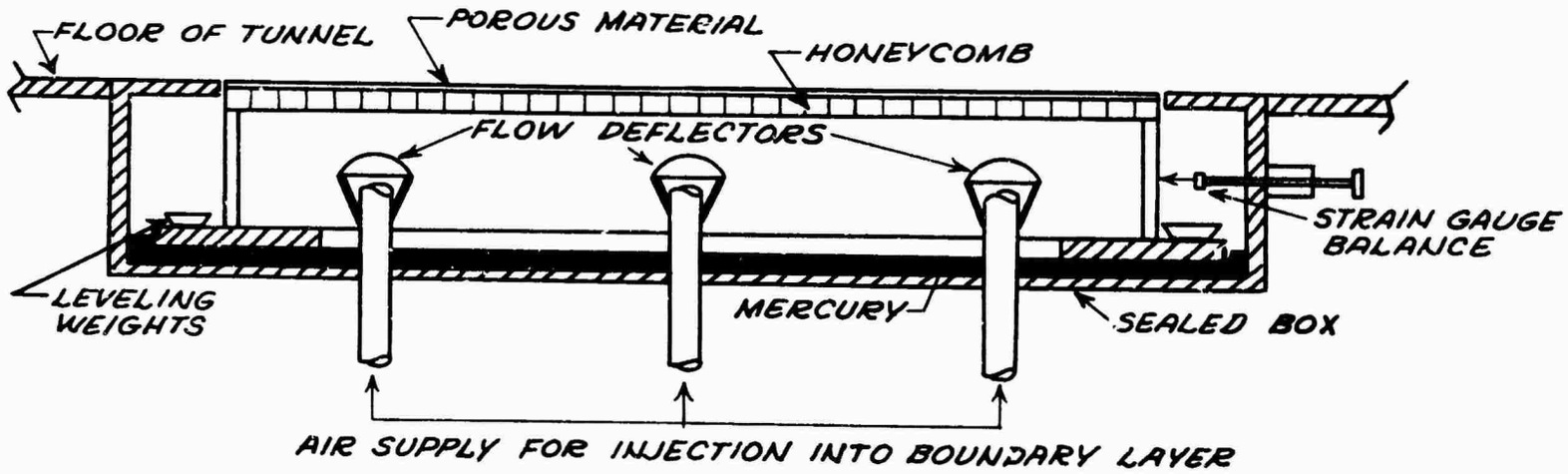

Figure 10. Cross Section Drawing of the Floating Element.

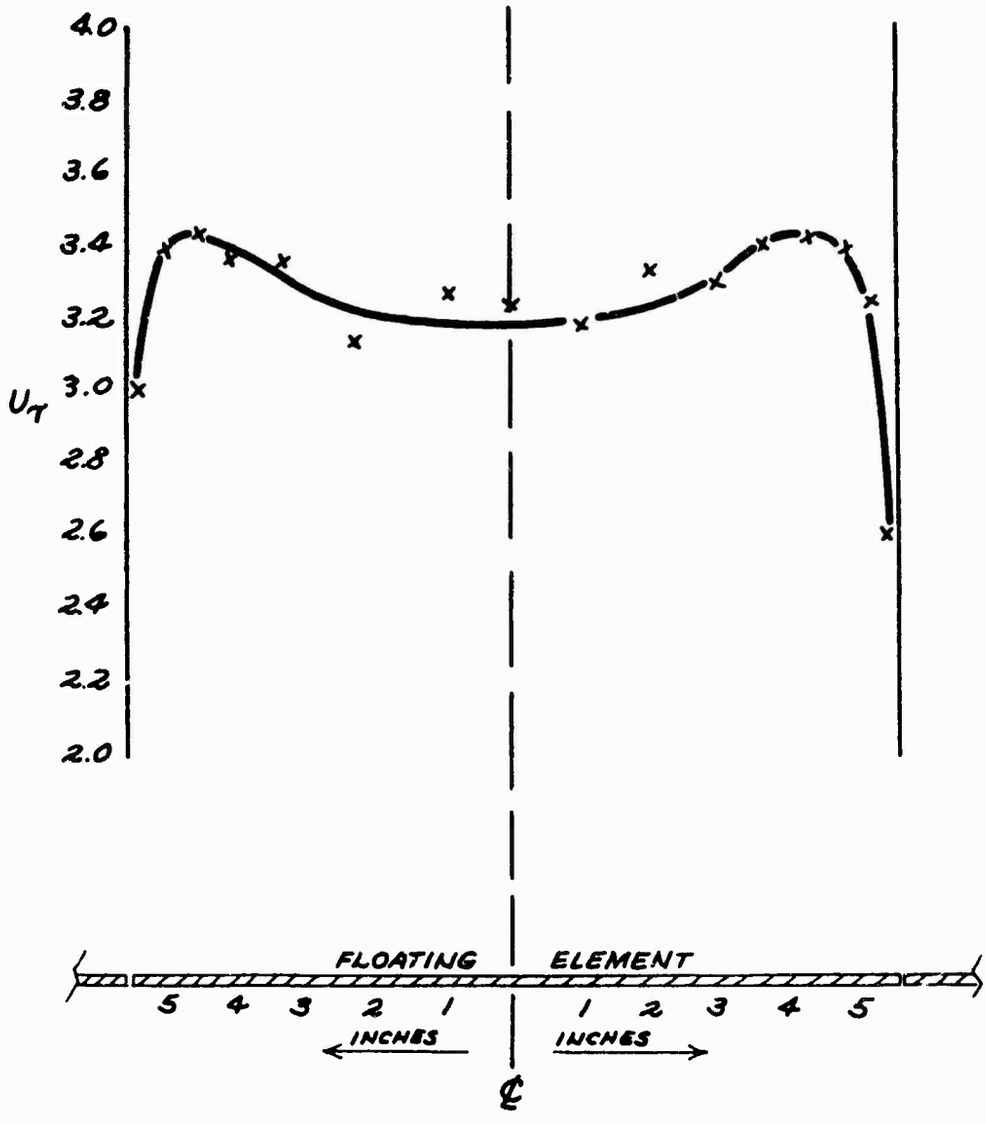

Figure 11. Variation of U_τ Across the Floating Element.

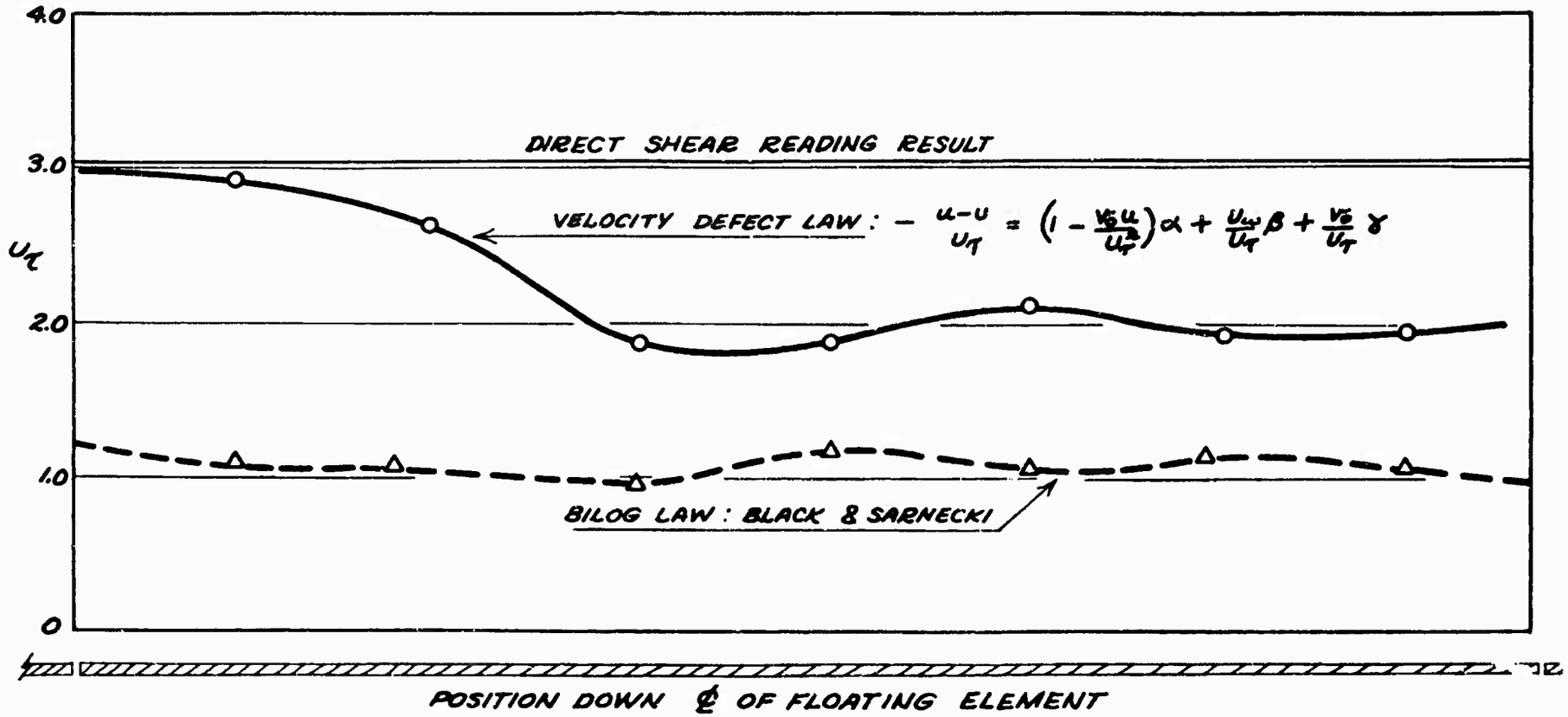

Figure 12. Variation of U_τ Along the Center-Line of the Floating Element.

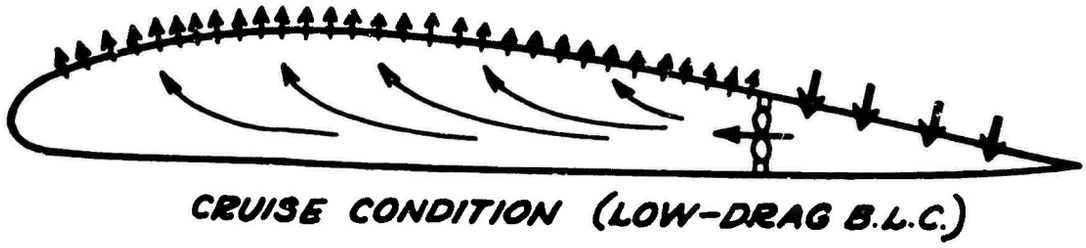

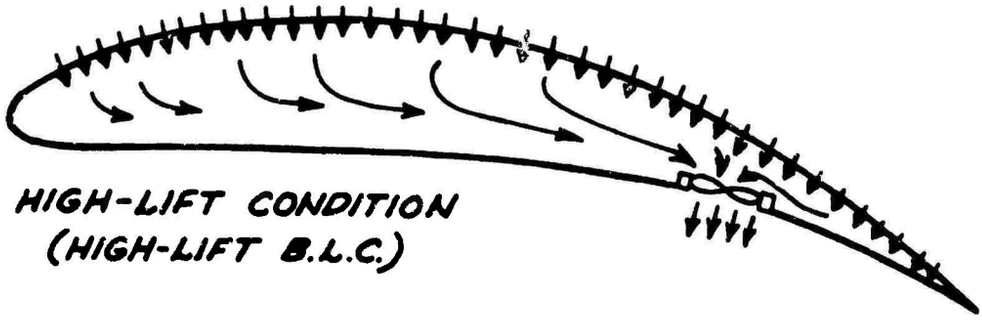

Figure 13. Suggested Combined Boundary Layer Control System.

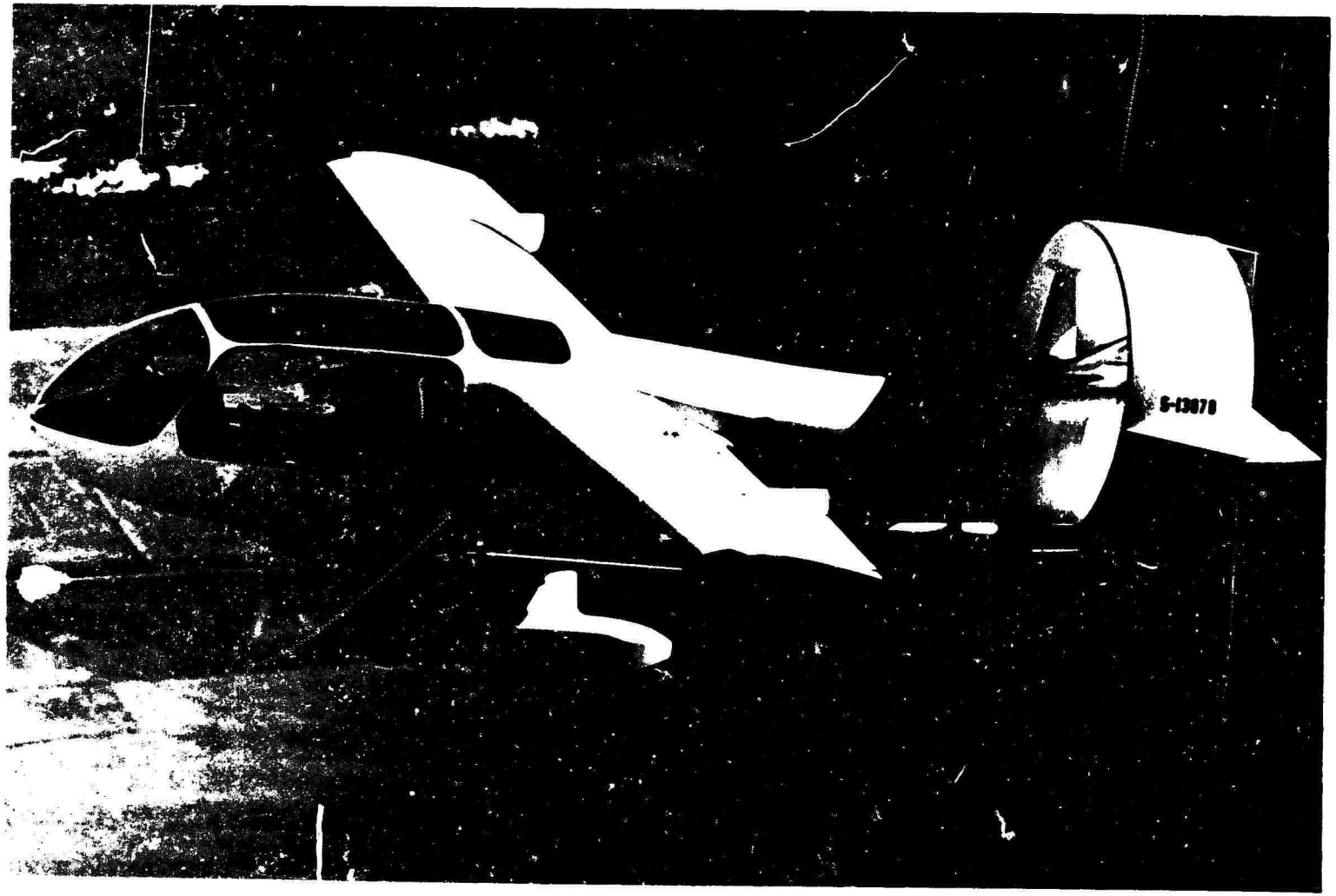

Figure 14. XV-11A High-Lift Boundary Layer Control Research Vehicle.